ANALYSES PERTAINING TO THE REDUCTION OF NON-SPECULAR SCATTERING

Technical Report

by

T. B. A. Senior
Radiation Laboratory
The University of Michigan
Ann Arbor, MI 48109

Prepared for

Air Force Office of Scientific Research
under Grant No. 77-3188 ModA

December 1977

ABSTRACT

An important problem in connection with radar absorbers is the design of absorbing coatings to reduce 'non-specular' scattering contributors such as edges, traveling and creeping waves. The present study is directed at the first two. The surface treatment is simulated using an impedance boundary condition and the main tools employed are high frequency diffraction analyses and a computer program for the direct digital solution of the integral equation for the induced current. For simplicity attention is confined to a two-dimensional problem, and the body used to illustrate the techniques is a 15° half angle ogival cylinder illuminated by an H-polarized plane wave incident in a plane perpendicular to the generators of the cylinder. By a combination of analytical and numerical techniques, surface impedances are specified providing significant and broadband cross section reductions over given aspect ranges.

TABLE OF CONTENTS

1. INTRODUCTION

The problem of reducing the backscattering cross section of a target is a rather old one, and the specification, manufacture and application of radar absorbing materials is now a well-developed art. These materials are customarily designed to reduce the backscattering over a range of frequencies for normal (or near normal) incidence on a surface, but the fact is that many targets of concern are so shaped that in the aspect ranges of most interests no surfaces are viewed at normal incidence. This is true, for example, for many aircraft at front and rear aspects, but even in the absence of specular contributions, the scattering from the wings, fuselage, etc., can still be significant. It is therefore important to seek absorbing materials which are effective in reducing 'non-specular' scattering and the present study is directed to this end.

The three main types of non-specular scatterer are edges (or other discontinuities in the slope or higher derivatives of the surface), traveling waves and creeping waves. All are aspect and polarization dependent and diminish with increasing frequency. Their magnitudes are generally small compared with any specular contribution that may exist, but they can be important under all circumstances and most particularly when there is no specular scattering.

Traveling and creeping waves are forms of surface wave whose propensity to cling to surfaces sets them apart from edge-diffracted contributions. The waves are distinguished from one another mainly by the illumination of the surface on which they travel. Creeping waves are born at the shadow boundaries

of bodies whose radii of curvature are electrically large. They propagate into the shadow region following geodesic paths, leaking off energy in the direction of the forward tangent to the path as they go. As a result of this leakage, the wave attenuates as it progresses and its electromagnetic properties at any point are almost exclusively determined by the local geometry of the surface. It is evident that such a wave can traverse the rear of a smoothly curved body such as a circular cylinder, and on reaching the boundary of the shadow and lit regions, the energy radiated is in the backscattering direction. For a metallic body creeping waves are only an appreciable source of scattering when the incident electric field is perpendicular to the surface at the shadow boundary, but once established they are no longer dependent on the incident field. They are closely bound to the surface over which they travel and this fact, combined with their natural rate of decay even on a metallic surface, makes it possible to diminish their effect using lossy coatings.

Traveling waves are also significant only when the electric vector is perpendicular to the surface. They are supported by surfaces of large radius in the direction of travel almost all of which are illuminated, and in contrast to creeping waves, they tend to build up as they travel, being fed by the incident field. As regards backscattering, a traveling wave is harmless as long as it continues to travel forward, but when it reaches any discontinuity in the surface or its electrical properties, a portion may be reflected back to contribute to the backscattered field. The resulting field has a fan-shaped pattern characteristic of a traveling wave antenna. As in the case of creeping waves, a traveling wave contribution can be reduced by appropriately loading the surface.

The third source of non-specular scattering is edge diffraction as, for example, by the front and rear edges of an ogival cylinder. This also is strongly polarization dependent. Thus, for a plane wave at near edge-on incidence in a plane perpendicular to the axis of an ogival cylinder with its electric vector parallel to the edge (E polarization), the front edge is the primary source. On the other hand, for H polarization the rear edge is dominant, and its scattering can be reduced by the same method used for the traveling wave, but even so the front edge still contributes a small amount. It may therefore be necessary to treat the front edge as well to produce a substantial decrease in the scattering from the entire body.

In three previous studies (Knott et al, 1973b; Knott and Senior, 1974; Senior and Liepa, 1977) techniques were developed for reducing non-specular scattering using surface treatments and/or resistive sheets extending out from the body. The present work is a continuation of these but is exclusively concerned with the specification of a surface treatment to reduce edge and traveling wave contributions to the backscattered field. The surface treatment is simulated using an impedance boundary condition and the main tools employed are high frequency diffraction analyses and a computer program for the direct digital solution of the integral equation for the induced current. For simplicity attention is confined to a two-dimensional problem and the model used to illustrate the techniques is a 15 degree half angle ogival cylinder illuminated by an H-polarized plane wave incident in a plane perpendicular to the generators of the cylinder. The task confronting us is to devise schemes for broadband reduction of the backscattering cross section with particular reference to a range of aspects about edge-on.

2. GENERAL CONSIDERATIONS

Our analyses and computations are based on the use of an impedance boundary condition to simulate the effect of a coating applied to the surface. It is assumed that the (normalized) surface impedance η is a function only of the local properties of the coating regardless of the field and the geometry of the surface to which it is applied, and this is an assumption which is incapable of prior validation. In particular, it is not evident that an actual coating will present the same impedance close to the edge of a body as it does when over a broad face, nor is there any assurance that a material can be found to yield a desired impedance independent of both the incident field and the surface geometry. In spite of these shortcomings, the concept of a surface impedance is a valuable one especially for a study such as this, and the fact that for bodies with a variety of different coatings good agreement has been found between measured scattering patterns and those computed using the appropriate surface impedance provides confidence in its validity.

For a surface whose impedance is specified at every point, the impedance (or Leontovich) boundary condition can be written as

$$\underline{E} - (\hat{n} \cdot \underline{E})\hat{n} = \eta Z \hat{n} \times \underline{H} \qquad (1)$$

where $\hat{n}$ is the unit vector outward normal and η is the surface impedance relative to the intrinsic impedance Z of the free space medium above the surface. η may vary over the surface and is zero for perfect conductivity. The derivation of (1) has been discussed by Senior (1960) and we remark that in contrast to the analogous boundary condition involving the normal derivative of the field, (1) does not contain any tangential derivatives of η.

An immediate consequence of (1) is that the surface supports electric and magnetic currents whose densities $\underline{K} = \hat{n} \wedge \underline{H}$ and $\underline{K}^+ = - \hat{n} \wedge \underline{E}$ respectively are related by

$$\underline{K}^* = - \eta Z \hat{n} \wedge \underline{K} ,$$

and in general both are non-zero. By trivial manipulation, (1) can also be expressed as

$$\underline{H} - (\hat{n} \cdot \underline{H})\hat{n} = - \frac{Y}{\eta} \hat{n} \wedge \underline{E} \qquad (2)$$

(Senior, 1962) where $Y = 1/Z$. This the dual of (1) under the transformation $\underline{E} \to \underline{H}$, $\underline{H} \to -\underline{E}$, $Z \leftrightarrow Y$, $\eta \to 1/\eta$, implying $\underline{K} \to \underline{K}^*$ and $\underline{K}^* \to -\underline{K}$. It follows that in spite of our concentration on the case of H polarization, the analogous results for E polarization can be obtained by replacing η by $1/\eta$.

If an H polarized plane wave is incident in a plane perpendicular to the generators of a cylinder whose profile is C, the problem is a scalar one for the component H_z parallel to the generators. The electric current is now in the direction of the tangent to the profile, i.e. $\underline{K} = \hat{s}K$, and the scattered magnetic field is $\underline{H}^S = \hat{z}H^S$ with

$$H^S (\underline{\rho}) = \frac{ik}{4} \int_C \left\{ \hat{n}' \cdot \hat{r} \, H_1^{(1)}(kr) + i\eta(s') H_0^{(1)}(kr) \right\} K(s')ds' \qquad (3)$$

where $\underline{r}$ $(= r\hat{r}) = \underline{\rho} - \underline{\rho}'$ is the vector from the integration point to the point of observation and $H_0^{(1)}$, $H_1^{(1)}$ are Hankel functions of the first kind of orders zero and one respectively. A time factor $e^{-i\omega t}$ is assumed and suppressed.

On taking the limit as the observation point approaches C, we have

$$H^i(s) = \frac{1}{2}K(s) - \frac{ik}{4}\int_C \left\{\hat{n}' \cdot \hat{r}\, H_1^{(1)}(kr) + i\eta(s')H_0^{(1)}(kr)\right\} K(s')\, ds' \tag{4}$$

This is an integral equation for the surface electric current density K(s) and is the one on which the computer program RAMD (see Senior and Liepa, 1977) is based.

The first terms in the integrands of (3) and (4) are contributed by the electric current and the second by the magnetic current. In the far zone of the body the Hankel functions can be replaced by the leading terms in their asymptotic expansions for large argument to give

$$H^S(\underset{\sim}{\rho}) \sim \sqrt{\frac{2}{\pi k\rho}}\, e^{i(k\rho - \pi/4)} P \tag{5}$$

in which the far field amplitude P is

$$P = \frac{k}{4}\int_C \left\{\hat{n}' \cdot \hat{\rho} - \eta(s')\right\} K(s') e^{-ik\hat{\rho}\cdot\underset{\sim}{\rho}'} ds' \tag{6}$$

The form of this expression suggests three possible procedures for reducing the scattering in some chosen direction $\hat{\rho}$, and these could be employed singly or in combination:

(i) reduce the amplitude of the current over the entire surface of the body,

(ii) adjust the phase of the current to ensure that there is no stationary phase point in the range of integration, and

(iii) choose the surface impedance so that $\hat{n}' \cdot \hat{\rho} - \eta(s')$ is small over the surface.

The first two are the bases for the more conventional approaches to cross section reduction. An absorber does serve to reduce $|K|$, but not always by a sufficient amount to rely on this technique alone. Shaping of the body is directed at the second method, and the elimination of all specular reflections is, in fact, equivalent to the elimination of the stationary phase points associated with the incident field phase. Unfortunately, such shaping may also accentuate surface wave effects. In the case of an ogival cylinder there is a stationary phase point created by the (backward) traveling wave, and it is then necessary to reduce this portion of the surface field as much as possible.

The third method is more novel. If

$$\eta = \hat{n} \cdot \hat{\rho} \tag{7}$$

at every point of the surface, the scattering will be zero in the direction $\hat{\rho}$ and (presumably) small in some range of aspects about this direction. The required impedance depends neither on the frequency nor the angle of incidence and is always real, but there is a difficulty: for any closed surface the specification demands a negative real (active) impedance over a portion of the surface. Thus, to suppress the edge-on backscattering from an ogival

cylinder of half angle Ω , η must vary from $\sin\Omega$ at the front through zero at the middle to - $\sin\Omega$ at the back. We have verified (Senior and Liepa, 1977) the validity of the scheme by using program RAMD to compute the bistatic scattering from a cylinder. The impedance did null out the scattering in the backwards direction, and reduced it below that of the bare body within 18 degrees of edge-on while increasing it at larger angles. In an attempt to avoid the negative impedances, we also computed the scattering for an impedance equal to the modulus of the optimum, and for a treatment in which the cylinder was left bare where the optimum impedance is negative. Unfortunately, neither was effective, and the edge-on backscattering was actually larger than for the bare body.

Although the optimum surface impedance is non-physical for any finite body of non-zero thickness, one geometry for which it is both realizable and simple is the infinite wedge, and for edge-on incidence in particular the requirement is that

$$\eta = \sin\Omega \tag{8}$$

where Ω is the half angle of the wedge. This is not irrelevant to our task since the edges of the ogival cylinder resemble that of a wedge, and we shall now examine the scattering from a number of discontinuities in the surfaces of coated bodies.

3. SCATTERING BY EDGES AND OTHER DISCONTINUITIES

The problem of immediate concern to us is the backscattering from the front and rear edges of the ogival cylinder, and this can be analyzed using the infinite wedge as a model. We treat first a wedge of arbitrary angle and then particularize the results to the case of a half plane and a wedge of half angle 15 degrees. We then examine several types of impedance discontinuity on an otherwise smooth surface and compare the scattering with that provided by a geometric discontinuity.

3.1 Backscattering from a Wedge

A wedge of half angle Ω having the constant surface impedance η on both faces is illuminated by an H polarized plane wave incident at an angle ϕ_0 to the symmetry plane of the wedge (see Figure 3-1). As shown by Maliuzhinets (1959) the far field amplitude of the edge diffracted wave in the direction ϕ is then

$$P(\phi, \phi_0, \eta) = -\frac{i}{2} \frac{\cos \frac{1}{\nu}(\pi - \phi_0)}{\nu \Psi(\pi - \phi_0)} \left\{ \frac{\Psi(-\phi)}{\sin \frac{\phi}{\nu} + \sin \frac{1}{\nu}(\pi - \phi_0)} + \frac{\Psi(2\pi - \phi)}{\sin \frac{1}{\nu}(2\pi - \phi) - \sin \frac{1}{\nu}(\pi - \phi_0)} \right\} \quad (9)$$

where $\nu = 2(\pi - \Omega)/\pi = 2\Phi/\pi$. (10)

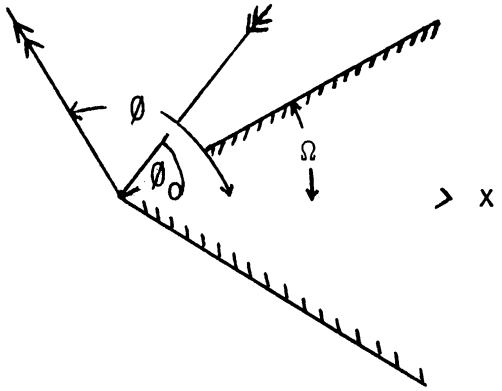

Figure 3-1: Wedge geometry.

It is sufficient to take $\Omega \leq \emptyset$, $\emptyset_0 \leq \pi$ and in the particular case of back-scattering ($\emptyset_0 = \emptyset$)

$$P(\emptyset, \emptyset, \eta) = -\frac{i}{4} \frac{\cos \frac{1}{\nu}(\pi - \emptyset)}{\nu \sin \frac{\pi}{2\nu}} \left\{ \frac{1}{\cos \frac{1}{\nu}(\frac{\pi}{2} - \emptyset)} \frac{\Psi(-\emptyset)}{\Psi(\pi - \emptyset)} \right.$$

$$\left. + \frac{1}{\cos \frac{1}{\nu}(\frac{3\pi}{2} - \emptyset)} \frac{\Psi(2\pi - \emptyset)}{\Psi(\pi - \emptyset)} \right\} . \qquad (11)$$

The function Ψ is given as the solution of a difference equation and can be expressed in terms of the special functions Ψ_Φ introduced by Maliuzhinets:

$$\Psi(\alpha) = \psi_\Phi(\alpha + \Phi + \chi)\, \psi_\Phi(\alpha + \Phi - \chi)\, \psi_\Phi(\alpha - \Phi + \chi)\, \psi_\Phi(\alpha - \Phi - \chi)$$

$$= \left\{ \psi_\Phi(\Phi) \right\}^4 \psi_{\Phi/2}(\alpha + \chi)\, \psi_{\Phi/2}(\alpha - \chi)$$

where $\eta = \cos \chi$. (12)

Hence

$$\Psi\ (\pi - \emptyset) = \left\{\psi_\Phi\ (\Phi)\right\}^4\ \psi_{\Phi/2}\ (\pi - \emptyset + \chi)\ \psi_{\Phi/2}\ (\pi - \emptyset - \chi)$$

and

$$\Psi\ (-\emptyset) = \left\{\psi_\Phi\ (\Phi)\right\}^4\ \psi_{\Phi/2}\ (-\emptyset + \chi)\ \psi_{\Phi/2}\ (-\emptyset - \chi)$$

$$= \left\{\psi_\Phi\ (\Phi)\ \psi_{\Phi/2}\ (\pi/2)\right\}^4 \cos\frac{1}{\nu}\left(\frac{\pi}{2} - \emptyset + \chi\right) \cos\frac{1}{\nu}\left(\frac{\pi}{2} - \emptyset - \chi\right)$$

$$\cdot \left\{\psi_{\Phi/2}\ (\pi - \emptyset + \chi)\ \psi_{\Phi/2}\ (\pi - \emptyset - \chi)\right\}^{-1}$$

(Maliuzhinets, 1959), giving

$$\frac{\Psi(-\emptyset)}{\Psi(\pi - \emptyset)} = \frac{1}{2}\left\{\cos\frac{2}{\nu}\left(\frac{\pi}{2} - \emptyset\right) + \cos\frac{2\chi}{\nu}\right\} g\ (\pi - \emptyset + \chi)\ g\ (\pi - \emptyset - \chi) \qquad (13)$$

in which

$$g\ (\alpha) = \left\{\frac{\psi_{\Phi/2}\ (\pi/2)}{\psi_{\Phi/2}\ (\alpha)}\right\}^2 . \qquad (14)$$

Similarly

$$\frac{\Psi\ (2\pi - \emptyset)}{\Psi\ (\pi - \emptyset)} = \frac{1}{2}\left\{\cos\frac{2}{\nu}\left(\frac{3\pi}{2} - \emptyset\right) + \cos\frac{2\chi}{\nu}\right\} g\ (\pi - \emptyset + \chi)\ g\ (\pi - \emptyset - \chi) \qquad (15)$$

and when (13) and (15) are substituted into (11) we have

$$P\ (\emptyset, \emptyset, \eta) = -\frac{i}{2\nu}\ \frac{\cos^2\frac{1}{\nu}(\pi - \emptyset)\ \cot\frac{\pi}{2\nu}}{\cos\frac{1}{\nu}\left(\frac{\pi}{2} - \emptyset\right)\cos\frac{1}{\nu}\left(\frac{3\pi}{2} - \emptyset\right)}\left\{\cos\frac{1}{\nu}\left(\frac{\pi}{2} - \emptyset\right)\right.$$

$$\left. \cdot \cos\frac{1}{\nu}\left(\frac{3\pi}{2} - \emptyset\right) - \sin^2\frac{\chi}{\nu}\right\} g\ (\pi - \emptyset + \chi)\ g\ (\pi - \emptyset - \chi).$$

(16)

Certain conclusions can be drawn which do not require a knowledge of the function g (α) and are valid for wedges of all angles. In general P is infinite when $\cos \frac{1}{\nu} (\frac{3\pi}{2} - \phi) = 0$, corresponding to the direction $\phi = \pi/2 + \Omega$ of specular reflection from the upper face of the wedge. For angles in the immediate vicinity of this direction we may replace ϕ by $\pi/2 + \Omega$ in all factors except the cosine to get

$$P(\phi, \phi, \eta) \sim \frac{i}{4\pi} \frac{\sin^2 \frac{\chi}{\nu}}{\cos \frac{1}{\nu} (\frac{3\pi}{2} - \phi)} g(\frac{\pi}{2} - \Omega + \chi)\, g(\frac{\pi}{2} - \Omega - \chi) .$$

But

$$\psi_{\Phi/2} (\tfrac{\pi}{2} - \Omega + \chi) = \psi_{\Phi/2} (\tfrac{3\pi}{2} - \Omega - \chi) \cot \tfrac{\chi}{2}$$

and

$$\psi_{\Phi/2} (\tfrac{\pi}{2} - \Omega + \chi)\, \psi_{\Phi/2} (\tfrac{\pi}{2} - \Omega - \chi) = \left\{\psi_{\Phi/2} (\pi/2)\right\}^2 \cot \tfrac{\chi}{2} \sin \tfrac{\chi}{\nu}$$

(Maliuzhinets, 1959). Hence

$$g(\tfrac{\pi}{2} - \Omega + \chi)\, g(\tfrac{\pi}{2} - \Omega - \chi) = \tan^2 \tfrac{\chi}{2} \operatorname{cosec}^2 \tfrac{\chi}{\nu}$$

implying

$$P(\phi, \phi, \eta) \sim \frac{i}{4\nu} \frac{\tan^2 \frac{\chi}{2}}{\cos \frac{1}{\nu} (\frac{3\pi}{2} - \phi)} = \frac{i}{4\nu} \frac{1 - \eta}{1 + \eta} \sec \frac{1}{\nu} (\frac{3\pi}{2} - \phi) .$$

The diffracted field is therefore infinite when $\phi = \pi/2 + \Omega$ except when $\eta = 1$, and since

$$P(\phi, \phi, \eta) \sim \frac{i}{4} \frac{1 - \eta}{1 + \eta} \frac{1}{\phi - \pi/2 - \Omega} \qquad (17)$$

for $\phi \sim \pi/2 + \Omega$, the singularity is identical to that displayed by the physical optics approximation.

For grazing incidence along the upper face $\phi = \Omega$ and $\cos \frac{1}{\nu} (\pi - \phi) = 0$. $P(\phi, \phi, \eta)$ is then zero provided $\eta \neq 0$. However, we caution that this is a situation in which a traveling wave may be excited and, in addition, plane wave illumination is not possible unless $\eta = 0$. Also

$$P\left(\frac{\pi}{2}, \frac{\pi}{2}, \eta\right) = -\frac{i}{2\nu} \frac{\cos^2 \frac{\pi}{2\nu} \cot \frac{\pi}{2\nu}}{\cos \frac{\pi}{\nu}} \left(\cos \frac{\pi}{\nu} - \sin^2 \frac{\chi}{\nu}\right) g\left(\frac{\pi}{2} + \chi\right) g\left(\frac{\pi}{2} - \chi\right)$$

which can be reduced to

$$P\left(\frac{\pi}{2}, \frac{\pi}{2}, \eta\right) = -\frac{i}{4\nu} \frac{\left(1 + \cos \frac{\pi}{\nu}\right)^2}{\sin \frac{\pi}{\nu}} \left\{1 - \frac{\sin^2 \frac{\chi}{\nu}}{\cos \frac{\pi}{\nu}}\right\} \sec^2 \frac{\chi}{\nu} \qquad (18)$$

using the expression (14) for $g(\alpha)$ and the relations given by Maliuzhinets (1959). In the particular case $\eta = 1$, i.e. $\chi = 0$,

$$P\left(\frac{\pi}{2}, \frac{\pi}{2}, 1\right) = -\frac{i}{4\nu} \frac{\left(1 + \cos \frac{\pi}{\nu}\right)^2}{\sin \frac{\pi}{\nu}}$$

whereas for a perfectly conducting wedge

$$P\left(\frac{\pi}{2}, \frac{\pi}{2}, 0\right) = -\frac{i}{4\nu} \left(3 - \sec \frac{\pi}{\nu}\right) \cot \frac{\pi}{2\nu}$$

(Bowman et al., 1969; p. 263). For $\Omega = 15^\circ$ ($\nu = 11/6$),

$$P\left(\frac{\pi}{2}, \frac{\pi}{2}, 1\right) = -i\ 0.10134$$

compared with

$$P\left(\frac{\pi}{2}, \frac{\pi}{2}, 0\right) = -i\ 1.18475.$$

Our final observation is the most important of all. As evident from (16), $P(\phi, \phi, \eta)$ is zero if

$$\sin \frac{\chi}{\nu} = \left\{ \cos \frac{1}{\nu} \left(\frac{\pi}{2} - \phi\right) \cos \frac{1}{\nu} \left(\frac{3\pi}{2} - \phi\right) \right\}^{1/2} \tag{19}$$

and for any wedge and any angle ϕ it is now possible to determine χ and hence η such that the edge diffracted field is zero in the backscattering direction. Results for $\phi = 0(5)180^{o}$ and three different wedge angles are given in Table 3-1. If $\phi = \pi$ (edge-on incidence), (19) reduces to

$$\sin \frac{\chi}{\nu} = \cos \frac{\pi}{2\nu}$$

implying

$$\eta = \sin \Omega$$

(cf equation 8). In all cases η is real and positive, corresponding to a purely resistive coating, with $\eta < (>)\ 1$ if $\phi > (<)\ \pi/2 + \Omega$. For a half plane ($\nu = 2$) the requirement is simply

$$\eta = 1 + \cos \phi \ . \tag{20}$$

To proceed further, however, it is necessary to determine the function $g(\alpha)$ for the wedge in question and we shall now examine two particular cases.

3.1.1 Half Plane

If $\Omega = 0$ ($\Phi = \pi$) so that $\nu = 2$, (16) yields

$$P(\phi, \phi, \eta) = -\frac{i}{8} \frac{1 - \cos \phi}{\cos \phi} (1 + \cos \phi - \eta)\, g(\pi - \phi + \chi)\, g(\pi - \phi - \chi) \tag{21}$$

where, from (14),

$$g(\alpha) = \left\{ \frac{\psi_{\pi/2}(\pi/2)}{\psi_{\pi/2}(\alpha)} \right\}^{2} \ . \tag{22}$$

Ø (degrees)	η		
	Ω = 0	Ω = 15°	Ω = 45°
180	0	0.25882	0.70711
175	0.00381	0.26287	0.71124
170	0.01519	0.27497	0.72357
165	0.03407	0.29498	0.74382
160	0.06031	0.32267	0.77157
155	0.09369	0.35771	0.80628
150	0.13397	0.39973	0.84725
145	0.18085	0.44825	0.89375
140	0.23396	0.50276	0.94495
135	0.29289	0.56269	1
130	0.35721	0.62743	1.05802
125	0.42642	0.69634	1.11814
120	0.5	0.76874	1.17950
115	0.57738	0.84396	1.24125
110	0.65798	0.92128	1.30258
105	0.74118	1	1.36271
100	0.82635	1.07941	1.42091
95	0.91284	1.15879	1.47647
90	1	1.23746	1.52876

Ø (degrees)	η		
	Ω = 0	Ω = 15°	Ω = 45°
85	1.08716	1.31472	1.57719
80	1.17365	1.38991	1.62122
75	1.25882	1.46240	1.66037
70	1.34202	1.53155	1.69422
65	1.42262	1.59679	1.72241
60	1.5	1.65758	1.74464
55	1.57358	1.71340	1.76069
50	1.64279	1.76380	1.77038
45	1.70711	1.80834	1.77363
40	1.76604	1.84668	-------
35	1.81915	1.87848	-------
30	1.86603	1.90349	-------
25	1.90631	1.92150	-------
20	1.93969	1.93236	-------
15	1.96593	1.93600	-------
10	1.98481	-------	-------
5	1.99619	-------	-------
0	2	-------	-------

Table 1: Impedances for zero edge diffraction.

But

$$\psi_{\pi/2}(\alpha) = \exp\left\{\frac{1}{4\pi}\int_0^{\alpha}\frac{2u - \pi\sin u}{\cos u}\,du\right\}$$

(Maliuzhinets, 1959) and since

$$\psi_{\pi}(\alpha) = \left(\frac{\sqrt{2}\cos\frac{\alpha}{2} + 1}{\sqrt{2} + 1}\right)^{1/2} \exp\left\{-\frac{1}{8\pi}\int_0^{\alpha}\frac{2u - \pi\sin u}{\cos u}\,du\right\}$$

(Bowman, 1967), it follows that

$$\psi_{\pi/2}(\alpha) = \frac{\sqrt{2}\cos\frac{\alpha}{2} + 1}{\sqrt{2} + 1}\left\{\psi_{\pi}(\alpha)\right\}^{-2}$$

giving

$$g(\alpha) = \left(\frac{2}{\sqrt{2}\cos\frac{\alpha}{2} + 1}\right)^{2}\left\{\frac{\psi_{\pi}(\alpha)}{\psi_{\pi}(\pi/2)}\right\}^{4} \tag{23}$$

The function $\psi_{\pi}(\alpha)$ has been tabulated by Bucci (1974) for a range of complex α.

Alternatively, in terms of the function

$$f(\alpha) = (1 + \sin\alpha)^{-1/4}\exp\left\{-\frac{1}{2\pi}\int_0^{\pi/2-\alpha}\frac{u\,du}{\sin u}\right\} \tag{24}$$

introduced by Senior (1975),

$$g(\alpha) = \frac{(1 + \sin\alpha)^{1/2}}{\cos\frac{1}{2}\left(\frac{\pi}{2} - \alpha\right)}\left\{f(\alpha)\right\}^{2} \tag{25}$$

and when this is substituted into (21), we have

$$P(\phi, \phi, \eta) = -\frac{i}{4}\,\frac{1 - \cos\phi}{\cos\phi}(1 + \cos\phi - \eta)\left\{f(\pi - \phi + \chi)\,f(\pi - \phi - \chi)\right\}^{2}. \tag{26}$$

In the particular case of edge-on incidence ($\phi = \pi$),

$$P(\pi, \pi, \eta) = -\frac{i\eta}{2}\left\{f(\chi)\right\}^4 \tag{27}$$

where we have used the fact that $f(\alpha)$ is an even function, as evident from its alternative representation

$$f(\alpha) = (\cos\alpha)^{-1/4} \exp\left\{\frac{1}{2\pi}\int_{\alpha}^{i\infty}\frac{v\,dv}{\cos v}\right\} \quad . \tag{28}$$

Equation (27) differs from the analogous expression in Senior (1975) only in having η replaced by $1/\eta$, as necessary by the change from E to H polarization.

A program has been written to compute $f(\chi)$ for all real η, but (24) and (28) can be used to provide asymptotic approximations to $f(\chi)$ whose accuracy is adequate for many practical purposes. Thus, if $|\eta| << 1$ then $\chi \simeq \pi/2 - \eta$ and (24) yields

$$f(\chi) \simeq 2^{-1/4} \exp\left(-\frac{\eta}{2\pi}\right) \tag{29}$$

so that

$$P(\pi, \pi, \eta) \simeq -\frac{i\eta}{4} \exp\left(-\frac{2\eta}{\pi}\right) \tag{30}$$

implying

$$P(\pi, \pi, 0) = 0 \quad . \tag{31}$$

On the other hand, for $|\eta| >> 1$

$$f(\chi) \simeq \eta^{-1/4} \exp\left\{-\frac{1}{2\pi\eta}\left[1 + \ln(2\eta)\right]\right\} \tag{32}$$

giving

$$P(\pi, \pi, \eta) \simeq -\frac{i}{2} \exp\left\{-\frac{2}{\pi\eta}\left[1 + \ln(2\eta)\right]\right\} \tag{33}$$

and implying

$$P(\pi, \pi, \infty) = -\frac{i}{2} \tag{34}$$

corresponding to a perfectly conducting half plane with E polarization. It now follows that if* $\eta = |\eta| e^{i\theta}$, $|\theta| \leq \pi/2$,

$$|P(\pi, \pi, \eta)| \simeq \frac{1}{4} |\eta| \exp\left\{-\frac{2}{\pi} |\eta| \cos\theta\right\} \qquad (|\eta| << 1) \tag{35}$$

$$|P(\pi, \pi, \eta)| \simeq \frac{1}{2} \exp\left\{-\frac{2}{\pi |\eta|}\left[(1 + \ln(2|\eta|)\cos\theta + \theta \sin\theta\right]\right\}$$

$$(|\eta| >> 1) \tag{36}$$

and these are independent of the sign of θ. Between them the two expressions provide rather accurate coverage of the entire range $0 \leq |\eta| \leq \infty$, with an error of no more than about 5 percent with the possible exception of the interval $0.8 < |\eta| < 2$.

---

* With η defined in this manner and $\eta = \cos\chi$,

$$\chi = \chi_r - i\chi_i$$

where, for $|\eta| \leq 1$,

$$\sin\chi_r = 2^{-1/2}\left\{\sqrt{(1 - |\eta|^2)^2 + 4|\eta|^2 \sin^2\theta} + 1 - |\eta|^2\right\}^{1/2}$$

$$\sinh\chi_i = \pm 2^{-1/2}\left\{\sqrt{(1 - |\eta|^2)^2 + 4|\eta|^2 \sin^2\theta} - 1 + |\eta|^2\right\}^{1/2}$$

and for $|\eta| > 1$

$$\sin\chi_r = \pm 2^{-1/2}\left\{\sqrt{(1 - |\eta|^2)^2 + 4|\eta|^2 \sin^2\theta} + 1 - |\eta|^2\right\}^{1/2}$$

$$\sinh\chi_i = 2^{-1/2}\left\{\sqrt{(1 - |\eta|^2)^2 + 4|\eta|^2 \sin^2\theta} - 1 + |\eta|^2\right\}^{1/2}$$

with the upper (lower) sign for $\theta >$ (< 0).

We have used (35) and (36) supplemented by the tabulation of Bucci (1974) to compute $|P(\pi, \pi, \eta)|$ as a function of $|\eta|$ for different values of θ. The results for $\theta = 0$, $\pi/4$ and $\pi/2$ are shown in Figure 3-2 and it is seen that arg η has most effect for $|\eta|$ somewhat greater than unity. If $\theta = \pi/2$ corresponding to a reactive surface, the exponent in (24) is purely imaginary, and as noted by Kay (1957) the modulus of the scattered field then has a simple algebraic expression. From (24)

$$|f(\chi)| = (1 + \sqrt{1 + |\eta|^2})^{-1/4}$$

giving

$$|P(\pi, \pi, \eta)| = \frac{1}{2} |\eta| (1 + \sqrt{1 + |\eta|^2})^{-1} \qquad (37)$$

for arg $\eta = \pi/2$.

Since $P(\pi, \pi, 0) = 0$, the metallic surface is actually the optimum for minimum backscattering at edge-on incidence, and $|P(\emptyset, \emptyset, 0)|$ is plotted as a function of $\emptyset$ in Figure 3-3. Alternatively, we can null out the backscattering in any direction $\emptyset \neq \pi/2$ by choosing η in accordance with (20), and Figure 3-3 also shows the curve for $\eta = 0.13397$ for which the null is at $\emptyset = 150°$. Both fields are, of course, infinite in the specular direction $\emptyset = 90°$, but the angular range where the field is large decreases with increasing $\eta \leq 1$.

3.1.2 Wedge of Half Angle 15°

For a wedge of half angle $\Omega = \pi - \Phi$ with $\Phi = \frac{n\pi}{4m}$ where m and n are integers with n odd, Maliuzhinets' function $\psi_\Phi(\alpha)$ can be expressed as a product of trigonometric factors. A particular case is $\Omega = 15°$, i.e., $\Phi = 11\pi/12$ implying $\nu = 11/6$, for which $m = 3$ and $n = 11$, and we then have

$$\psi_\Phi(\alpha) = \frac{h(\alpha)}{h(o)}$$

where $h(\alpha)$ is the even function

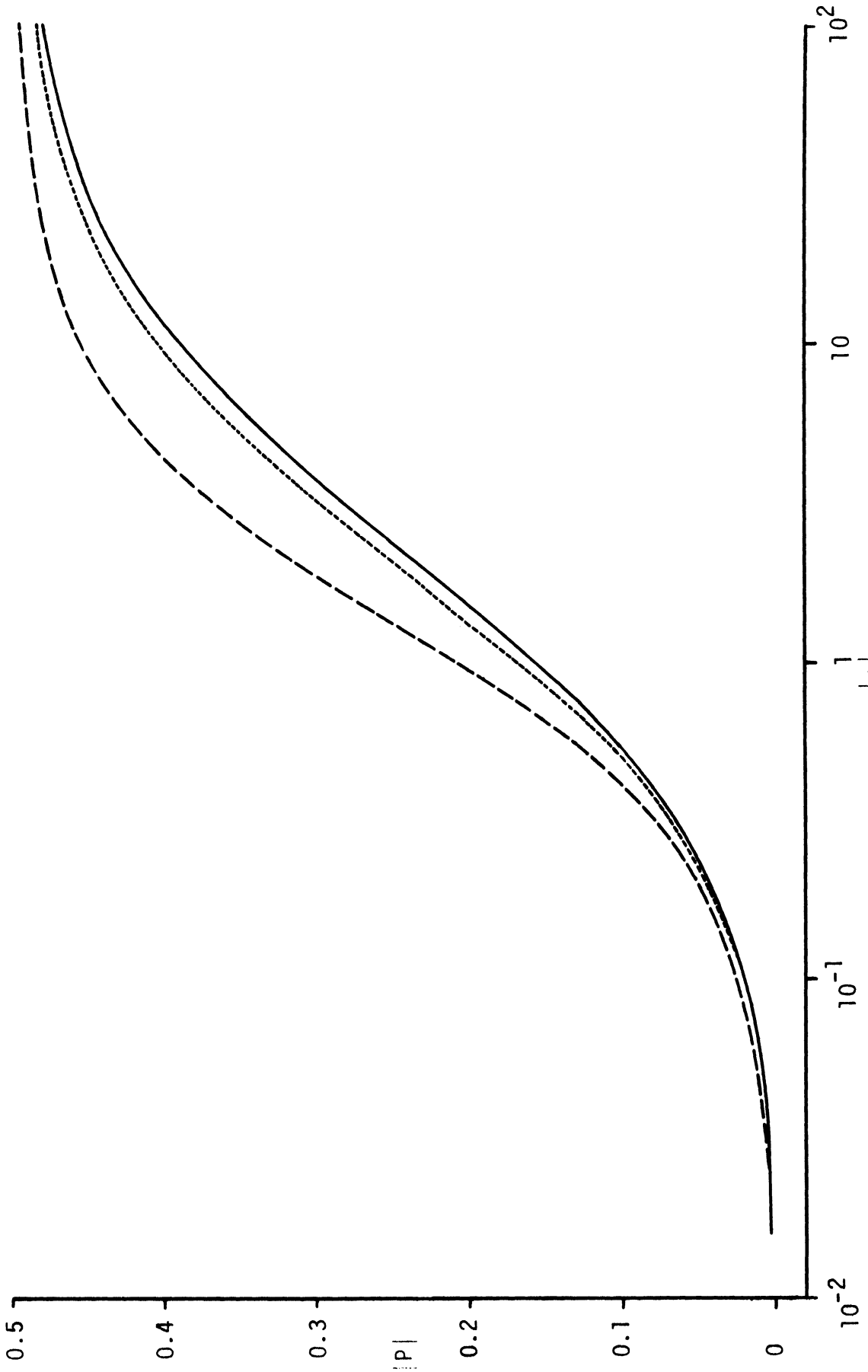

Figure 3-2: Edge-on backscattering for a half plane with impedance $\eta = |\eta| e^{\pm i\theta}$ with $\theta = 0$ (——), $\pi/4$ (- - - -) and $\pi/2$ (— — —).

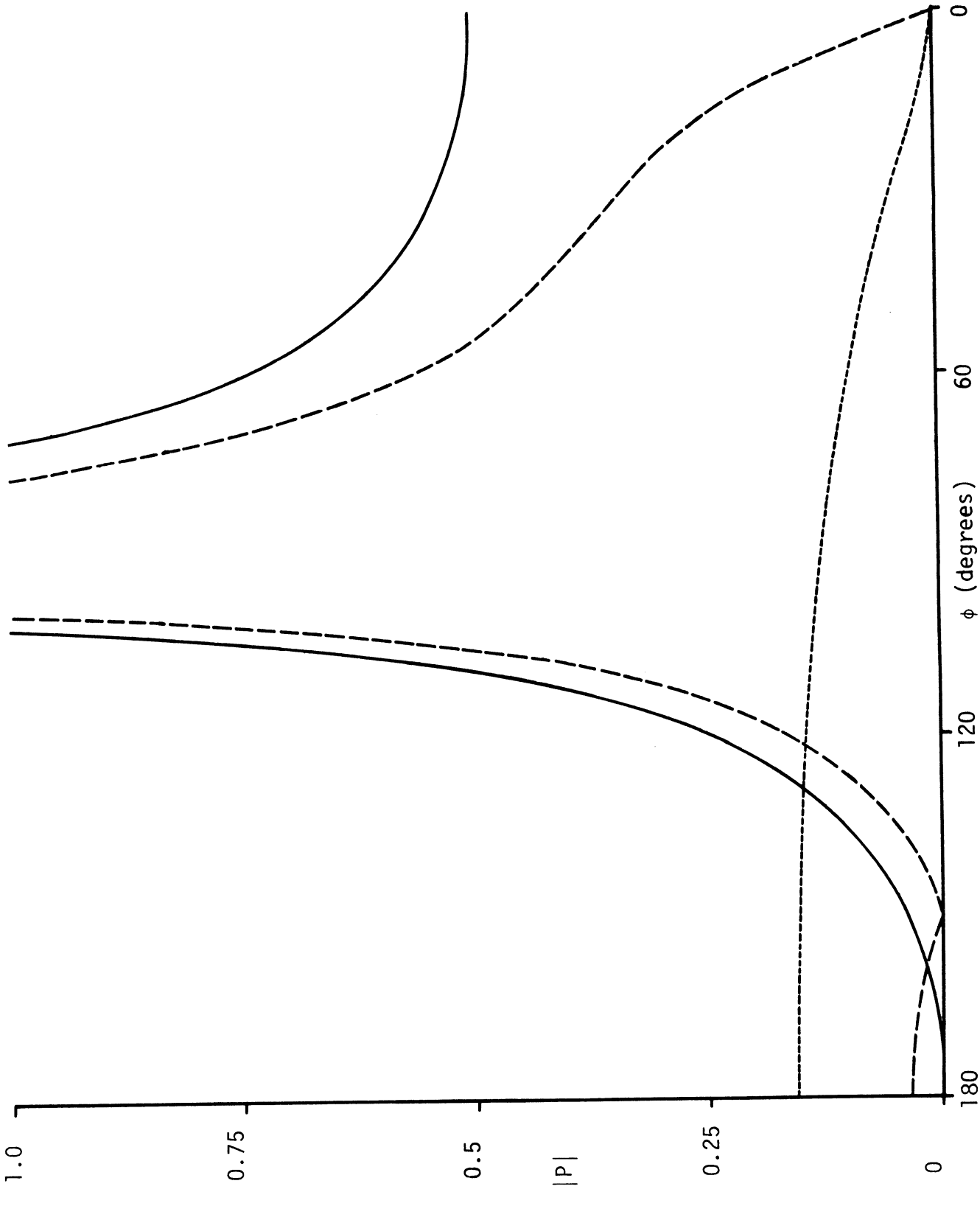

Figure 3-3: Backscattering from a half plane with impedance $\eta = 0$ (———), 0.13397 (— — — —) and 1 (-----).

$$h(\alpha) = \sec\frac{\alpha}{22}\;\frac{\prod_{p=1}^{3}\left\{\cos\frac{\alpha}{11}+\cos\frac{2p-1}{11}\pi\right\}\prod_{p=1}^{6}\left\{\cos\frac{\alpha}{11}+\cos\frac{6p-10}{33}\pi\right\}}{\prod_{p=1}^{2}\left\{\cos\frac{\alpha}{11}+\cos\frac{2p}{11}\pi\right\}\prod_{p=1}^{5}\left\{\cos\frac{\alpha}{11}+\cos\frac{6p-7}{33}\pi\right\}}\,.$$

It follows that

$$\psi_{\Phi/2}(\alpha) = \frac{\psi_{\Phi}(\alpha+\Phi)}{\psi_{\Phi}(\Phi)}\cdot\frac{\psi_{\Phi}(\alpha-\Phi)}{\psi_{\Phi}(\Phi)} = \frac{h(\alpha+\Phi)}{h(\Phi)}\cdot\frac{h(\alpha-\Phi)}{h(\Phi)}$$

giving

$$g(\alpha) = \left\{\frac{h(\frac{\pi}{2}+\frac{11}{12}\pi)}{h(\alpha+\frac{11}{12}\pi)}\right\}^2\left\{\frac{h(\frac{\pi}{2}-\frac{11}{12}\pi)}{h(\alpha-\frac{11}{12}\pi)}\right\}^2$$

and hence, from (16),

$$P(\emptyset,\emptyset,\eta) = -\,i\,0.23632\;\frac{\cos^2\frac{6}{11}(\pi-\emptyset)}{\cos\frac{6}{11}(\frac{\pi}{2}-\emptyset)\cos\frac{6}{11}(\frac{3\pi}{2}-\emptyset)}$$

$$\cdot\left\{\cos\frac{6}{11}(\tfrac{\pi}{2}-\emptyset)\cos\frac{6}{11}(\tfrac{3\pi}{2}-\emptyset)-\sin^2\frac{6\chi}{11}\right\}$$

$$\cdot\left\{\frac{h(\frac{17}{12}\pi)}{h(\frac{23}{12}\pi-\emptyset+\chi)}\;\frac{h(\frac{5}{12}\pi)}{h(\frac{\pi}{12}-\emptyset+\chi)}\;\frac{h(\frac{17}{12}\pi)}{h(\frac{23}{12}\pi-\emptyset-\chi)}\;\frac{h(\frac{5}{12}\pi)}{h(\frac{\pi}{12}-\emptyset-\chi)}\right\}^2. \qquad (38)$$

We have computed this expression as a function of $\emptyset$ for a variety of η and the results for $\eta = 0(0.25)2.0$ are plotted in Figures 3-4 and 3-5 (note the expanded scale of the latter figure). In contrast to the situation with a half plane, the edge-on backscattering is no longer zero for perfect conductivity, but can be made zero by choosing η appropriately. From Table 3-1 the required impedance is $\eta = 0.25882$ and the resulting edge diffracted field is shown in Figure 3-6. It is essential that the impedance be real to obtain the effect. If $\arg\eta \neq 0$ (or π), there is no longer a zero in the backscattered

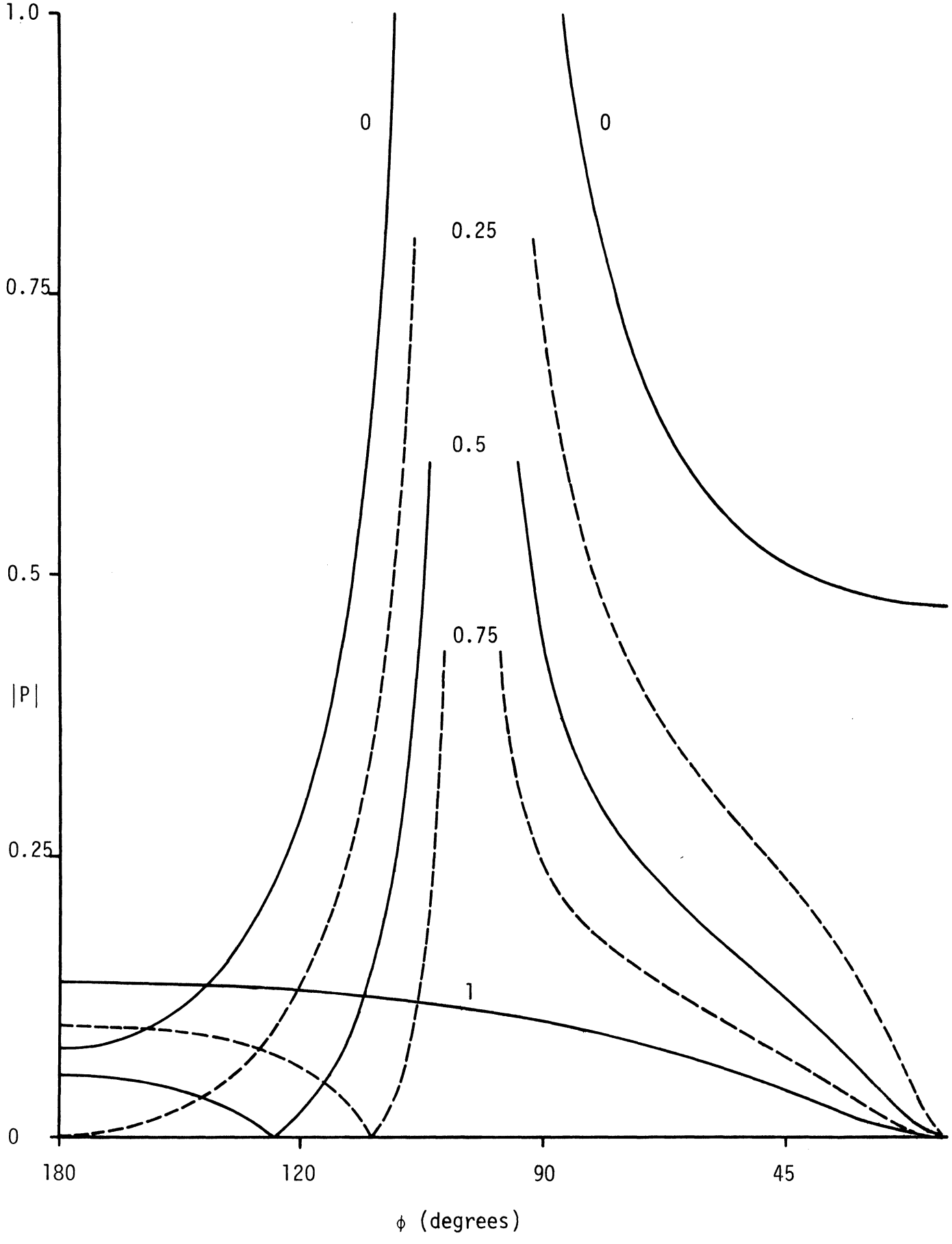

Figure 3-4: Backscattering from a 15° half angle wedge having the real impedance shown.

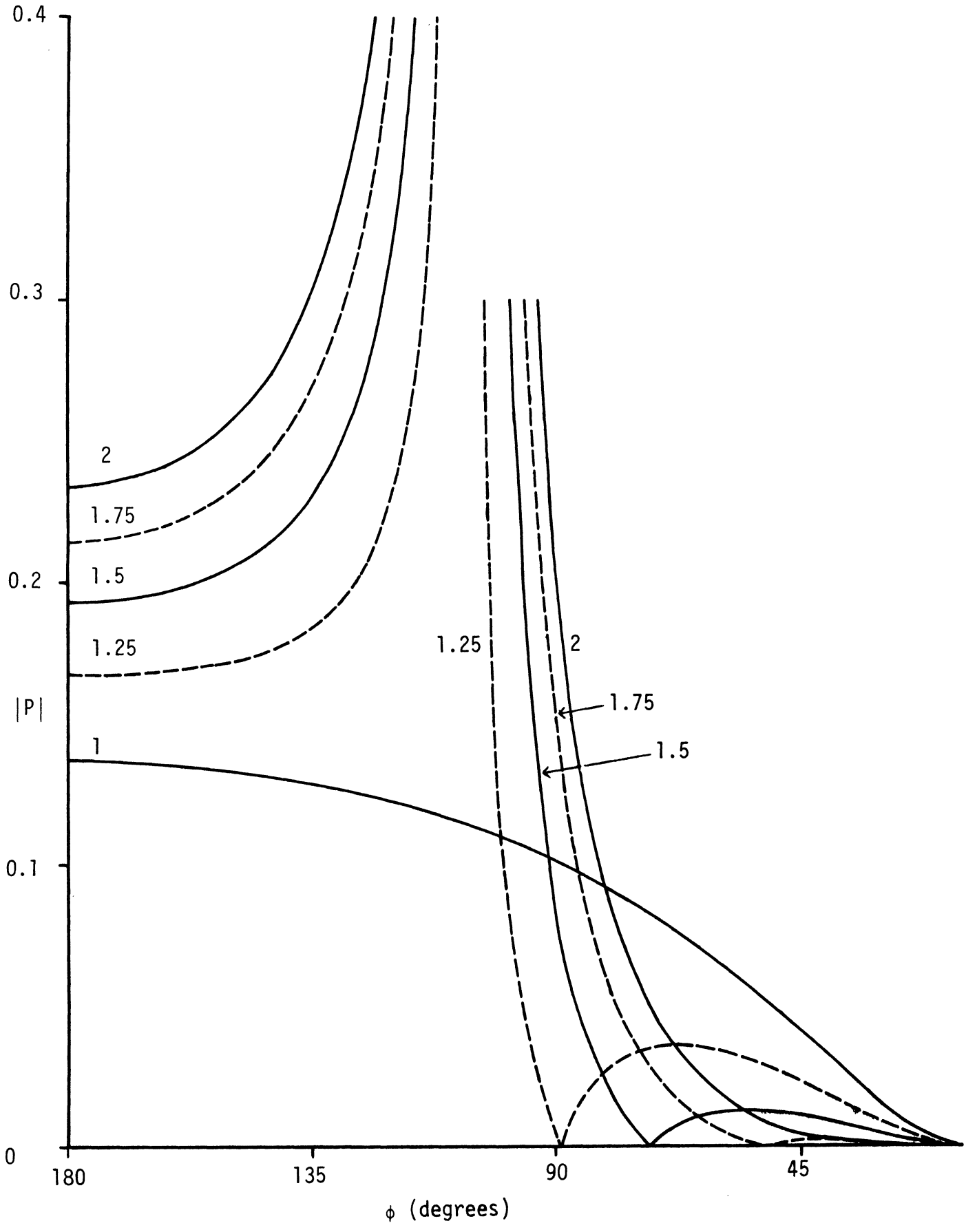

Figure 3-5: Backscattering from a 15° half angle wedge having the real impedance shown.

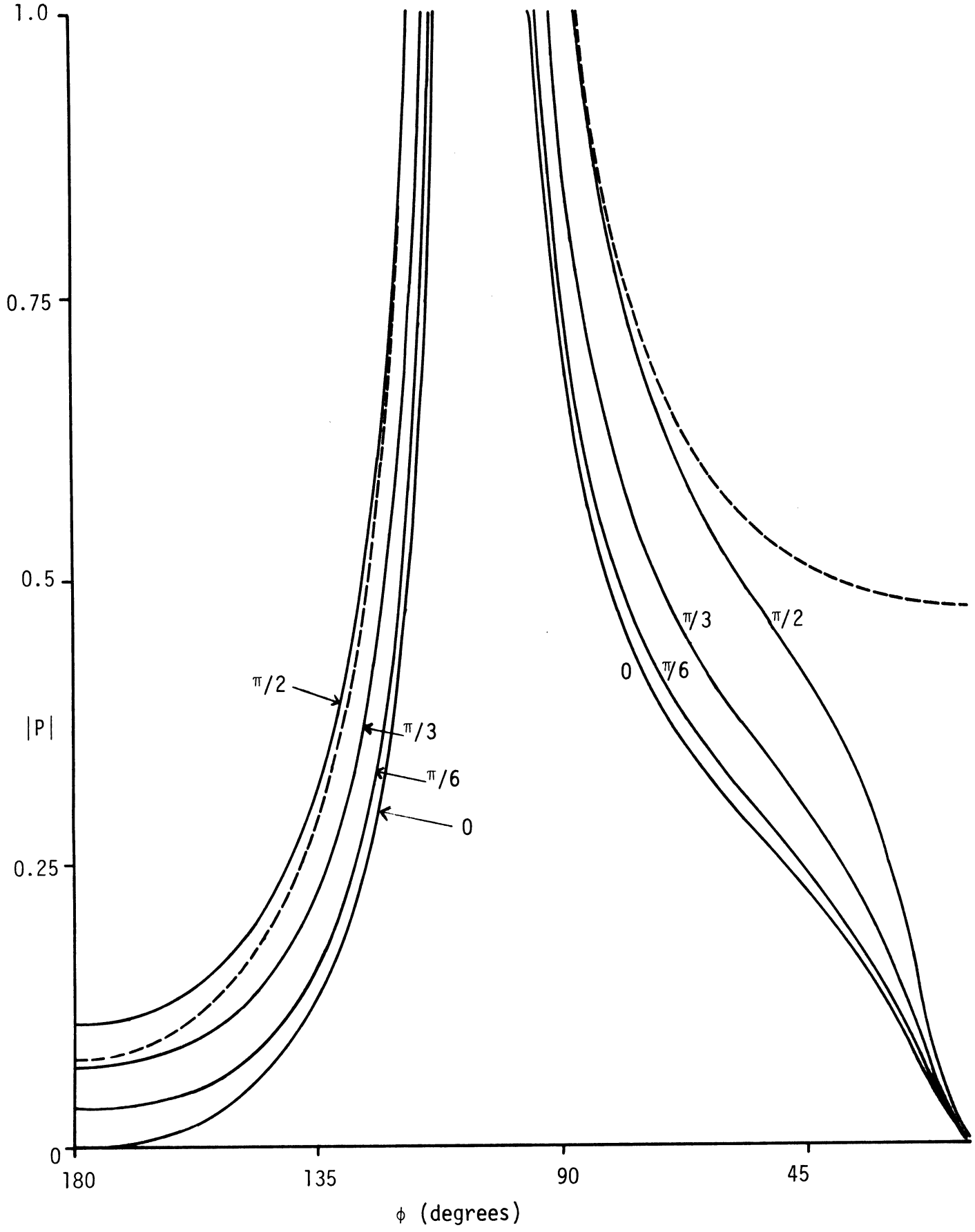

Figure 3-6: Backscattering from a 15° half angle wedge with impedance $\eta = 0.13397e^{\pm i\theta}$ for $\theta = 0, \pi/6, \pi/3$ and $\pi/2$. The broken line is for a perfectly conducting wedge ($\eta = 0$).

field and this is illustrated by the curves for $\eta = 0.25882\, e^{i\theta}$ with $\theta = \pi/6$, $\pi/3$, and $\pi/2$ included in Figure 3-6. For the purely reactive impedance ($\theta = \pi/2$) the scattering is comparable to that from the perfectly conducting wedge.

If the desire is to reduce the backscattering over some range of aspects about edge-on, it is more effective to null the field at an angle less than 180°, even at the expense of an increase in the edge-on return. The impedance necessary to produce a null at any given ϕ in the range $150° \leq \phi \leq 180°$ is shown in Figure 3-7, and the edge-on backscattering as a function of η, $0.1 \leq \eta \leq 0.4$, is plotted in Figure 3-8. The average cross section reduction which can be achieved can be judged from Figure 3-9 showing the backscattered field for the four impedances creating zeros at 150, 155, 160 and 165°. Over the range from $\phi = 150°$ to 180° the average power reduction is greatest for $\eta = 0.32267$ (null at $\phi = 160°$) and is -17.7 dB, although the edge-on reduction is then only -13.8 dB. Once again, much of the performance is lost if η is not real. If, for example, $\eta = 0.32267\, e^{i\theta}$ with $\theta \neq 0$, there is no longer a null at $\phi = 160°$. The entire curve is now raised above that for $\theta = 0$, but as seen from Figure 3-10 the curves for small θ still have local minima at aspects determined to a first approximation by Re. η.

3.2 Impedance Discontinuities

To minimize the backscattering cross section of a body over a range of aspects it may be necessary for the impedance to be a function of position on the surface, and this could result in discontinuities in the impedance or its surface derivatives. It is therefore of interest to examine the scattering from such a line singularity.

We can treat the case of a jump discontinuity in η by considering a wedge of half angle $\Omega = \pi/2$ with different face impedances (see Figure 3-11). From (9) with $\nu = 1$ we then have

$$P(\phi, \phi_0) = \frac{i}{2} \frac{\cos \phi_0}{\sin \phi + \sin \phi_0} \left\{ \frac{\Psi(-\phi)}{\Psi(\pi - \phi_0)} - \frac{\Psi(2\pi - \phi)}{\Psi(\pi - \phi_0)} \right\} \tag{39}$$

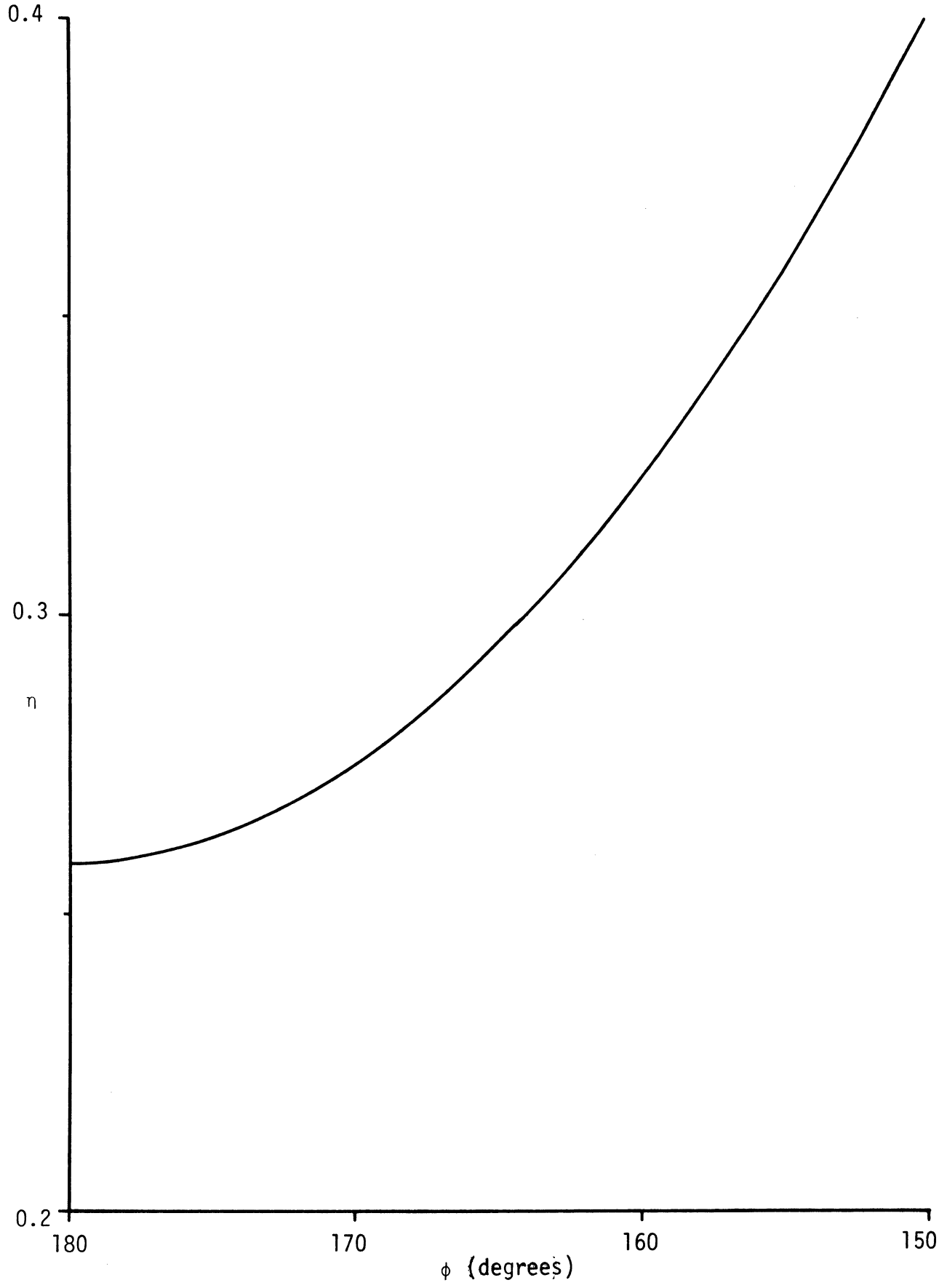

Figure 3-7: The impedance for zero backscattered field in the direction ϕ.

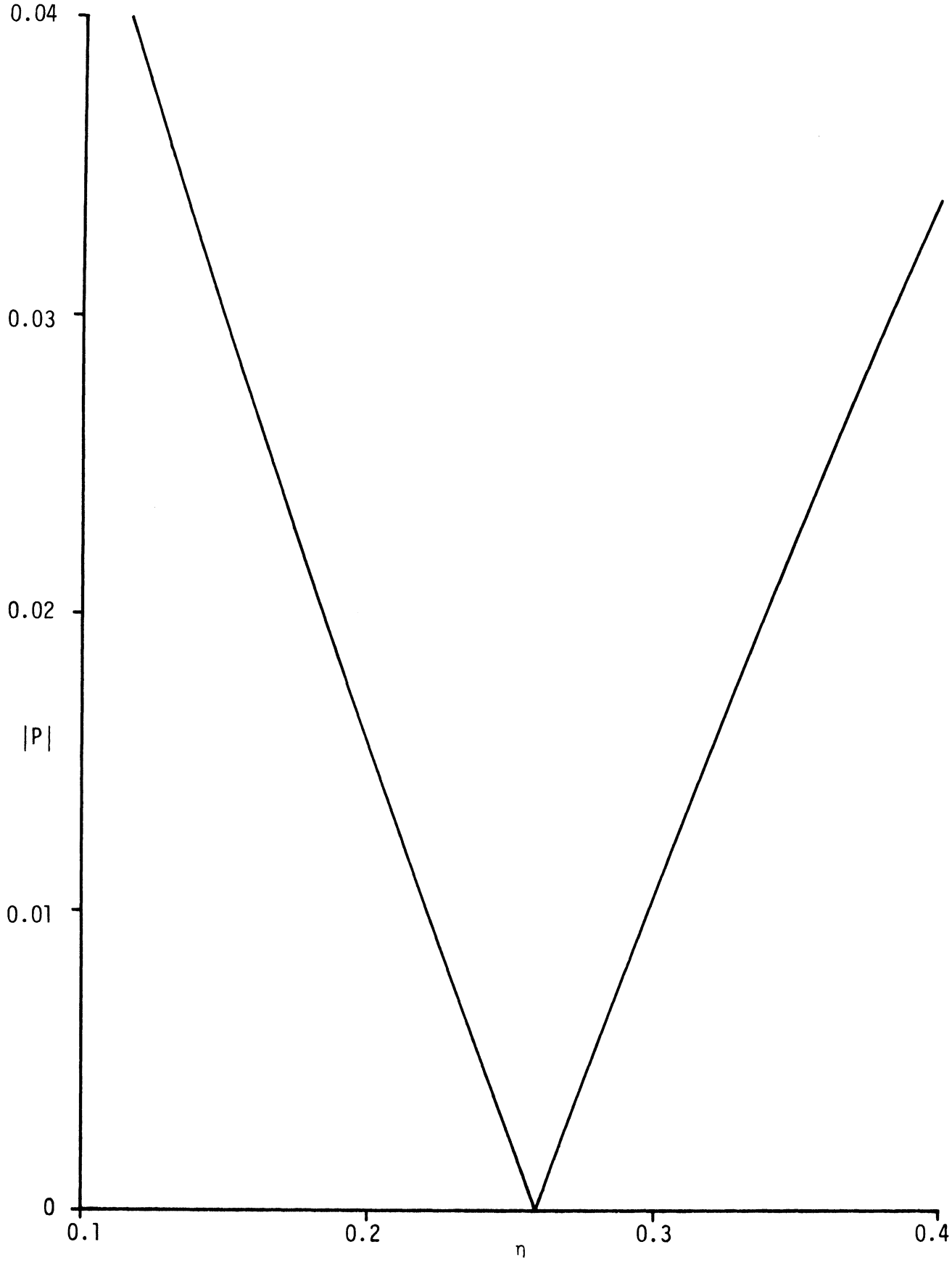

Figure 3-8: Edge-on backscattering as a function of η.

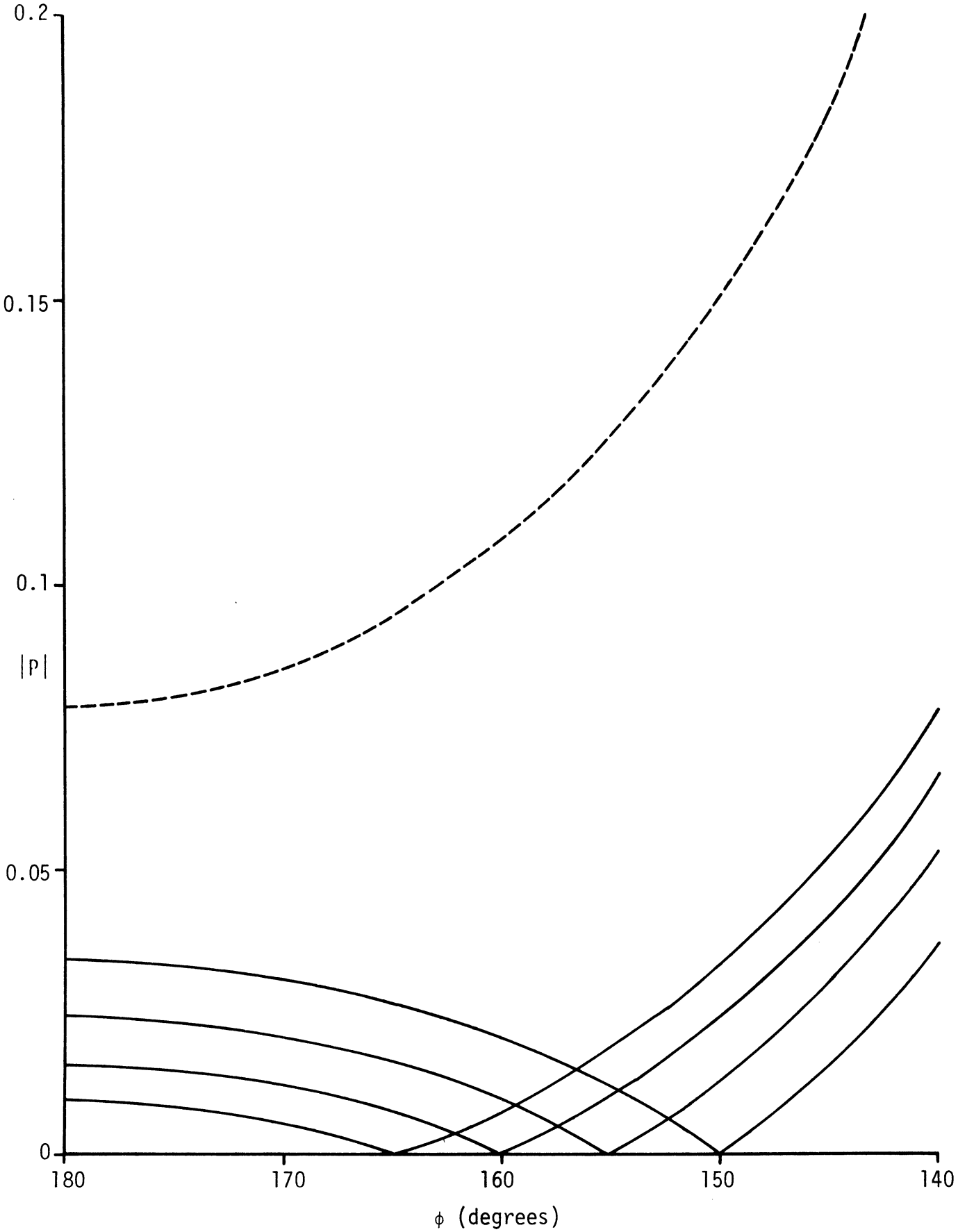

Figure 3-9: Backscattering from 15° half angle wedges with impedances η = 0.29498, 0.32267, 0.35771 and 0.39973, creating zeros at ϕ = 165, 160, 155 and 150° respectively. The broken line is for a perfectly conducting wedge (η = 0).

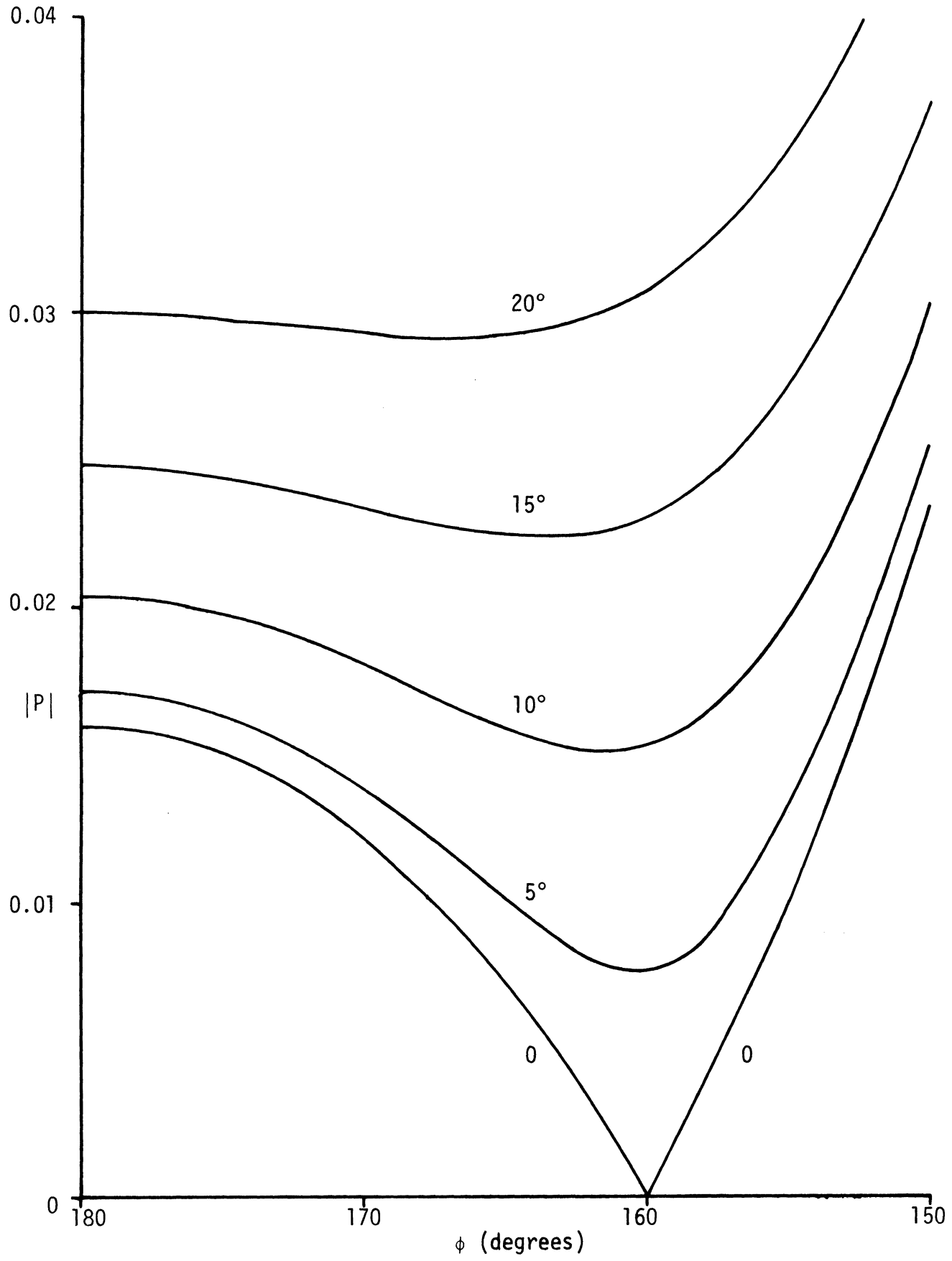

Figure 3-10: Backscattering from a 15° half angle wedge with impedance $\eta = 0.32267\, e^{i0}$ for the θ shown.

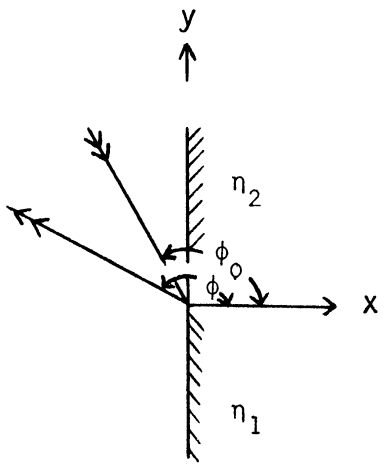

Figure 3-11: Geometry for impedance discontinuity.

where

$$\Psi(\alpha) = \psi_{\pi/2}\left(\alpha + \frac{\pi}{2} + \chi_2\right)\psi_{\pi/2}\left(\alpha + \frac{\pi}{2} - \chi_2\right)\psi_{\pi/2}\left(\alpha - \frac{\pi}{2} + \chi_1\right)\psi_{\pi/2}\left(\alpha - \frac{\pi}{2} - \chi_1\right) \tag{40}$$

(Maliuzhinets, 1959) with $\pi/2 \leq \emptyset, \emptyset_o \leq 3\pi/2$. In (40)

$$\eta_{1,2} = \cos \chi_{1,2} \quad . \tag{41}$$

Since

$$\psi_{\pi/2}\left(\alpha + \frac{\pi}{2}\right)\psi_{\pi/2}\left(\alpha - \frac{\pi}{2}\right) = \left\{\psi_{\pi/2}\left(\frac{\pi}{2}\right)\right\}^2 \cos\frac{1}{2}\left(\alpha + \frac{\pi}{2}\right) \quad ,$$

$$\Psi(\pi - \emptyset_o) = \psi_{\pi/2}\left(\frac{3\pi}{2} - \emptyset_o + \chi_2\right)\psi_{\pi/2}\left(\frac{3\pi}{2} - \emptyset_o - \chi_2\right)\psi_{\pi/2}\left(\frac{\pi}{2} - \emptyset_o + \chi_1\right)\psi_{\pi/2}\left(\frac{\pi}{2} - \emptyset_o - \chi_1\right)$$

$$= -\frac{1}{2}\left(\cos \emptyset_o - \eta_1\right)\left\{\psi_{\pi/2}\left(\frac{\pi}{2}\right)\right\}^4 \frac{\psi_{\pi/2}\left(\frac{3\pi}{2} - \emptyset_o + \chi_2\right)\psi_{\pi/2}\left(\frac{3\pi}{2} - \emptyset_o - \chi_2\right)}{\psi_{\pi/2}\left(\frac{3\pi}{2} - \emptyset_o + \chi_1\right)\psi_{\pi/2}\left(\frac{3\pi}{2} - \emptyset_o - \chi_1\right)} \quad .$$

Similarly

$$\Psi(2\pi - \phi) = \psi_{\pi/2}(\tfrac{5\pi}{2} - \phi + \chi_2)\psi_{\pi/2}(\tfrac{5\pi}{2} - \phi - \chi_2)\psi_{\pi/2}(\tfrac{3\pi}{2} - \phi + \chi_1)\psi_{\pi/2}(\tfrac{3\pi}{2} - \phi - \chi_1)$$

$$= \frac{1}{2}(\cos\phi - \eta_2)\left\{\psi_{\pi/2}(\tfrac{\pi}{2})\right\}^4 \frac{\psi_{\pi/2}(\tfrac{3\pi}{2} - \phi + \chi_1)\psi_{\pi/2}(\tfrac{3\pi}{2} - \phi - \chi_1)}{\psi_{\pi/2}(\tfrac{3\pi}{2} - \phi + \chi_2)\psi_{\pi/2}(\tfrac{3\pi}{2} - \phi - \chi_2)}$$

and

$$\Psi(-\phi) = \psi_{\pi/2}(\tfrac{\pi}{2} - \phi + \chi_2)\psi_{\pi/2}(\tfrac{\pi}{2} - \phi - \chi_2)\psi_{\pi/2}(-\tfrac{\pi}{2} - \phi + \chi_1)\psi_{\pi/2}(-\tfrac{\pi}{2} - \phi - \chi_1)$$

$$= \frac{(\cos\phi + \eta_1)(\cos\phi - \eta_2)}{(\cos\phi - \eta_1)(\cos\phi + \eta_2)}\ \Psi(2\pi - \phi)$$

on using the fact that

$$\psi_{\pi/2}(\alpha - \pi) = \tan\tfrac{1}{2}(\alpha + \tfrac{\pi}{2})\psi_{\pi/2}(\alpha + \pi)\ .$$

Hence

$$P(\phi, \phi_o) = i(\eta_2 - \eta_1)\frac{\cos\phi\cos\phi_o}{\sin\phi + \sin\phi_o}\ \frac{1}{(\cos\phi - \eta_1)(\cos\phi_o - \eta_1)}$$

$$\cdot \frac{\psi_{\pi/2}(\tfrac{3\pi}{2} - \phi + \chi_1)\psi_{\pi/2}(\tfrac{3\pi}{2} - \phi - \chi_1)\psi_{\pi/2}(\tfrac{3\pi}{2} - \phi_o + \chi_1)\psi_{\pi/2}(\tfrac{3\pi}{2} - \phi_o - \chi_1)}{\psi_{\pi/2}(\tfrac{3\pi}{2} - \phi + \chi_2)\psi_{\pi/2}(\tfrac{3\pi}{2} - \phi - \chi_2)\psi_{\pi/2}(\tfrac{3\pi}{2} - \phi_o + \chi_2)\psi_{\pi/2}(\tfrac{3\pi}{2} - \phi_o - \chi_2)} \tag{42}$$

and in the particular case of backscattering ($\phi_o = \phi$)

$$P(\phi, \phi) = \frac{i}{2}(\eta_2 - \eta_1)\sec\theta\left(\frac{\sin\theta}{\sin\theta + \eta_1}\right)^2 \frac{g(\pi - \theta + \chi_2)g(\pi - \theta - \chi_2)}{g(\pi - \theta + \chi_1)g(\pi - \theta - \chi_1)} \tag{43}$$

where $g(\alpha)$ is given by (14) and $\theta = \emptyset - \pi/2$ is the angle measured from the surface with impedance η_2.

For a small discontinuity in the impedance such that $\eta_2 = \eta$, $\eta_1 = \eta + \Delta$ we have, to the first order in Δ,

$$P(\emptyset, \emptyset) = -\frac{i}{2}\Delta \sec\theta \left(\frac{\sin\theta}{\sin\theta + \eta}\right)^2 \tag{44}$$

since the product of the g functions is unity to this order. The expression is identical to that obtained by Kaminetzky and Keller (1972) by applying boundary layer techniques to a surface of large but finite radius, and is qualitatively similar to that for the edge-diffracted field of a metallic wedge whose angle is close to π. The scattering increases with increasing $\theta < \pi/2$ and for grazing incidence

$$P = -\frac{i\Delta}{2} \tag{45}$$

if $\eta = 0$. This shows the importance of having a surface treatment commence with a discontinuity in the impedance which is as small as possible and, hopefully, zero if we are to avoid introducing another source of scattering. On the other hand, if $\eta \neq 0$, for $\theta = 0$

$$P = 0 \tag{46}$$

but it is then no longer possible to have a plane wave at grazing incidence, and for any surface wave that may exist the reflection coefficient is not necessarily zero.

If the impedance is a continuous function (perfect fairing of a coating), there may still be discontinuities in its first derivative and these could now produce diffraction. The asymptotic analysis of Kaminetzky and Keller (1972) also provides an expression for the scattering from a small discontinuity of this type, and in the backscattering direction

$$P(\emptyset, \emptyset) = -\frac{\Delta'}{4k}\sec^2\theta \left(\frac{\sin\theta}{\sin\theta + \eta}\right)^2 \tag{47}$$

where $\Delta' = [\frac{\partial \eta}{\partial y}]_{y=0-}^{y=0+}$. The result is somewhat similar to that for a line discontinuity in curvature of a perfectly conducting body (Senior, 1972). For grazing incidence ($\theta = 0$) with $\eta = 0$

$$P(0, 0) = -\frac{\Delta'}{4k} \tag{48}$$

and because of the k^{-1} factor the practical significance of this type of scattering is much less than for a discontinuity in η. If $\eta \neq 0$

$$P(0, 0) = 0 \tag{49}$$

but we again caution that no account has been taken of any surface waves that may exist. Even a discontinuity in the first (or higher) derivative of the impedance can reflect a surface wave, and in previous numerical studies of cross section reduction techniques it was found necessary to eliminate discontinuities in the first derivative as well as in the impedance itself.

4. CROSS SECTION REDUCTION OF AN OGIVAL CYLINDER

For surface treatments which can be simulated by a surface impedance, we can use the foregoing analyses to aid in the specification of an impedance for maximum cross section reduction. To illustrate the concepts and procedures involved, we consider the case of an ogival cylinder of half angle 15 degrees (see Figure 4-1) having the following dimensions:

half angle (Ω)	=	15 degrees	
surface radius (R)	=	34.3536 cm	
surface length, top	=	17.9876 cm	(= $2R\Omega$)
overall length (ℓ)	=	17.7828 cm	(= $2R\sin\Omega$)

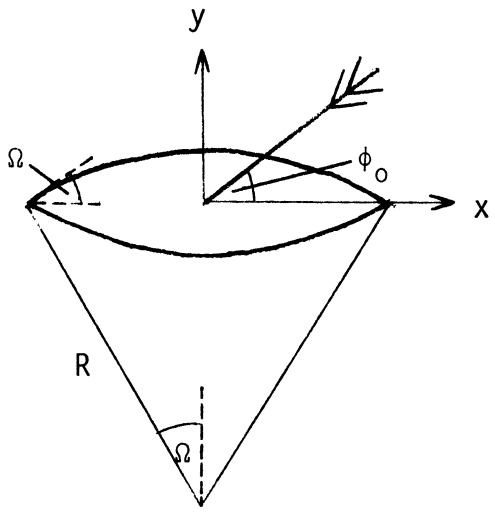

Figure 4-1: Ogival cylinder geometry.

A plane electromagnetic wave is incident at an angle ϕ_0 to the negative x-axis in a plane perpendicular to the generators of the cylinder with its magnetic vector parallel to the generators (H polarization), so that

$$H_z^i = e^{-ik(x\cos\phi_0 + y\sin\phi_0)} \tag{50}$$

The far zone scattered field

$$H_z^s(\phi, \phi_0) \sim \sqrt{\frac{2}{\pi k\rho}}\, e^{i(k\rho - \pi/4)}\, P(\phi, \phi_0)$$

is observed in a direction ϕ where $\phi_0 = \phi$ for backscattering, and the task is to minimize the backscattering cross section

$$\sigma(\phi) = \frac{2\lambda}{\pi} |P(\phi, \phi)|^2 \tag{51}$$

with particular reference to the range of angles $\pm$ 30 degrees about edge-on: $\phi = \pi$ (= 180 degrees). Obviously the impedance should be chosen the same on the top and bottom surfaces of the cylinder, and we can therefore confine attention to $0 \leq \phi \leq$ 180 degrees.

Our aim is to reduce the backscattering over a wide range of frequencies from (about) 5 GHz on up on the assumption that the surface impedance is frequency independent and can be chosen at will. At 5 GHz λ = 5.99585 cm and since the body is then 3λ long it is reasonable to expect that high frequency asymptotic techniques can be used to analyze the scattering. Two of the main contributors to the scattering are the front and rear edges, with the latter

contributing either directly or via a surface wave on the body. As the frequency and/or the aspect changes, constructive and destructive interference will produce a backscattering cross section which varies, and to achieve a broadband reduction it is necessary that the contributors be individually reduced.

The primary tools in our investigation are a computer program for the numerical solution of the integral equation (4) by the moment method and an explicit analytic/integral expression for the backscattered field developed using asymptotic techniques. Program RAMD solves (4) for any specified surface impedance $\eta(s)$ and, hence, determines the far zone scattered field. All our computations used 96 samplint points distributed uniformly over the two sides of the cylinder, implying a cell size $\lambda/16$.

For the three constant impedances η = 0, 0.5 and 1 the backscattering cross sections $\sigma(\phi)$ at 5 GHz computed in this manner are shown in Figure 4-2. The case η = 0 represents the bare or perfectly conducting cylinder. The cross section decreases via a series of oscillations from broadside ($\phi = 90^{o}$) to edge-on ($\phi = 180^{o}$), and we observe the rather broad lobe centered on $\phi = 158^{o}$ which can be attributed to a traveling wave. Increasing the impedance to 0.5 decreases the broadside return by about 10 dB, but decreases even more the scattering for $\phi \gtrsim 140^{o}$ and effectively suppresses any traveling wave return. By increasing η to 1 we achieve a further 22 dB reduction in the broadside cross section. The pattern now consists of a series of lobes of almost equal amplitude, but for $\phi \simeq 180^{o}$ the scattering actually exceeds the bare body value.

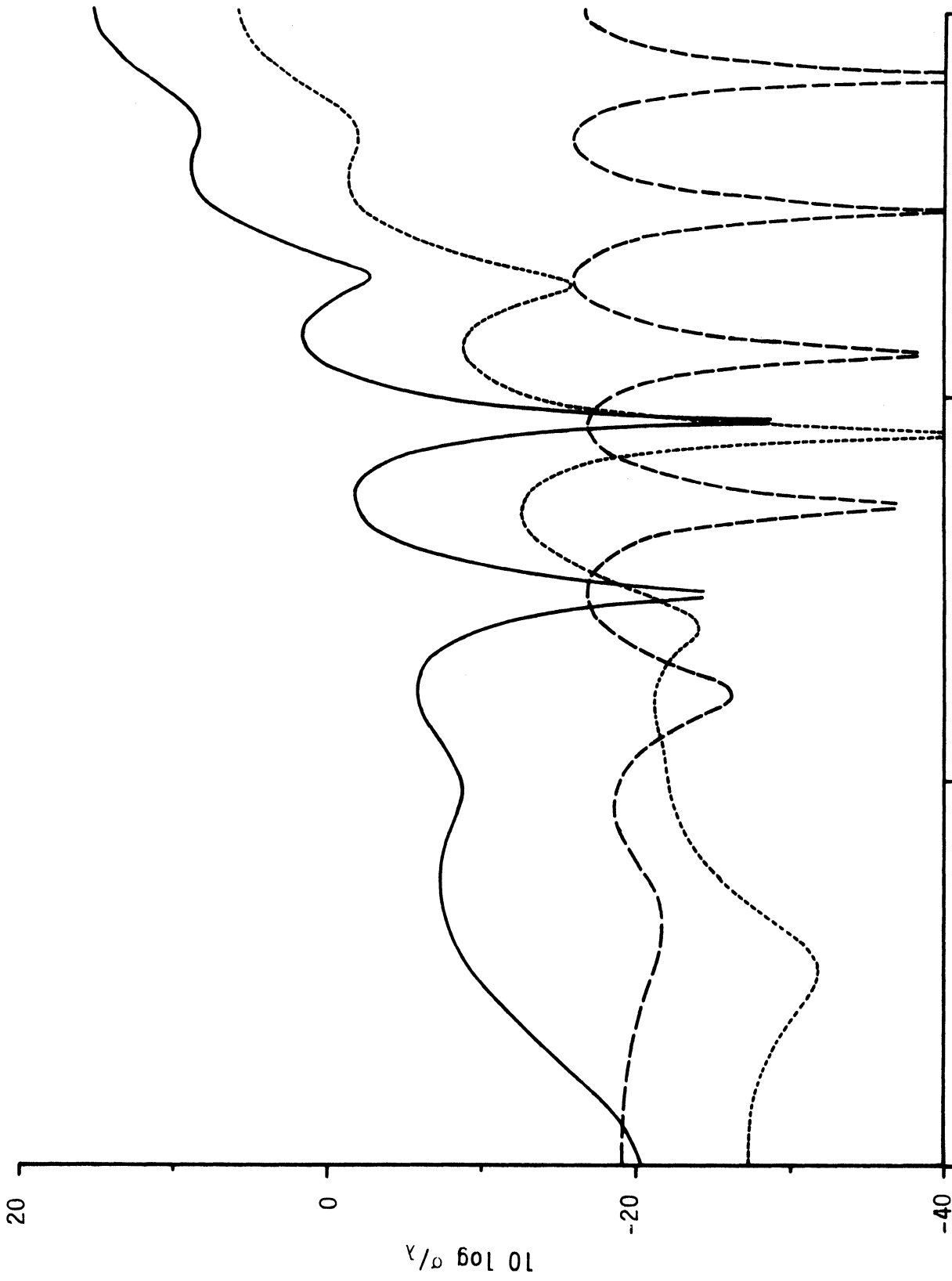

Figure 4-2: Backscattering cross section of the 15° half angle ogival cylinder with uniform impedance $\eta = 0$ (———), 0.5 (- - - -) and 1(— — — —) at 5 GHz.

The amplitudes and (normalized) phases of the corresponding surface fields $K = H_z$ are shown in Figures 4-3 and 4-4 respectively. The physical optics approximation is

$$K^{p\cdot o} = \frac{2\,\hat{n}\cdot\hat{i}}{\hat{n}\cdot\hat{i} - \eta}\, e^{ik\,\hat{i}\cdot\underline{r}} \tag{52}$$

where the notation is as defined in Appendix B. As η increases, the increasing suppression of any (backward) traveling wave component is clearly evident from Figure 4-3, and for $\eta \gtrsim 0.5$ the physical optics approximation is remarkably accurate. This is true for the phase as well as the amplitude, and in Figure 4-4 we have plotted arg K - arg $K^{p\cdot o}$.

In view of this agreement, an analytical approximation which combines the physical optics expression for the backscattered field with the edge waves of Chapter 3 should provide a reasonable estimate of the scattering. The necessary formulae are derived in Appendix B and a program has been written to evaluate the physical optics integral numerically for any specified (continuous) surface impedance η and hence compute the backscattering cross section. For $15^o < \phi < 165^o$ only the upper surface of the ogival cylinder contributes and the resulting cross sections for $\eta = 0$ and 1 are plotted as functions of ϕ, $90^o \leq \phi \leq 165^o$, in Figure 4-5. Since the theory ignores any surface (or traveling) waves that may exist, the accuracy of the prediction could be expected to improve as η increases towards unity, but in actual fact the curves for both $\eta = 0$ and 1 agree almost equally well with those computed using program RAMD and have a common failing: the maxima and minima are progressively displaced.

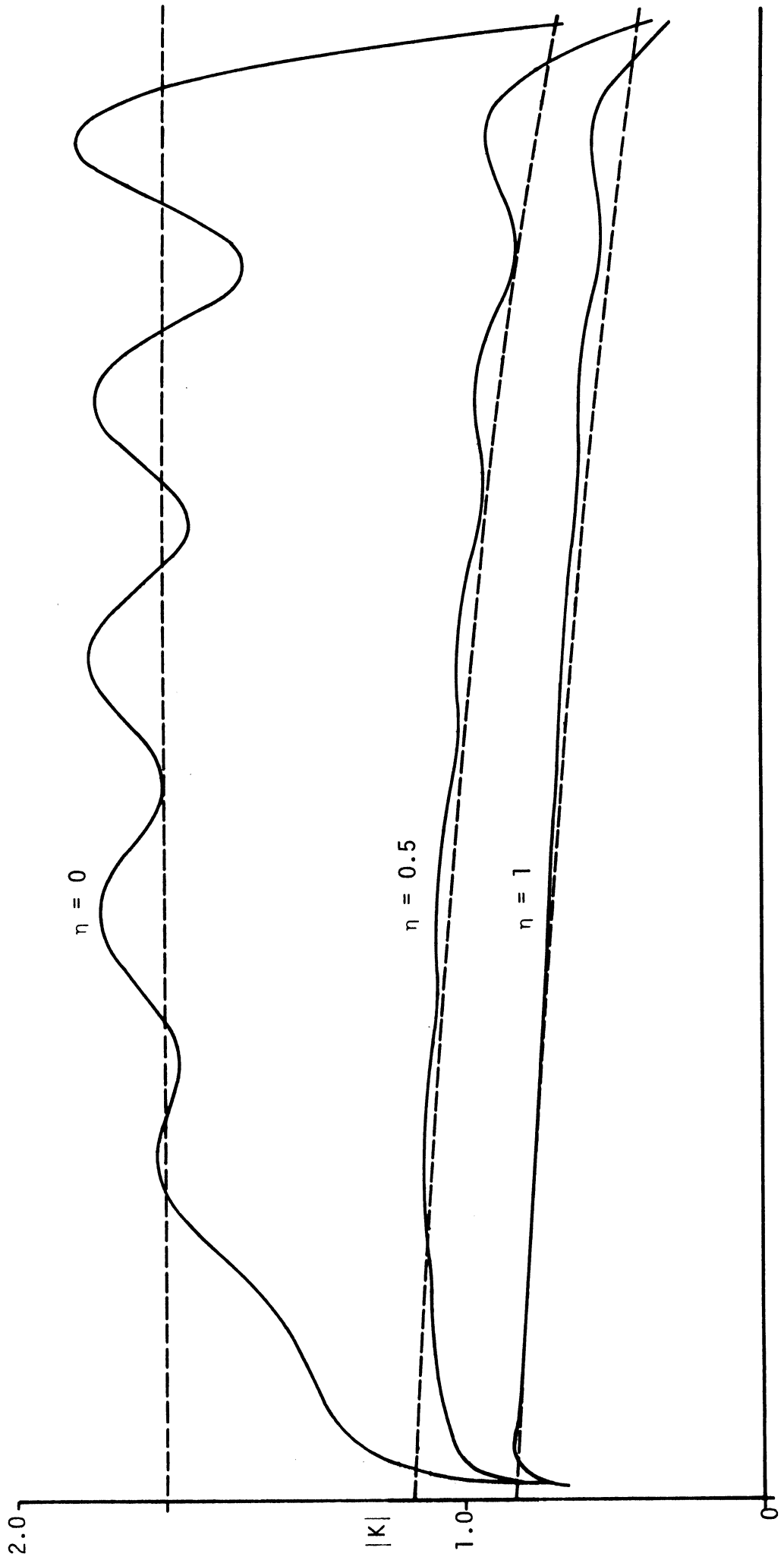

Figure 4-3: Amplitudes of currents induced on the 15° half angle ogival cylinder with uniform impedances shown when illuminated at $\phi = 150°$; f = 5 GHz. The broken lines are the physical optics approximation (55).

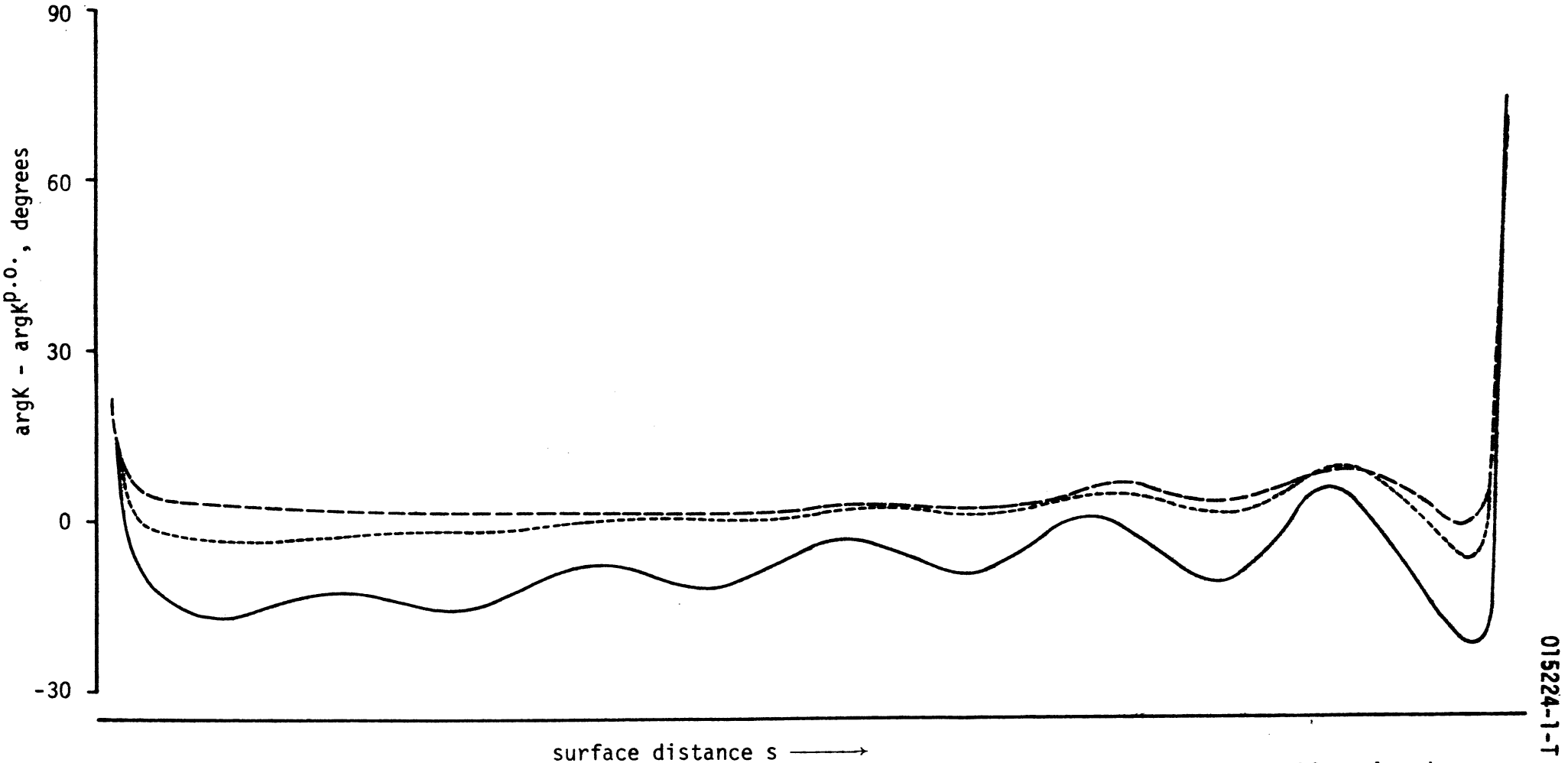

Figure 4-4: Relative phase of currents induced on the 15° half angle ogival cylinder with the uniform impedance $\eta = 0$ (———), $\eta = 0.5$ (-----) and $\eta = 1$ (— — — —). Illumination at $\phi = 150°$; f = 5 GHz.

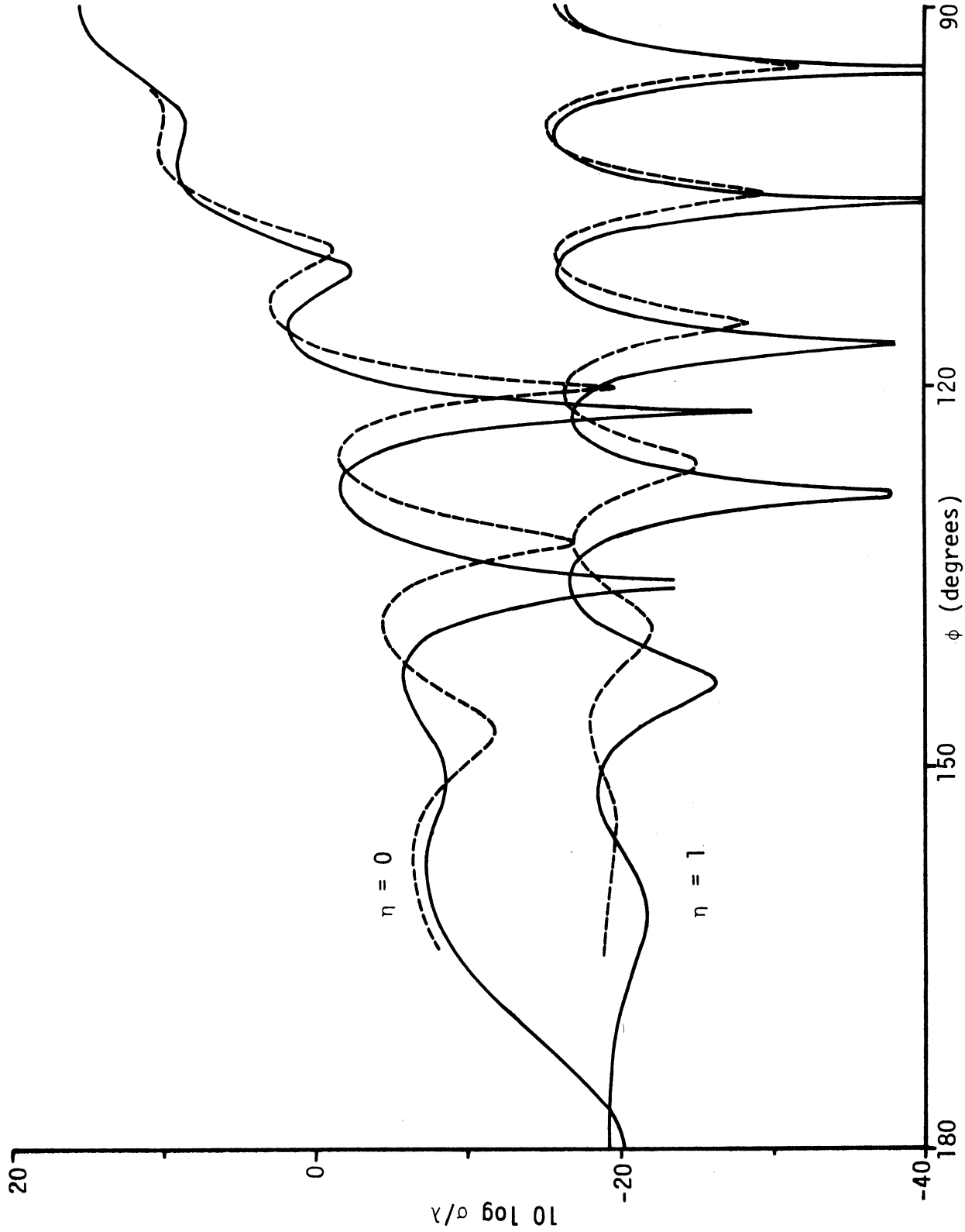

Figure 4-5: Backscattering cross section of the 15° half angle ogival cylinder with uniform impedance shown computed at 5 GHz using RAMD (———) and the analytical approximation (- - - - -).

The reason for this displacement has not been found. With the analytical approximation the minima occur at almost precisely the angles corresponding to destructive interference between the two edge waves regardless of η, i.e., at

$$\phi = \cos^{-1}\left(-\frac{m\lambda}{4\ell}\right)$$

where m is an odd (even) integer if the two edge contributions have the same (opposite) sign for incidence at the angle ϕ. With the output from RAMD, however, the locations of the minima are consistent with the destructive interference between two edge waves emanating from the ends of a body whose length ℓ' is slightly less than ℓ. From the computed backscattering cross sections for f = 4.5(0.1)5.5 GHz and η = 0, 0.5 and 1, the 4 or 5 clearly defined minima in the range $95^{o} < \phi < 150^{o}$ have been read off and the equivalent lengths ℓ' deduced. For any one η the results are virtually independent of frequency and show only a weak dependence on the minima locations, with ℓ' ranging from 0.97ℓ for η = 0, to 0.94ℓ for η = 0.5 and back to 0.96ℓ for η = 1. Although it is believed that the effect is real, there is no obvious explanation, and we are forced to conclude that the minima are not exclusively determined by the edge waves from two identical wedges located at the ends of the cylinder.

In spite of this shortcoming, the analytical approximation appears to accurately predict the main contributors to the scattering for aspects $\phi < 165^{o}$ and can be used to devise and evaluate techniques for cross section reduction in this range. As an illustration, consider the problem of reducing the backscattering cross section at broadside ($\phi = \pi/2$). As seen from (B.8) there

are three contributors to the far field amplitude: the two edges and the (unterminated) surface, and since we are not interested in phase cancellation as a means of cross section reduction, it is necessary to seek a surface impedance which will reduce the individual contributors. Clearly this should be symmetric fore and aft, i.e. $\eta(-\alpha) = \eta(\alpha)$, in which case

$$P(\pi/2) = 2P^{W}(\pi/2, \pi/2, \eta_2) + P^{surf}(\pi/2) \tag{53}$$

and a convenient measure of the backscattering averaged over frequencies is then

$$\tilde{\sigma} = \sigma_1 + \sigma_2$$

where

$$\frac{\sigma_1}{\lambda} = \frac{2}{\pi} |2P^{W}(\pi/2, \pi/2, \eta_2)|^2$$

and

$$\frac{\sigma_2}{\lambda} = \frac{2}{\pi} |P^{surf}(\pi/2)|^2 .$$

This enables us to restrict our use of the analytic approximation to the single frequency f = 5 GHz.

For the bare body ($\eta = 0$) $|P^{W}| = 1.1846$ and $|P^{surf}| = 5.2236$, giving $\tilde{\sigma}/\lambda = 12.62$ dB. As evident from Figure 4-5, there is a marked improvement on going to the uniform impedance $\eta = 1$: $|P^{W}| = 0.10134$ and $|P^{surf}| = 0.02454$, producing the much smaller cross section $\tilde{\sigma}/\lambda = -15.76$ dB, and this impedance was the starting point for our investigation. We can null out the surface contribution by choosing

$$\eta = \cos\alpha$$

(see B.9), but then $|P^W| = 0.11816$ and $\tilde{\sigma}/\lambda = -14.49$ dB. To reduce P^W and still keep P^{surf} small, we first examined the effect of adding 'tips' to the cosine variation so as to raise the impedance to a value η_2 at the edges. The actual profile used was

$$\eta = \cos\alpha \quad , \qquad |\alpha| \leq \alpha_2$$

$$\eta = \eta_1 \left\{ 1 - \left(\frac{\Omega - \alpha}{\Omega - \alpha_2} \right) \right\}^2 + \frac{\Omega - \alpha}{\Omega - \alpha_2} \left\{ 2 - \left(\frac{\Omega - \alpha}{\Omega - \alpha_2} \right) \right\} \cos \alpha_2$$

$$- (\Omega - \alpha) \left\{ 1 - \left(\frac{\Omega - \alpha}{\Omega - \alpha_2} \right) \right\} \sin \alpha_2 \quad , \qquad \alpha_2 < |\alpha| \leq \Omega$$

(see Figure 4-6) for which the impedance and its first derivative are continuous, $0 \leq |\alpha| \leq \Omega$, but due (apparently) to the contributions of the concave regions, no combination of α_2 and η_2 was found to reduce $\tilde{\sigma}/\lambda$ below its value for the uniform impedance $\eta = 1$.

We now reverted to the uniform impedance and added tips to produce the profile

$$\eta = 1 \qquad |\alpha| \leq \alpha_2$$

$$\eta = \eta_2 + (1 - \eta_2) \sin \frac{\pi(\Omega - |\alpha|)}{2(\Omega - \alpha_2)} \qquad \alpha_2 < |\alpha| \leq \Omega$$

Starting with $\alpha_2 = 0.18786$ corresponding to a tip length of 1 inch, the cross sections were determined for a sequence of increasing $\eta_2 > 1$ to determine

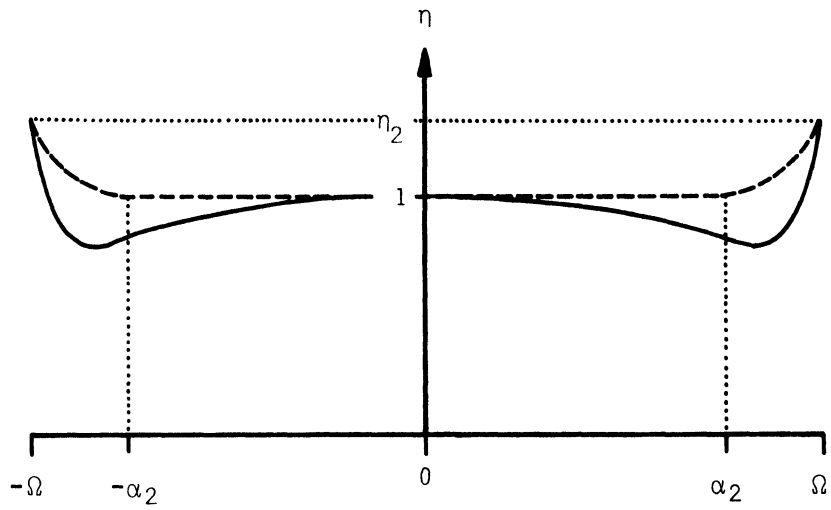

Figure 4-6: Impedance profiles for broadside incidence.

the minimum $\tilde{\sigma}/\lambda$. The results are listed below and in each case the minimum occurs for $\eta_2 = 1.115$:

$\alpha_2 = 0.18786$, $\tilde{\sigma}/\lambda = -18.65$ dB

0.22483 = -18.77

0.25441 = -18.89

0.26106 = -18.89

where the tip lengths are 1, 0.5, 0.1 and 0.01 inches respectively. Although it is doubtful whether the full effect would be realized if the length was less than about $\lambda/4$, it is evident that by raising the impedance at the edges to 0.115 we can reduce the average cross section 3 dB below that for the uniform impedance, thereby achieving more than 31 dB reduction in the cross section of the bare body over a wide frequency range.

In an aspect region about edge-on ($\phi = \pi$) the analytical approximation is significantly in error because of the omission of surface wave effects, and it is then necessary to resort to the computer program RAMD. To illustrate this we consider the problem of minimizing the backscattering cross section over an angular range of $\pm$ 30 degrees about edge-on. The problem is one of practical importance and similar to that previously investigated by Senior and Liepa (1977).

Although the analytical approximation is no longer applicable, the underlying concepts are still valid and, in particular, the edges of the cylinder continue to play a dominant role in the scattering. This is evident

from computed data for the backscattering cross section at edge-on incidence. The results for the uniform impedances η = 0 and 1 at f = 4.5(0.1)5.5 GHz are plotted in Figure 4-7, and since the frequency variation is close to sinusoidal, we can determine the magnitudes of the two contributors to the scattering from the levels of the maxima and minima. Thus, for η = 0,

$$|P_1| = 0.077, \qquad |P_2| = 0.046$$

whereas for η = 1

$$|P_1| = 0.135, \qquad |P_2| = 0.010 .$$

For a 15 degree half-angle wedge, P = i0.078 and -i0.137 for η = 0 and 1 respectively, and these now serve to identify P_1 with the scattering from the front edge of the ogival cylinder. Presumably, therefore, P_2 is due to the rear edge whose contribution appears as a result of surface waves on the cylinder.

This process can be repeated at other aspects throughout the angular region. As $\emptyset$ decreases it is clear that at least one of the contributors is no longer frequency independent, but if we attribute the entire frequency variation to the rear edge contribution we can compensate for it by using the differing levels of two adjacent maxima or minima to deduce the values appropriate to the 5 GHz frequency. The magnitudes of P_1 and P_2 obtained in this manner are shown for η = 0 in Figure 4-8. The close agreement between the lower set of values and the theoretical curve for the scattering from a wedge clearly identifies P_1 as the front edge contribution, and the minor departures are no more than to be expected in view of the deductive analysis employed. The

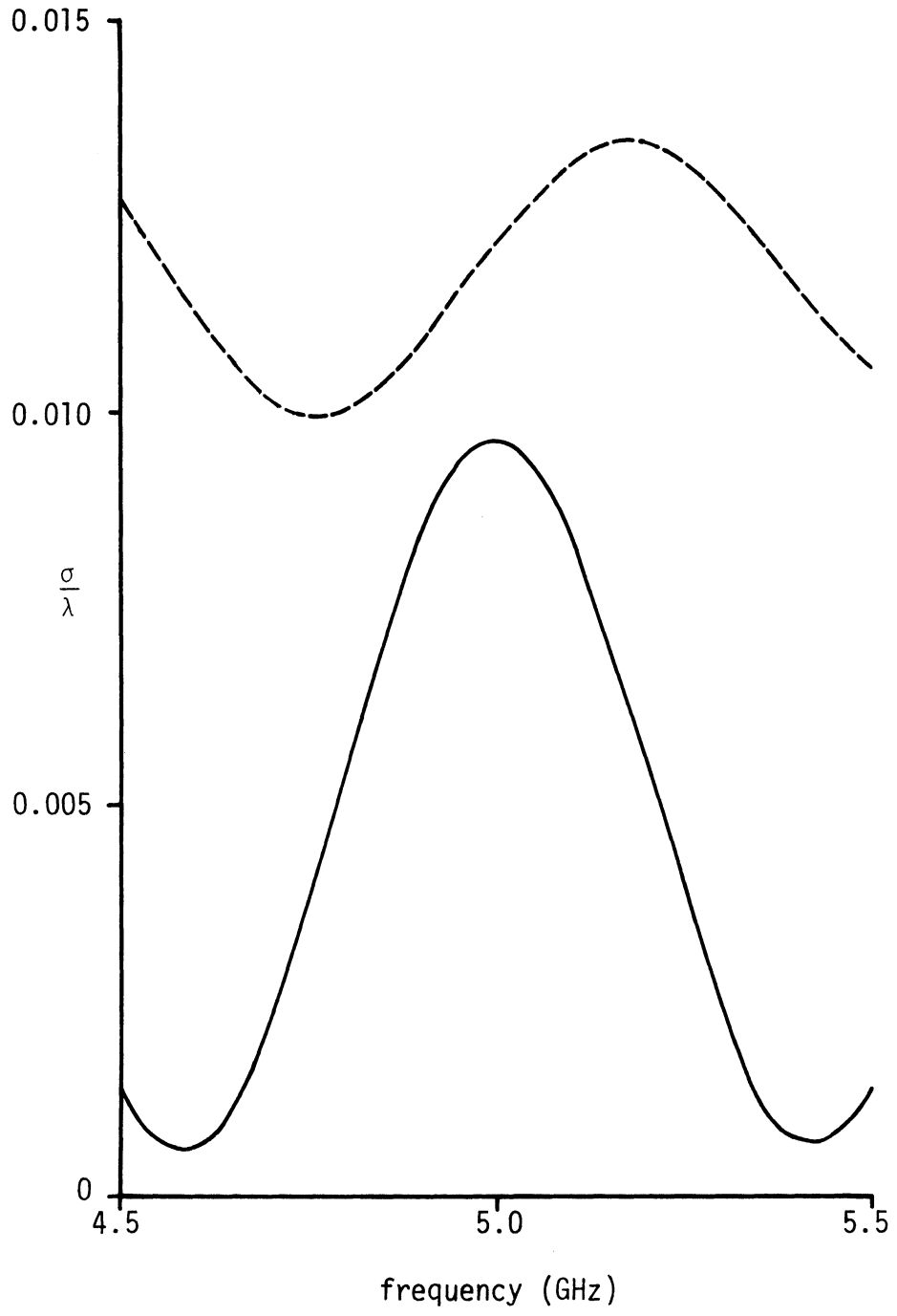

Figure 4-7: Edge-on backscattering cross sections of the 15° half angle ogival cylinder with impedance $\eta = 0$ (-----) and $\eta = 1$ (——).

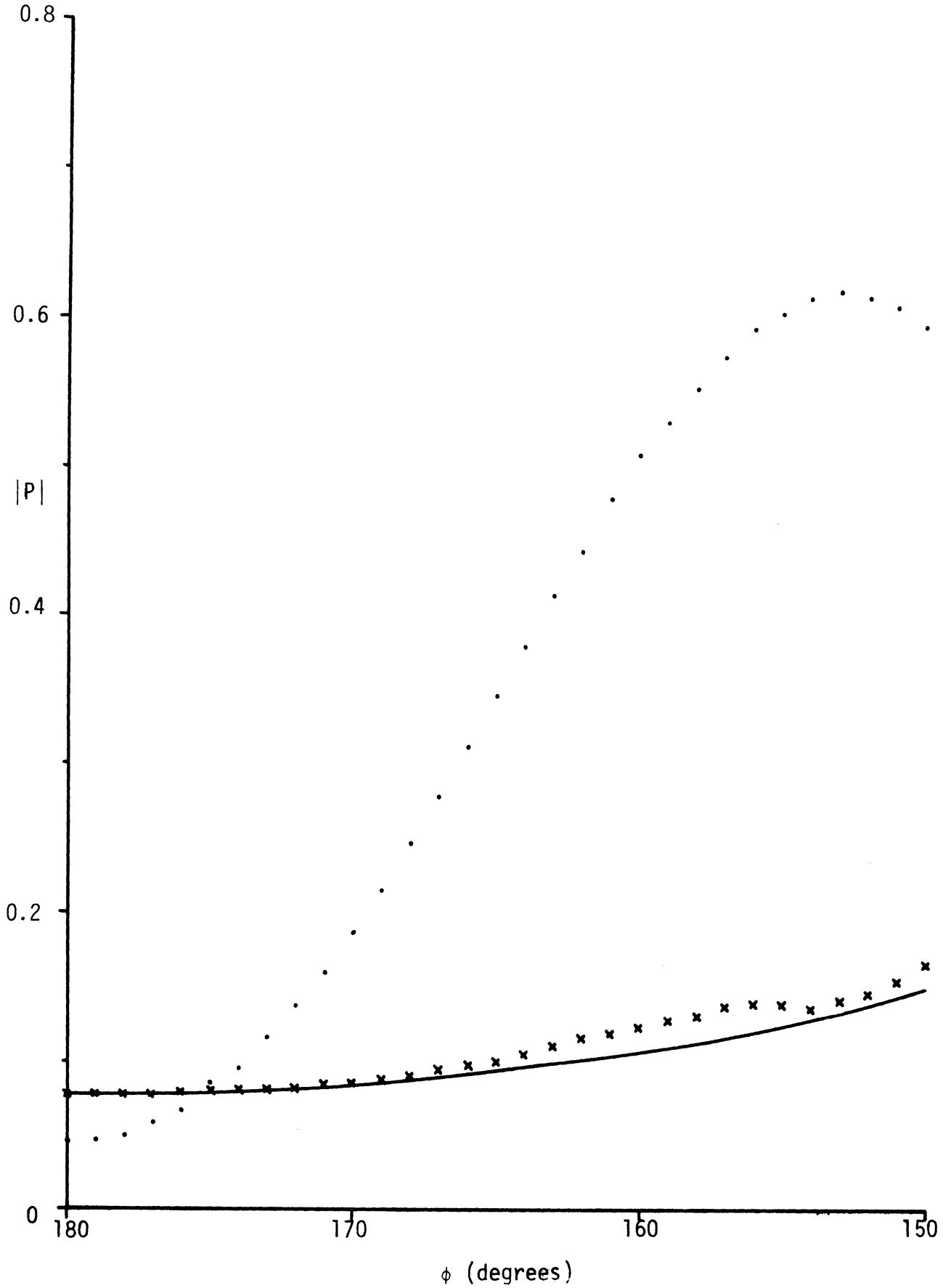

Figure 4-8: Deduced magnitudes for the front (xxx) and rear (•••) edge contributions for $\eta = 0$ at 5 GHz. The solid line is the theoretical result for a 15° half angle wedge coincident with the front edge.

other points then define the rear edge contribution P_2 whose magnitudes exceed those of the front edge for $\phi < 175^o$ and reach a local maximum at $\phi = 153^o$. This is almost precisely the location expected for the traveling wave peak according to the formula

$$\phi = 180 - 49.9\sqrt{\frac{\lambda}{\ell}} \quad , \text{degrees}$$

(Senior and Knott, 1968). As ϕ decreases below 153 degrees, $|P_2|$ also decreases and then increases again in accordance with the theoretical expression for (direct) scattering from a wedge coincident with the rear edge of the cylinder.

The above process for finding the magnitudes of the two contributors is a very tedious one and a number of other methods have been tried to reduce the labor. One that is reasonably effective is to draw cumulative plots of σ/λ versus ϕ at all of the frequencies and to sketch in the bounding curves. The latter are then assumed to represent

$$\frac{2}{\pi} |P_1 \pm P_2|^2$$

from which $|P_1|$ and $|P_2|$ can be found. The cumulative plots for $\eta = 0$ are shown in Figure 4-9, and the accuracy that would result from using the bounding curves can be gauged from the crosses showing the extrema deduced from Figure 4-8. The process is certainly much simpler but its accuracy is also less than that desired, particularly for those aspects and/or impedances where P_2 has a significant frequency dependence, and we have therefore used the original method in all our analyses. This requires the construction of individual plots of σ/λ versus frequency, $4.4 \leq f \leq 5.6$ GHz at each of the angles $\phi = 150(1)180^o$ for each impedance variation considered, but the results seem worth the labor.

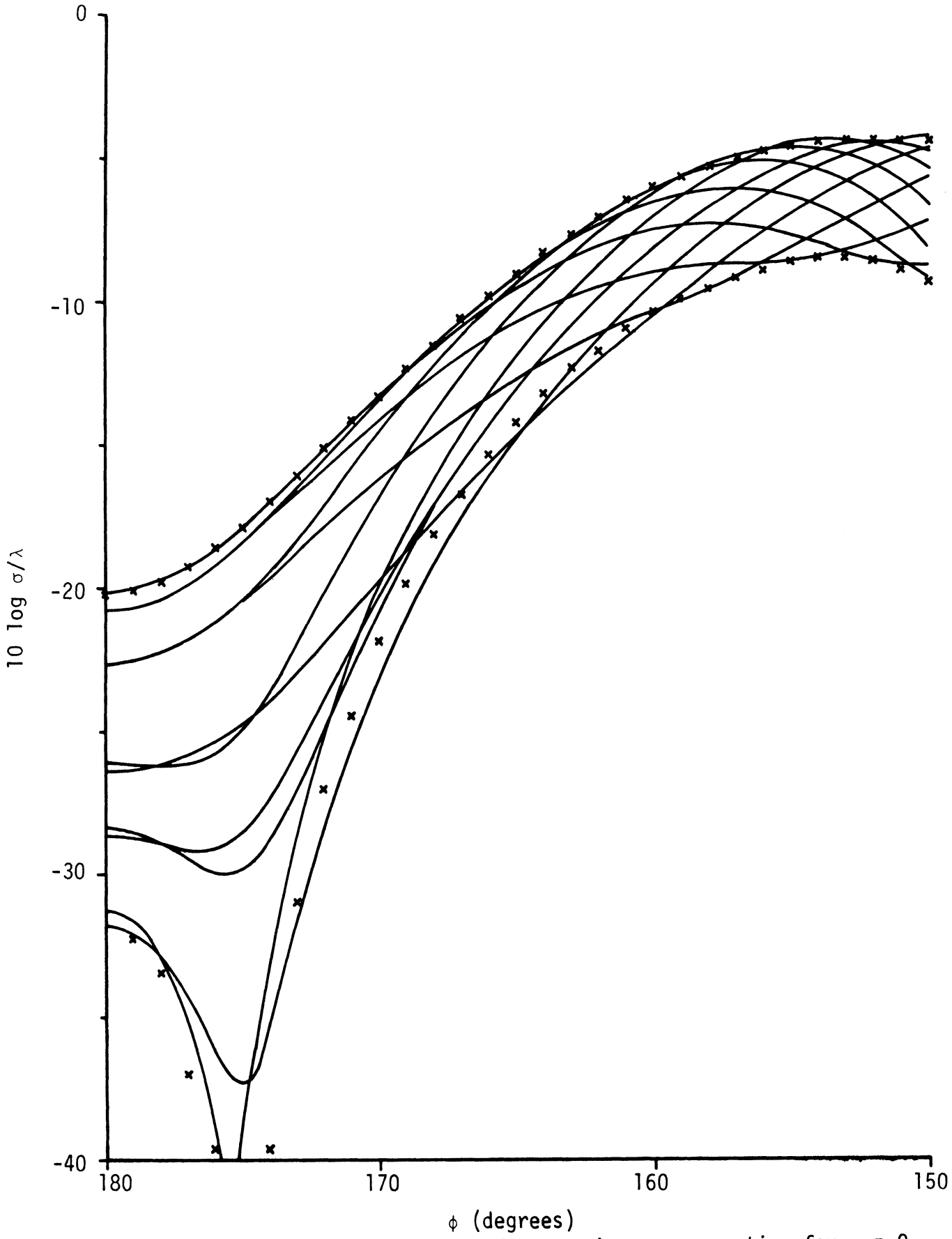

Figure 4-9: Cumulative plots of the backscattering cross section for $\eta = 0$. The crosses show $2/\pi\ (|P_1| \pm |P_2|)^2$ with $|P_1|$ and $|P_2|$ taken from Figure 4-8.

The values of $|P_1|$ and $|P_2|$ obtained appear accurate and meaningful and the only difficulties experienced were in seeking to deduce the frequency variation of $|P_2|$ from two adjacent and low minima. In such cases it was found desirable to extend the frequency range for which data is computed to include a second maximum and to use two maxima instead.

$|P_1|$ and $|P_2|$ for the four uniform impedances $\eta = 0$, 0.5, 1 and 2 are plotted as functions of ϕ, $150 \leq \phi \leq 180^0$, in Figures 4-10 and 4-11. The front edge contributions are in excellent agreement with the theoretical values (shown as the dashed curves in Figure 4-10) for a 15 degree half-angle wedge, and, as expected, the rear edge contribution decreases with increasing η, the decrease being most dramatic for $\phi \gtrsim 160^0$. To obtain a broadband reduction in the backscattering cross section it is necessary to reduce both sources individually, and in the case of P_2 it is obvious that η should be as large as possible. If, for example, $\eta = 1$, Figure 4-11 shows that $|P_2|$ is reduced by an amount ranging from 14 dB at 180 degrees to 18 dB at smaller angles. To reduce $|P_1|$, however, requires a value of η in the vicinity of 0.3, and based on the simulation of the leading edge by an infinite wedge we would expect $|P_1|$ to be zero at edge-on incidence if $\eta = 0.25882$.

To test this conjecture, data were now computed for the ogival cylinder with the uniform impedance $\eta = 0.25882$. The values of $|P_2|$ are included in Figure 4-11 and are comparable to estimates made by interpolating the results for $\eta = 0$ and 0.5. Figure 4-12 shows a plot of the corresponding front edge contribution along with the theoretical curve for a wedge. It is seen that $|P_1|$ decreases from 0.0038 at $\phi = 180^0$ to a minimum of 0.0028 at $\phi \simeq 174.5^0$ and then increases rather rapidly. From the consistency of the data points for adjacent values of ϕ it is believed that the effects are real, and the

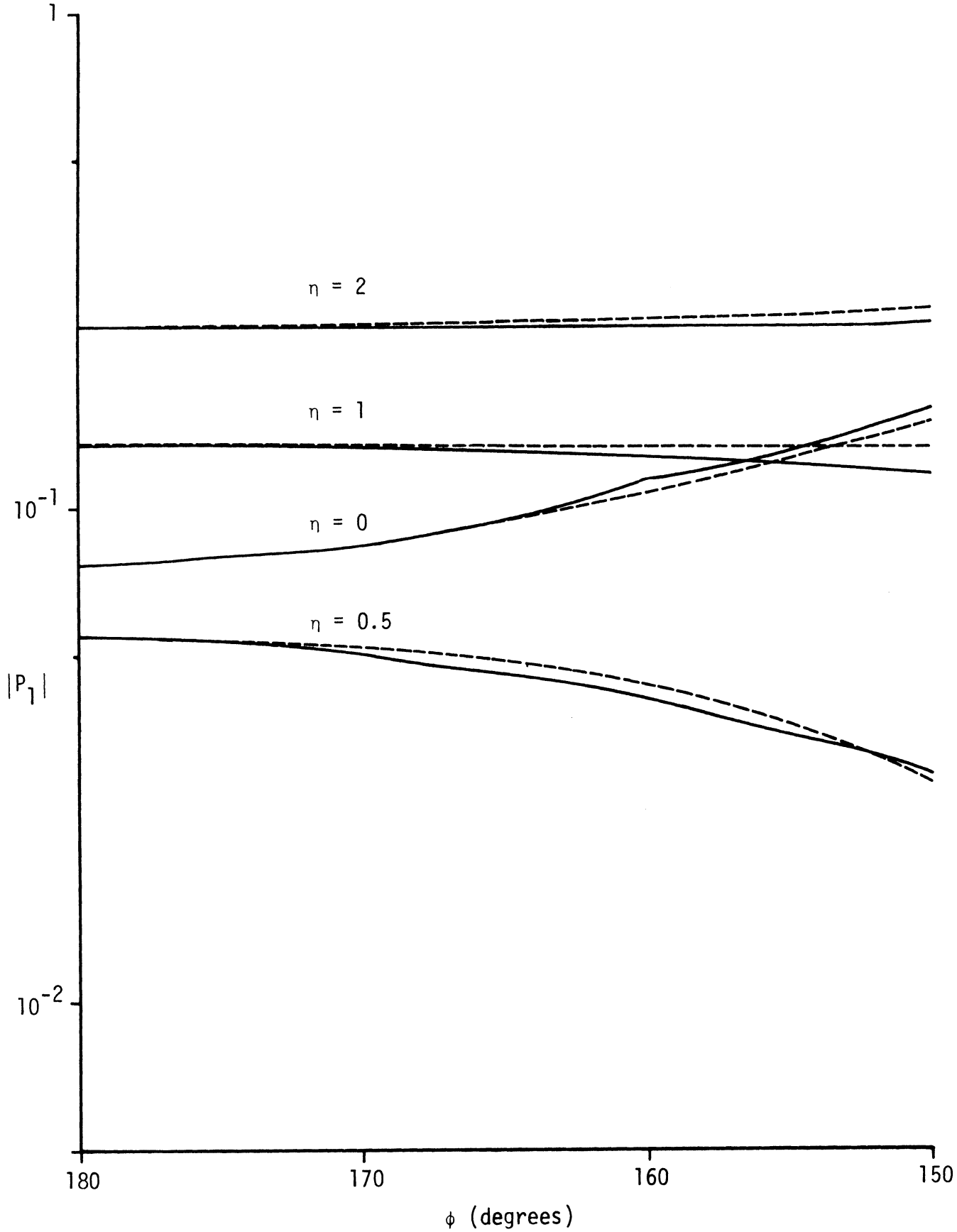

Figure 4-10: Deduced magnitudes of the front edge contribution for η = 0, 0.5, 1 and 2. The broken lines are the theoretical wedge results.

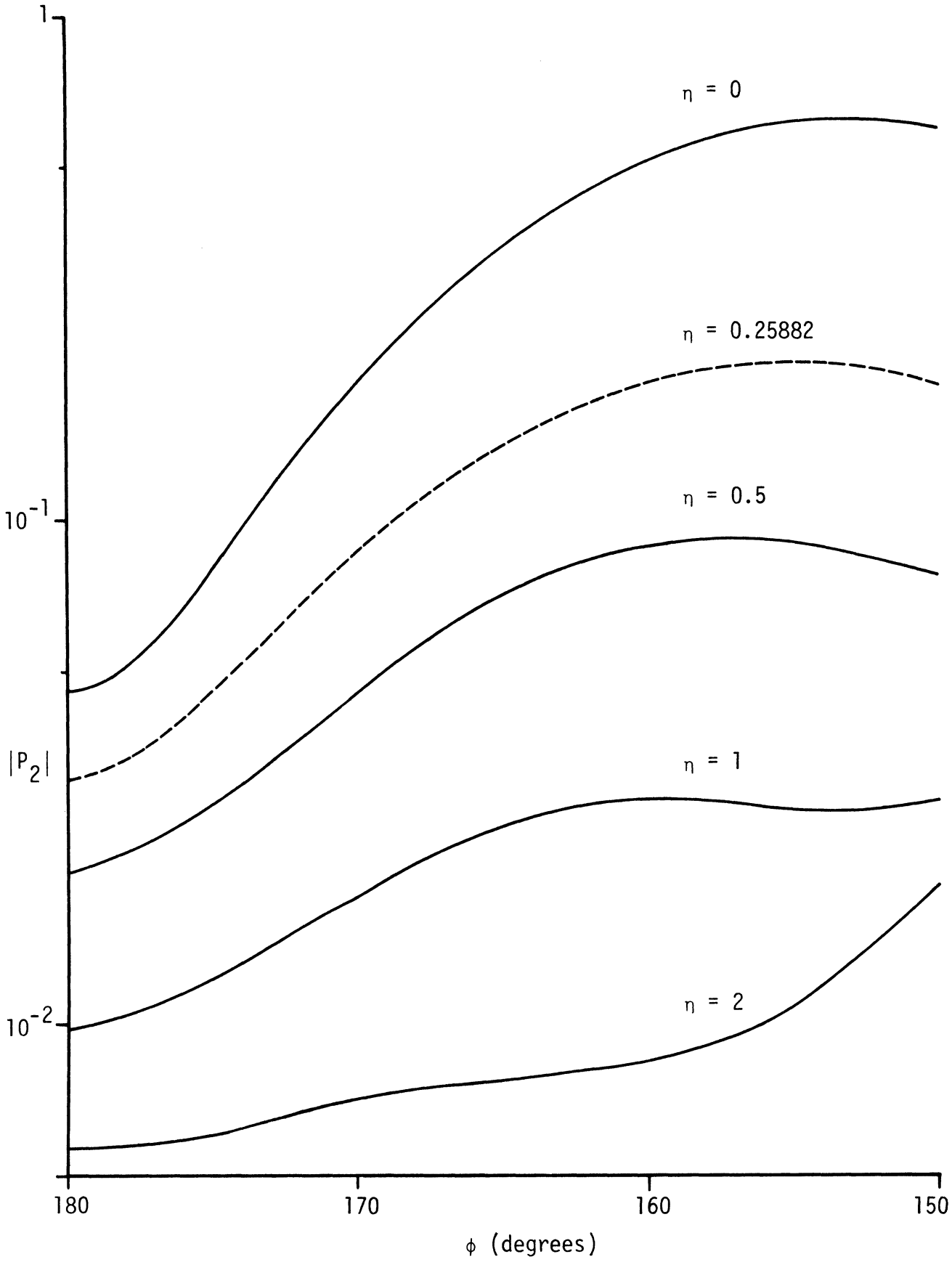

Figure 4-11: Deduced magnitudes of the rear edge contribution for η = 0, 0.5, 1, 2 and 0.25882.

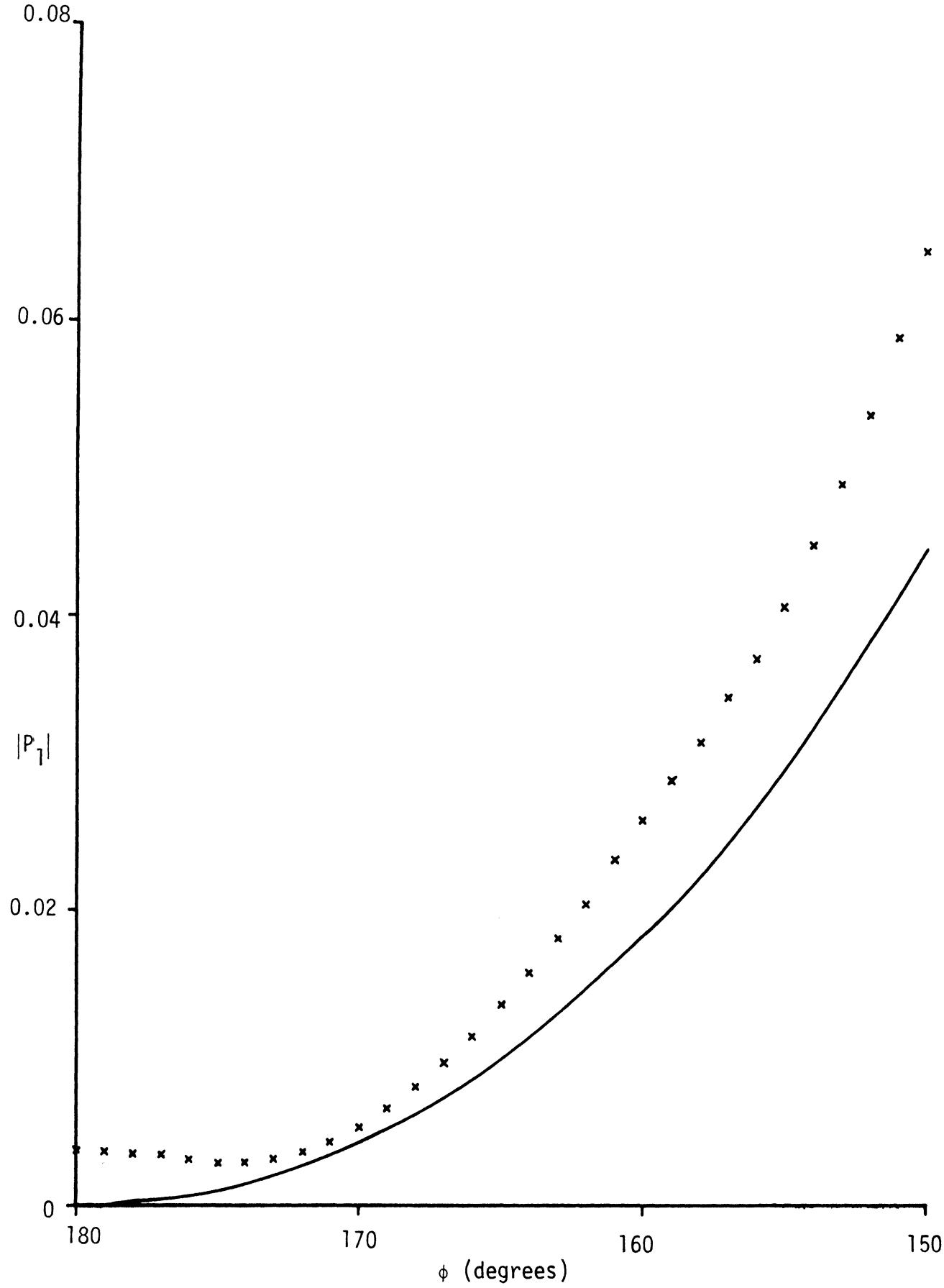

Figure 4-12: Deduced (xxx) magnitudes of the front edge contribution for η = 0.25882, compared with the theoretical wedge result (———).

rapid increase for $\phi < 170^0$ is compatible with the decreasing angle of the ogival cylinder compared with a wedge. For $\phi > 170^0$, however, no convincing explanation for the behavior has been found. The values of $|P_1|$ are consistent with those for a wedge having an impedance $\eta = |\eta|e^{i\sigma}$ with $|\eta| \simeq 0.264$ and $\sigma \simeq 2.5^0$, but for scattering at these low levels it is not unlikely that the curvature of the surface in the vicinity of the edge is also a contributing factor. We must also be careful not to lose perspective, and over the range $170 \leq \phi \leq 180^0$ the computed front edge contribution in Figure 4-12 is more than 25 dB below the already-low return for the perfectly conducting edge.

To reduce both the front and rear edge contributions we obviously require an impedance which is as large as possible over most of the surface (including the rear portion) to decrease the rear edge return, but which is also close to 0.25 in the vicinity of the front edge. In addition, the impedance variation should be smooth with no discontinuities in at least $\partial\eta/\partial s$ to avoid the introduction of new sources of scattering, and a general variation which meets these criteria is

$$\eta = \frac{1}{2}(\eta_m + \eta_1) - \frac{1}{2}(\eta_m - \eta_1)\cos \pi s/s_1 \quad , \qquad 0 \leq s \leq s_1$$

$$\eta = \eta_m \quad , \qquad s_1 \leq s \leq s_m \quad , \tag{55}$$

where η_1 is the impedance at the front and s is the surface distance measured from the front to the rear ($s = s_m$).

As an illustration, suppose that the maximum achievable $\eta(= \eta_m)$ is 1 and that the taper extends over the entire front half of the body, i.e., $s_1 = s_m/2$. For $\eta_1 = 0.25882$ the resulting front edge contribution is plotted in Figure 4-13,

where we have included for comparison the data for the uniform impedance $\eta = 0.25882$ and the theoretical wedge return. $|P_1|$ now has a very shallow minimum at $\phi = 178^0$, and is greater than it is for the uniform impedance. The impedance taper has therefore increased the front edge contribution, showing that $|P_1|$ is not entirely determined by the impedance at the edge. $|P_2|$ is plotted in Figure 4-14 with the corresponding curve for the uniform impedance $\eta = 1$. As expected, the rear edge contribution is greater than for the uniform impedance since the taper has removed some of the absorber from the surface.

The average cross section $\tilde{\sigma}$ obviously increases with decreasing ϕ and is dominated by the front edge contribution for $\phi < 160^0$. To reduce $\tilde{\sigma}$ it is therefore necessary to reduce $|P_1|$ for $\phi \lesssim 160^0$, and this we can do by increasing the value of η at the front edge, even though this may serve to increase $|P_1|$ for ϕ close to 180^0. With this objective in mind, results were obtained for the same s_1 and η_m as before, but with $\eta_1 = 0.26287$, 0.27497, 0.29498 and 0.39973. For a uniform impedance wedge these values are such as to produce zeros in the backscattering from the edge at $\phi = 175^0$, 170^0, 165^0 and 150^0 respectively. Not surprisingly, the effect on $|P_2|$ is relatively small. In all four cases the values lie between those for the uniform impedance $\eta = 1$ and for the tapered impedance commencing with $\eta_1 = 0.25882$, and to increase η_1 from 0.25882 to 0.26287 reduces $|P_2|$ by less than one percent. For the largest η_1 (= 0.39973) the data for $|P_2|$ are included in Figure 4-14.

With $|P_1|$, however, η_1 has a considerable effect and the data for the four values of η_1 are plotted in Figures 4-15 through 4-18, along with the corresponding curves for wedges and the uniform impedance η_1. As η_1 increases, $|P_1(180^0)|$ initially decreases, and then increases for $\eta_1 \gtrsim 0.28$. The minimum as a function of ϕ also becomes more pronounced, occurring at an angle somewhat greater than predicted by wedge theory. It is deepest for $\eta_1 = 0.29498$ but then rises rapidly with increasing η_1, suggesting that the net return from

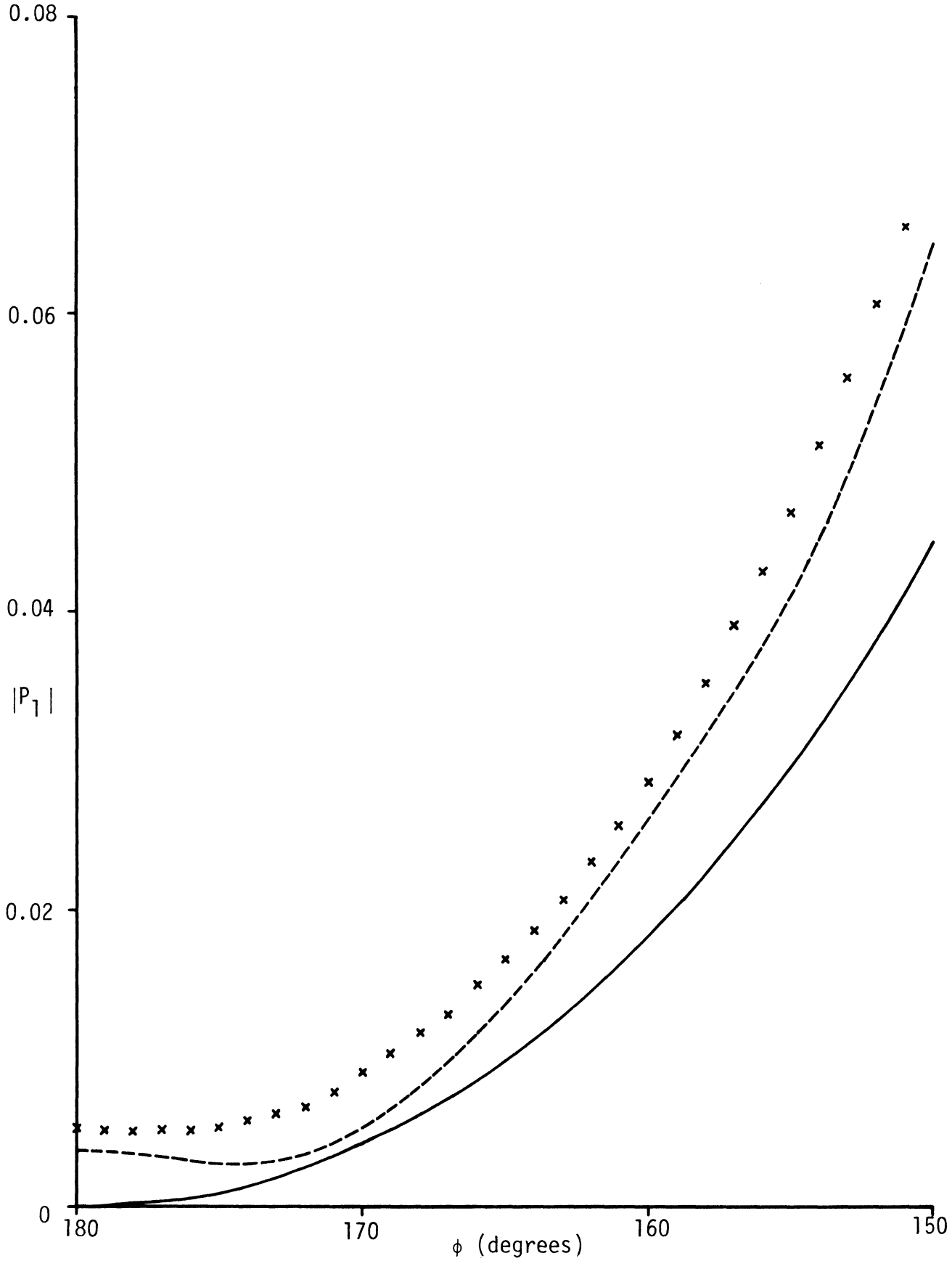

Figure 4-13: Deduced (xxx) magnitudes of the front edge contribution for the impedance profile (55) with $\eta_1 = 0.25882$, $\eta_m = 1$ and $s_1 = s_m/2$, compared with the magnitudes (----) and the theoretical wedge result (——) for the uniform impedance $\eta = 0.25882$.

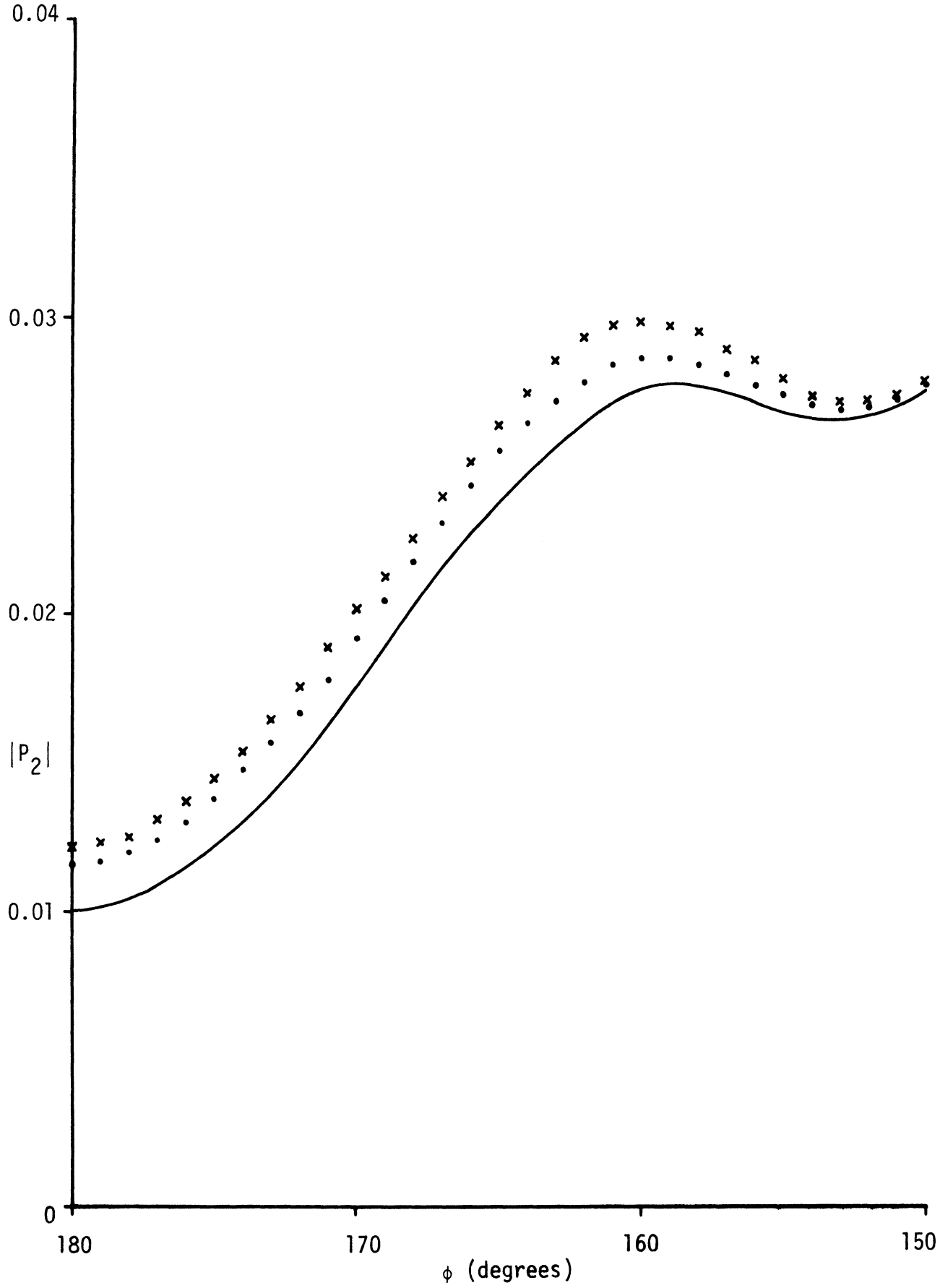

Figure 4-14: Deduced magnitudes for the rear edge contribution for the impedance profile (55) with $\eta_m = 1$, $s_1 = s_m/2$ and $\eta_1 = 0.25882$ (xxx), $\eta_1 = 0.39973$ (...), compared with the result (——) for the uniform impedance $\eta = 1$.

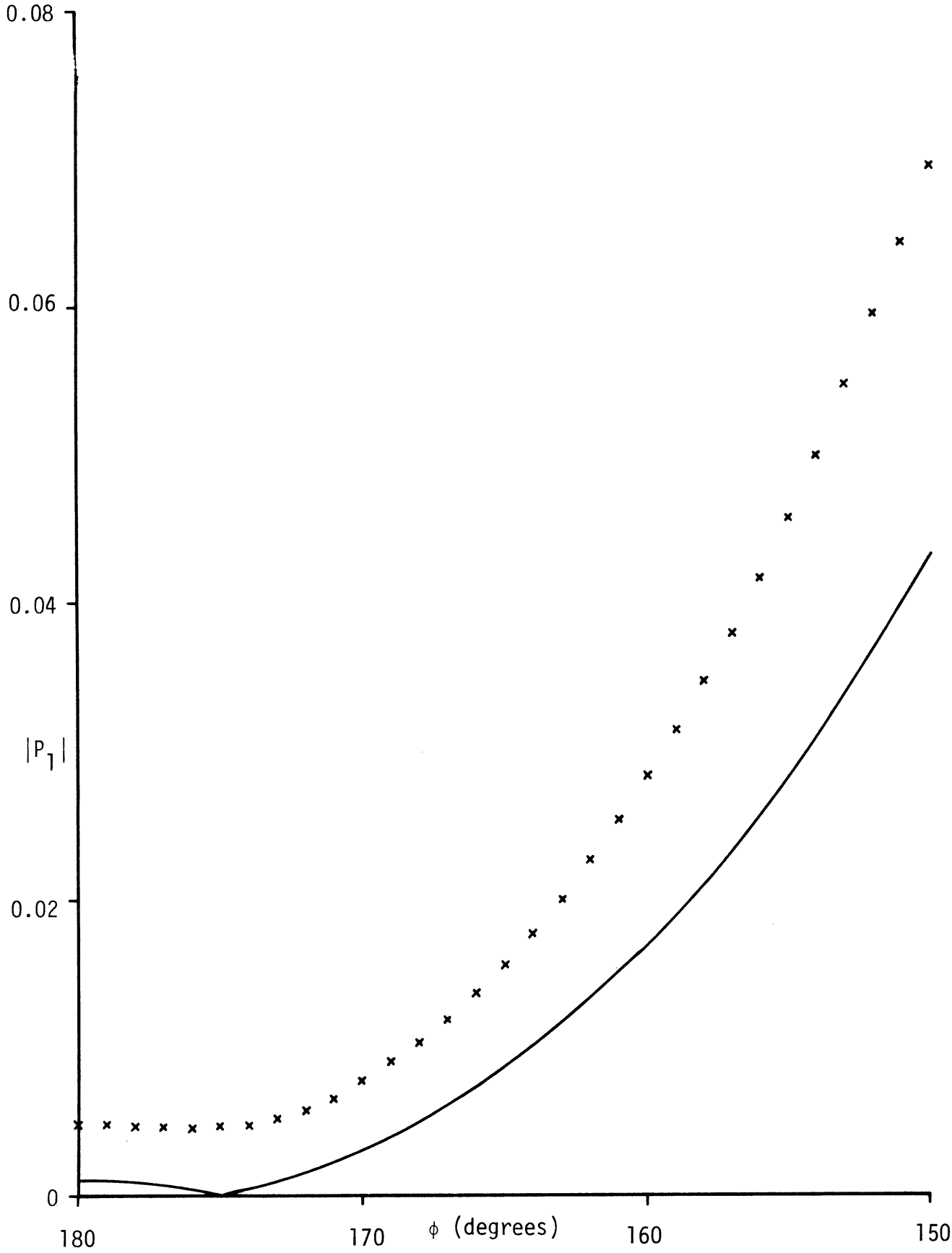

Figure 4-15: Deduced (xxx) magnitudes of the front edge contribution for the impedance profile (55) with $\eta_1 = 0.26287$, $\eta_m = 1$ and $s_1 = s_m/2$, compared with the theoretical wedge result for the uniform impedance $\eta = 0.26287$.

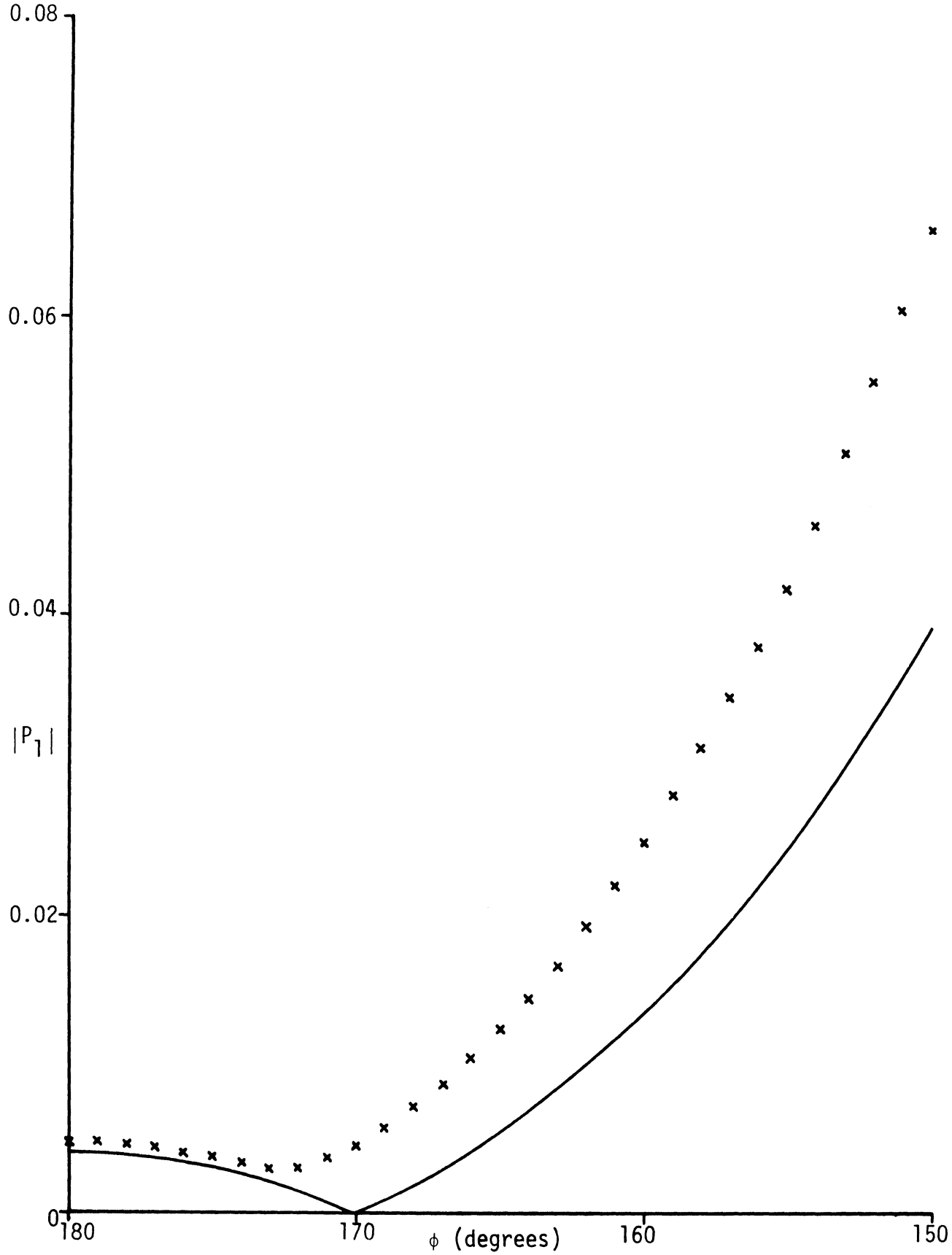

Figure 4-16: Deduced (xxx) magnitudes of the front edge contribution for the impedance profile (55) with $\eta_1 = 0.27497$, $\eta_m = 1$ and $s_1 = s_m/2$, compared with the theoretical wedge result for the uniform impedance $\eta = 0.27497$.

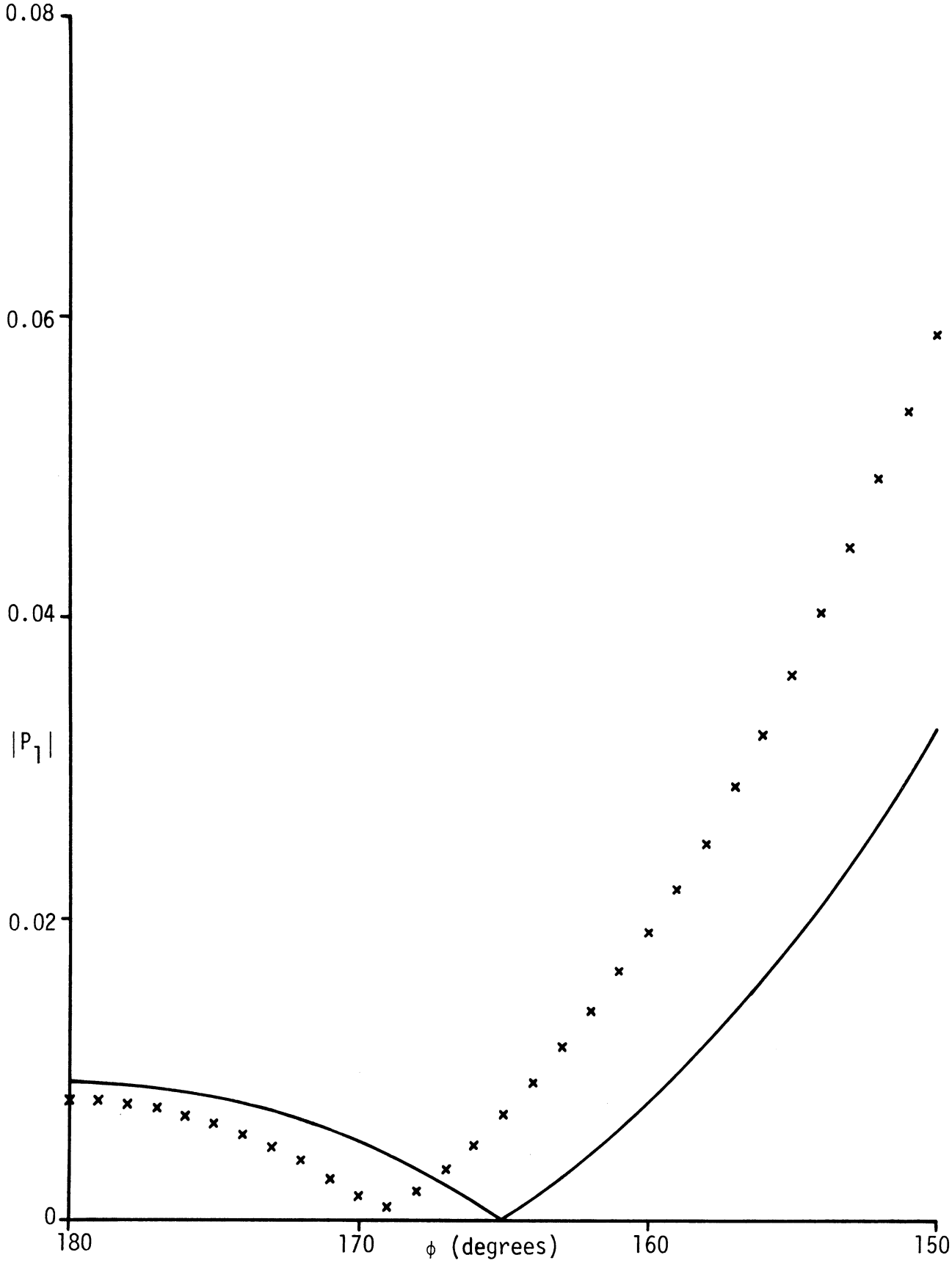

Figure 4-17: Deduced (xxx) magnitudes of the front edge contribution for the impedance profile (55) with $\eta_1 = 0.29498$, $\eta_m = 1$ and $s_1 = s_m/2$, compared with the theoretical wedge result for the uniform impedance $\eta = 0.29498$.

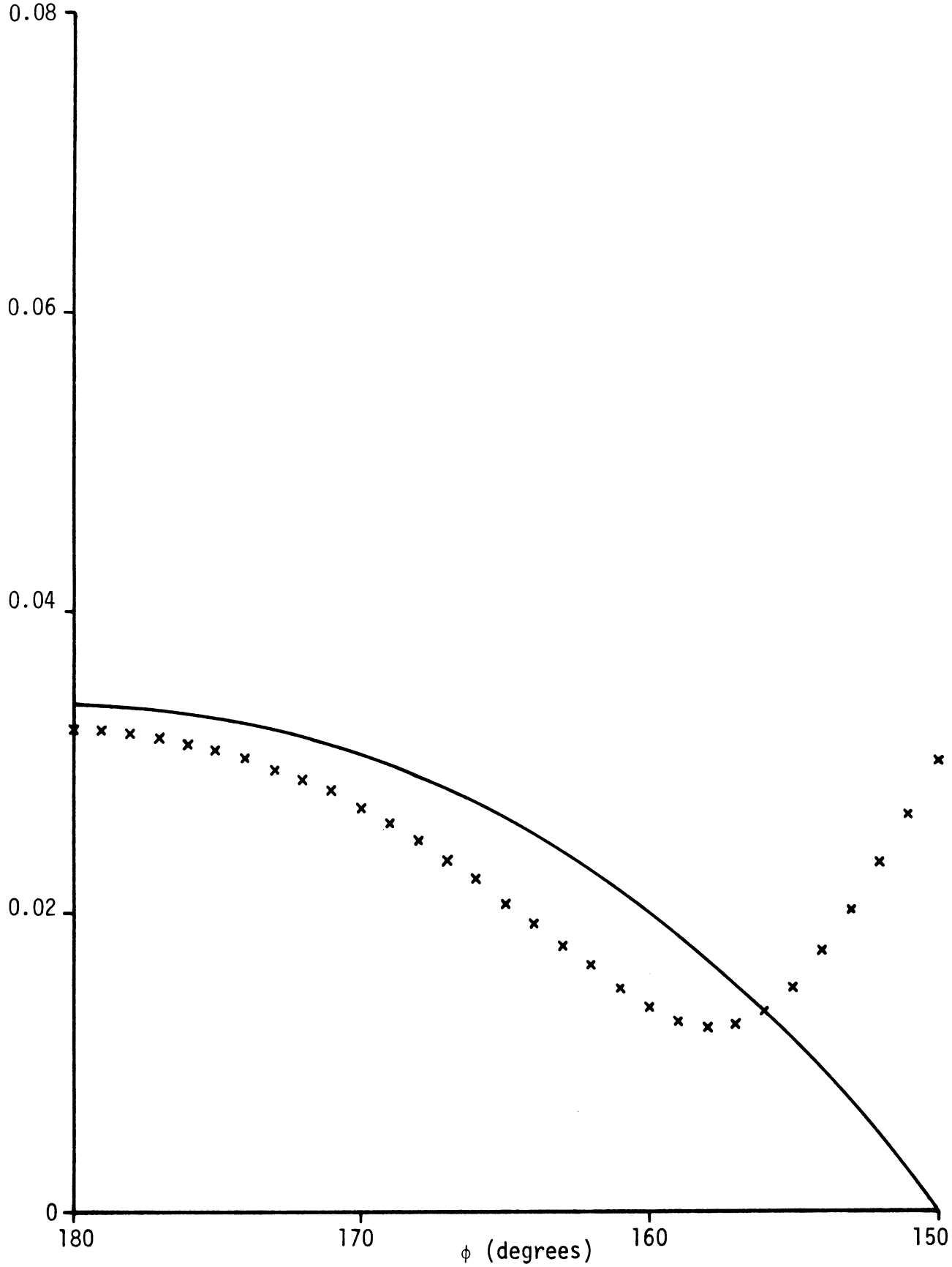

Figure 4-18: Deduced (xxx) magnitudes of the front edge contribution for the impedance profile (55) with $\eta_1 = 0.39973$, $\eta_m = 1$ and $s_1 = s_m/2$, compared with the theoretical wedge result for the uniform impedance $\eta = 0.39973$.

the front edge is made up of a contribution associated with the actual impedance at the edge and one due to the impedance variation.

For cross section reduction purposes the impedance profile that is most desirable depends on the particular objective, and in Figure 4-19 the average cross section $\tilde{\sigma}/\lambda$ is plotted as a function of $\emptyset$ for the above five values of η_1. The edge-on backscattering is least if $\eta_1 = 0.26287$ or 0.27497, but when the cross section is averaged over the entire range $180^o \geq \emptyset \geq 150^o$, the latter impedance is slightly superior, and reduces the average bare body cross section by 21.1 dB. However, the averaged (over angle) cross section is actually least for the impedance $\eta_1 = 0.39973$, which yields a reduction of 22.0 dB in the bare body return. It also gives the greatest reduction in the traveling wave lobe, and the resulting cross section is now almost constant over the entire aspect range.

We have also examined the effect of different impedance tapers using the same values of η_1 (= 0.25882) and η_m (= 1) as before, and, in particular, data have been computed for the cosinusoidal taper (55) with $s_1 = s_m/4$ and $s_m/8$. These correspond to taper lengths of only 0.75λ and 0.375λ respectively at 5 GHz, and not surporisingly even the front edge contribution now shows some frequency dependence, especially for $s_1 = s_m/8$. However, by using adjacent maxima and minima in the individual plots versus frequency, values of $|P_1|$ and $|P_2|$ have been deduced appropriate to 5 GHz, and the results for $|P_2|$ are shown in Figure 4-20. For the most part the data points lie between the curves for the uniform cylinder with $\eta = 1$ and the cylinder whose tapered impedance has $s_1 = s_m/2$, and the variability near $\emptyset = 155^o$ is no more than expected in view of the uncertainties in the deductive analyses. For the front edge contribution, however, the reduced values of s_1 substantially increase the scattering. As seen from Figure 4-21, the results for $s_m/4$ and $s_m/8$ are comparable to those

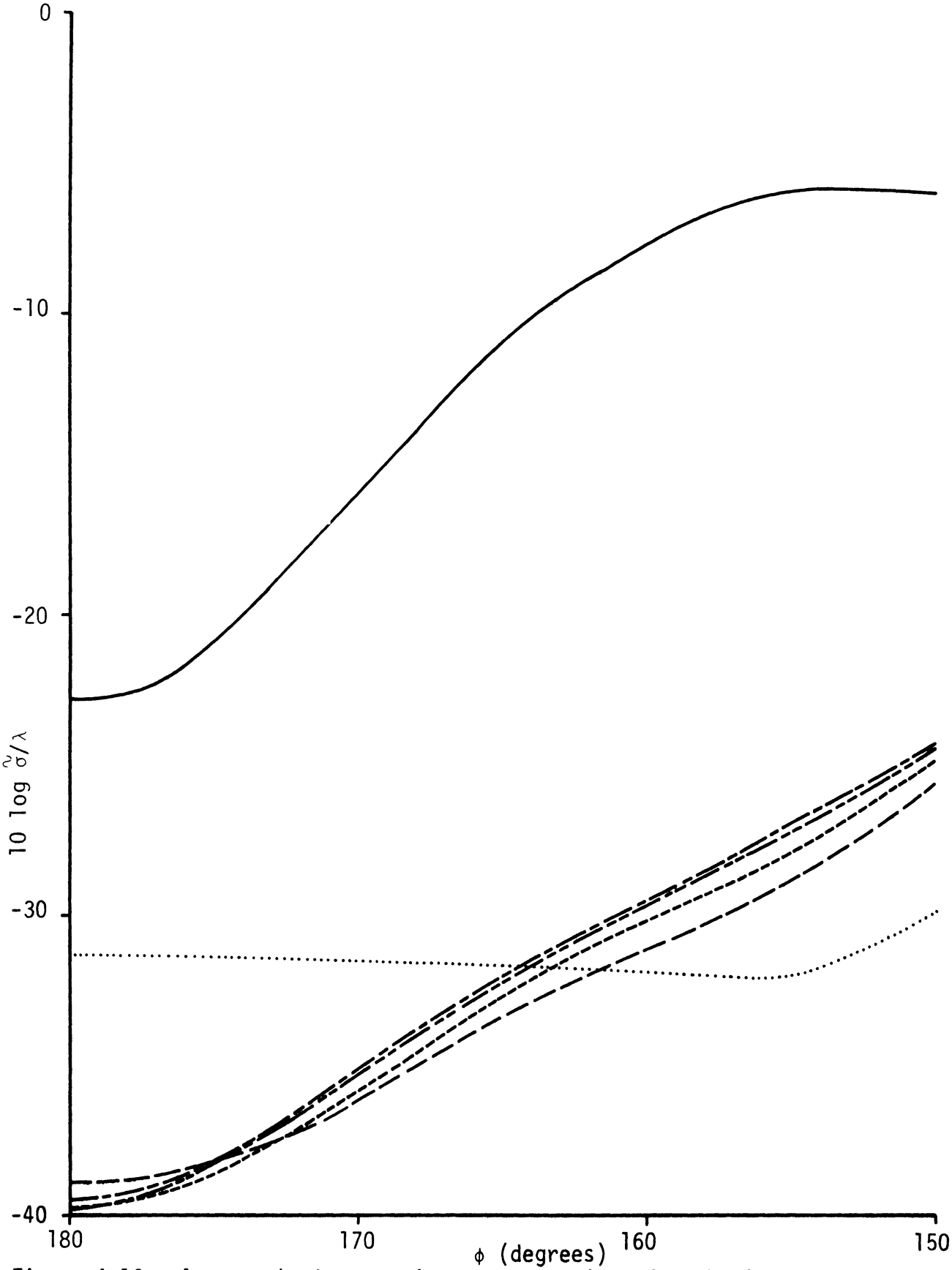

Figure 4-19: Average backscattering cross sections for the impedance profile (55) with $\eta_m = 1$, $s_1 - s_m/2$ and $\eta_1 = 0.25882$ (— - —), 0.26287 (— -- —), 0.27497 (---), 0.29498 (— — —), 0.39973 (···), compared with the bare body ($\eta = 0$) result (——).

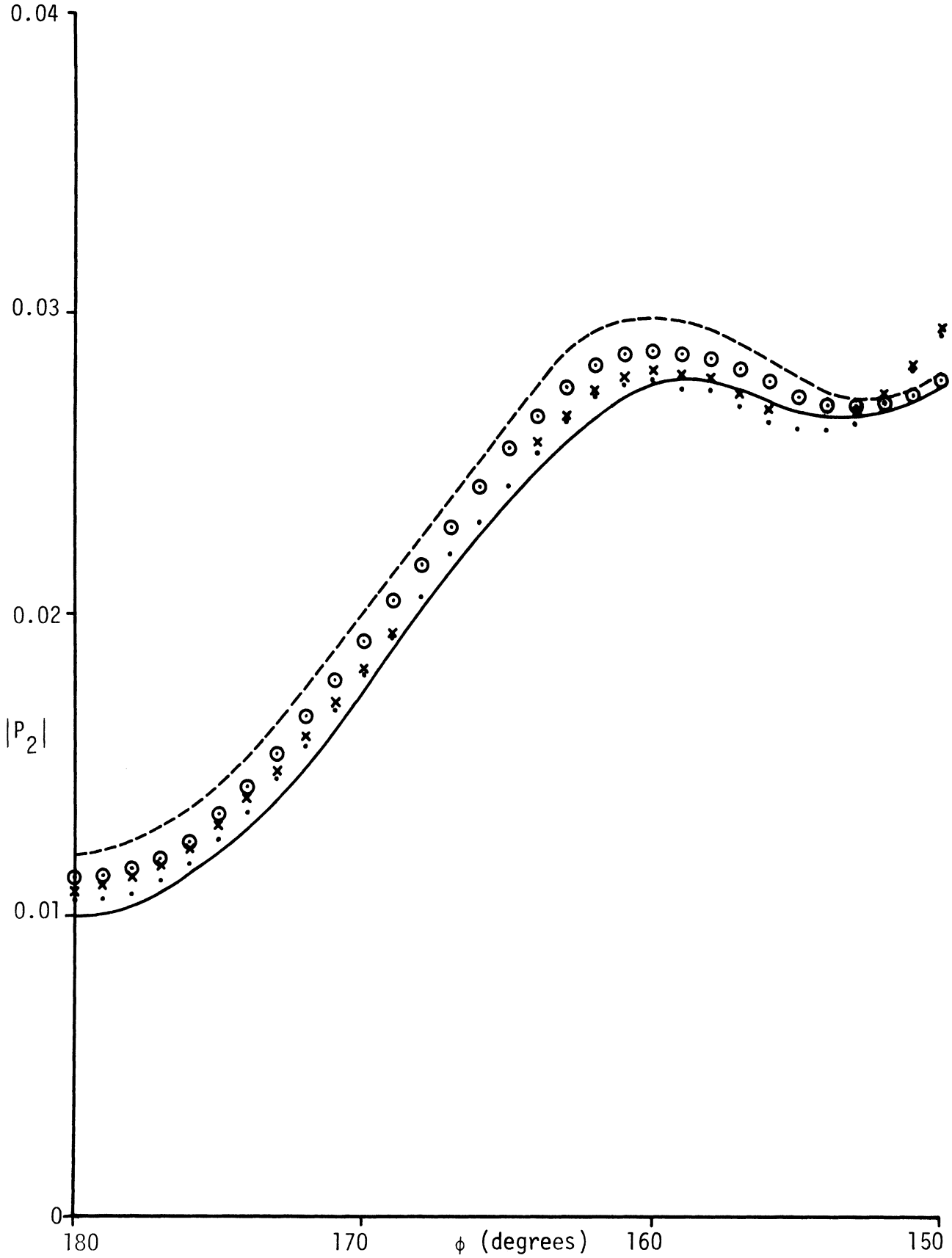

Figure 4-20: Deduced magnitudes of the rear edge contribution for: profile (55) with $\eta_1 = 0.25882$, $\eta_m = 1$ and $s_1 = s_m/2$ (---), $s_m/4$ (xxx), $s_m/8$ (•••); profile (56) with $\eta_1 = 0.25882$, $\eta_m = 1$ and $s_1 = s_m/2$ (000); uniform impedance $\eta = 1$ (——).

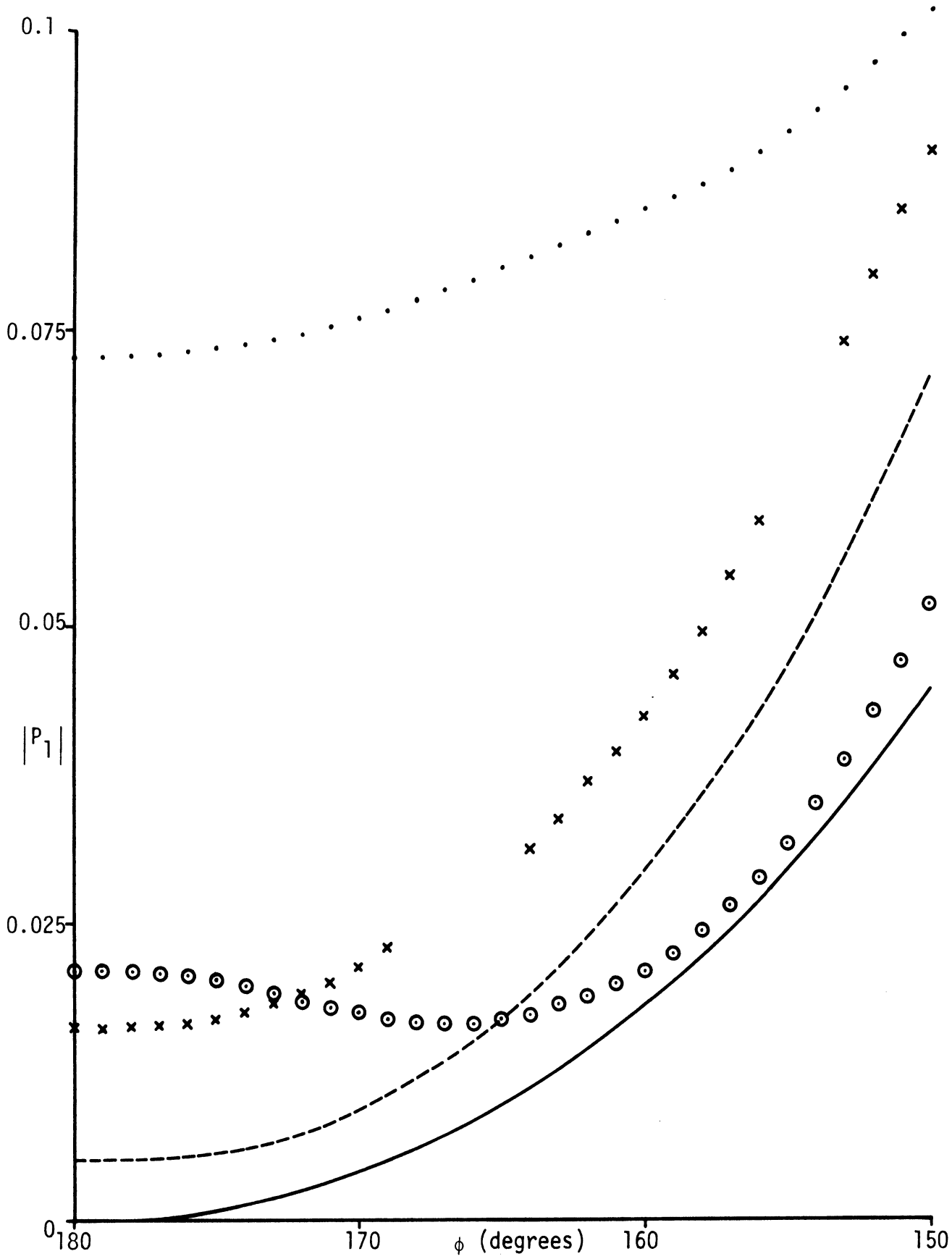

Figure 4-21: Deduced magnitudes of the front edge contribution for: profile (55) with $\eta_1 = 0.25882$, $\eta_m = 1$ and $s_1 = s_m/2$(---), $s_m/4$ (xxx), $s_m/8$ (···); profile (56) with $\eta_1 = 0.25882$, $\eta_m = 1$ and $s_1 = s_m/2$ (000); uniform impedance $\eta = 1$ (——).

for uniform impedance wedges (see Figure 3-8) with $\eta = 0.198$ and 0.017 respectively, and the large impedance slope now has more effect than the actual impedance at the edge.

As a further illustration of the effects of a rapid impedance variation, data have been obtained for the impedance profile

$$\eta = \eta_1 + (\eta_m - \eta_1) \sin \frac{\pi s}{2 s_1} \quad , \qquad 0 \leq s \leq s_1$$
$$\eta = \eta_m \quad , \qquad s_1 \leq s \leq s_m \tag{56}$$

with $\eta_1 = 0.25882$, $\eta_m = 1$ and $s_1 = s_m/2$, and the resulting values of $|P_2|$ and $|P_1|$ are included in Figures 4-20 and 4-21. $|P_2|$ is quite in accordance with expectations and is bracketted by the values for the uniform wedge and the wedge with the taper (55) extending over half the body, i.e., $s_1 = s_m/2$. $|P_1|$, however, is much greater than for the latter wedge, and the minimum centered on $\phi \simeq 166^0$ is suggestive of a complex (equivalent) edge impedance having $|\eta| \simeq 0.3$. For $\phi \leq 170^0$ $|P_1|$ is also less than for the analogous profile (55), implying a larger reduction in $\tilde{\sigma}$ in this aspect range, but if this is the objective, Figures 4-17 through 4-19 show that an even better performance can be achieved using the profile (55) with $\eta_1 \simeq 0.3$; and since the front edge contribution is virtually independent of frequency if $s_1 = s_m/2$, the results obtained are then meaningful for all frequencies $f \geq 5$ GHz.

In seeking to realize the above impedances using a coating, one of the main difficulties is the requirement that the impedance be real. As previously remarked, much of the desired reduction in the front edge contribution is lost if the impedance is complex and to demonstrate this fact computations were performed for the impedance profile (55) with $s_1 = s_m/2$, Re. $\eta_1 = 0.25882$, Re. $\eta_m = 1$ and arg $\eta = 30^0$ instead of 0. The results are shown in Figures 4-22

and 4-23. Over most of the aspect range the values of $|P_1|$ are substantially larger than for the case $\eta = 0$, and are reasonably approximated by the data for the corresponding uniform wedge. For the larger $\emptyset$, $|P_2|$ is similar to but somewhat smaller than for $\theta = 0$, suggesting that $|\eta|$ rather than $Re.\eta$ is the determining factor in this aspect range, but for $\emptyset \lesssim 165^0$ the curve shows hardly any evidence of the local maximum that previously characterized the rear edge return. Because of the changed shape of the curve, it would appear that $|P_2|$ is influenced by the value of the impedance at the rear as well as by the attenuation of the field on the surface. This is certainly not unreasonable physically and it is unfortunate that there is no easy way to separate the two effects.

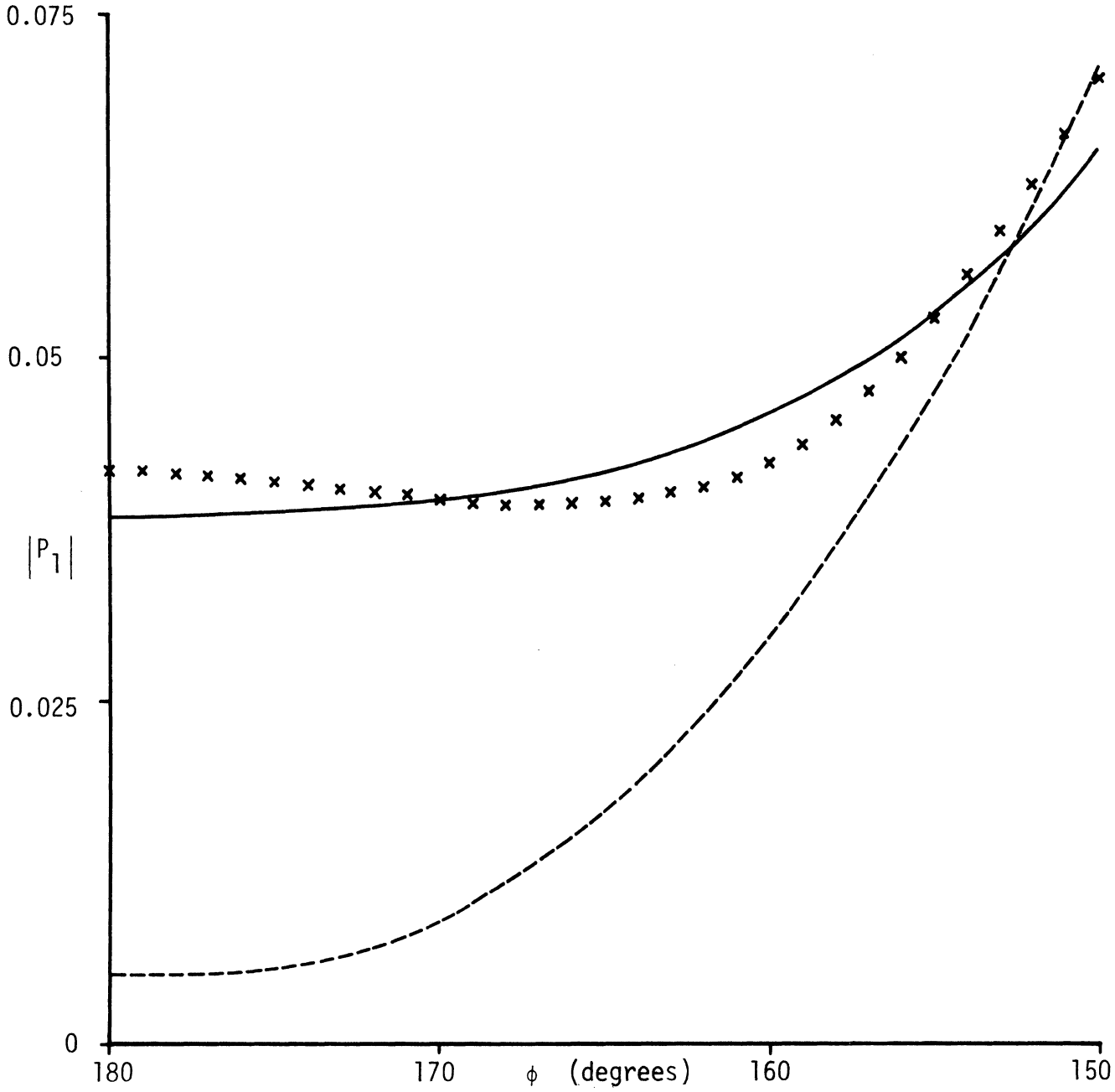

Figure 4-22: Deduced (xxx) magnitudes of the front edge contribution for the impedance profile (55) with Re. $\eta_1 = 0.25882$, $s_1 = s_m/2$ and arg $\eta = 30°$, compared with the results for arg $\eta = 0$ (---) and the theoretical wedge result (——) for the uniform impedance $\eta = 0.25882\ (1 + i/\sqrt{3})$.

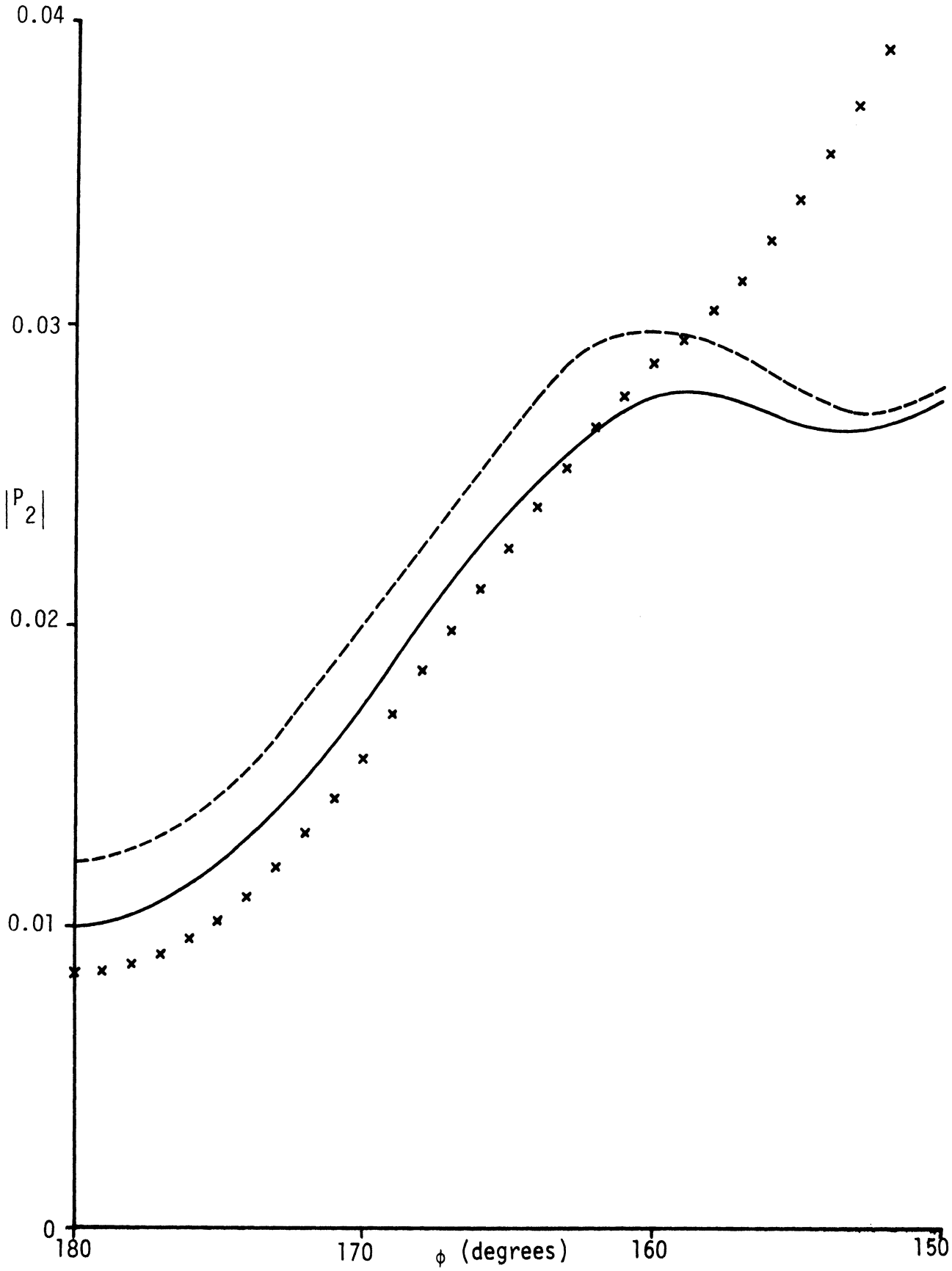

Figure 4-23: Deduced (xxx) magnitudes of the rear edge contribution for the impedance profile (55) with Re. $\eta_1 = 0.25882$, $s_1 = s_m/2$ and arg $\eta = 30°$, compared with the results for arg $\eta = 0$ (---) and the theoretical wedge result (——) for the uniform impedance $\eta = 0.25882\ (1 + i/\sqrt{3})$.

5. ACKNOWLEDGEMENT

The author is indebted to Mrs. Austra Liepa for the computer programming involved in this study.

6. REFERENCES

Bowman, J.J., T.B.A. Senior and P.L.E. Uslenghi (1969), "Electromagnetic and acoustic scattering by simple shapes", North-Holland Publishing Co., Amsterdam.

Bucci, O.M. (1974), "On a function occurring in the theory of scattering from an impedance half plane", Laboratorio di Onde Elettromagnetiche, Napoli, Italy.

Kaminetzky, L. and J.B. Keller (1972), "Diffraction coefficients for higher order edges and vertices", SIAM J. Appl. Math. 22(1), 109-134.

Kay, A.F. (1957), "Scattering of a surface wave by a discontinuity in normal reactance with applications to antenna problems", TRG Report AFCRC-TN-56-778.

Knott, E.F. and T.B.A. Senior (1973a), "Equivalent currents for a ring discontinuity", IEEE Trans. AP-21, 693-695.

Knott, E.F. and T.B.A. Senior (1973b), "Non-specular radar cross section study", The University of Michigan Radiation Laboratory Report No. 011062-1-T.

Knott, E.F. and T.B.A. Senior (1974), "Non-specular radar cross section study", The University of Michigan Radiation Laboratory Report No. 011764-1-F.

Maliuzhinets, G.D. (1959), "Excitation, reflection and emission of surface waves from a wedge with given face impedances", Sov. Phys. -Dokl. 3(4), 752-755.

Senior, T.B.A. (1960), "Impedance boundary conditions for imperfectly conducting surfaces", Appl. Sci. Res. 8(B), 418-436.

Senior, T.B.A. (1962), "A note on impedance boundary conditions", Can. J. Phys. 40, 663-665.

Senior, T.B.A. (1972), "The diffraction matrix for a discontinuity in curvature", IEEE Trans. AP-20(3), 326-333.

Senior, T.B.A. (1975), "Half plane edge diffraction", Radio Sci. 10 (6), 645-650.

Senior, T.B.A. and V.V. Liepa (1977), "Non-specular RAM", The University of Michigan Radiation Laboratory Report No. 014518-1-F.

Ufimtsev, P.Ya. (1962), "Method of edge waves in the physical theory of diffraction", Izd-Vo Sov. Radio, Moscow.

APPENDIX A. EDGE DIFFRACTION COEFFICIENT

A program has been written to compute the edge diffraction coefficient for backscattering from a 15° half angle wedge using the expression for P (Ø, Ø, η) given in (38). The required inputs are the real and imaginary parts of the angle χ satisfying (12), and a program listing and specimen output are as follows:

```
      COMPLEX X,F17,F17SQ,ARG,F5,F5SQ,SINE,Q,SINSQ,P15,FALFA
      DATA PI/3.1415927/,P11/2.8797933/,S11/.5454545/,
     &PI2/1.5707963/,RAD/.0174533/,DEG/57.2957795/
      ARG=CMPLX((17.*PI)/12.,0.)
      F17=FALFA(ARG)
      F17SQ=F17*F17
      ARG=CMPLX(-(5.*PI)/12.,0.)
      F5=FALFA(ARG)
      F5SQ=F5*F5
      ROOT2=SQRT(2.)
100   READ(5,500) X
500   FORMAT(2F10.5)
      WRITE(6,501)
501   FORMAT(1H1,' EDGE SCATTERING COEFFICIENT (15 DEGREES)')
      XR=REAL(X)
      XI=AIMAG(X)
      WRITE(6,510) XR,XI
510   FORMAT(1H0,5X,'X = (',F8.5,',',F8.5,' )'//,4X,
     &'PHI',12X,'MOD',11X,' ARG '/)
      SINE=CSIN(S11*X)
      SINSQ=SINE*SINE
      PHIP=180.
      PHI= 0.
      DO 200 I=1,34
      PHIR=RAD*PHI
      Q=F17SQ/(FALFA(X-PHIR+P11)*FALFA(X+PHIR+P11))
      Q=Q*F5SQ/(FALFA(X-PHIR-P11)*FALFA(X+PHIR-P11))
      COS6=COS(S11*PHIR)
      COS2=COS(S11*(PHIR-PI2))*COS(S11*(PHIR+PI2))
      P15=0.23632*COS6*COS6*(COS2-SINSQ)*Q*Q/COS2
      AMP=CABS(P15)
      PHASE=DEG*ATAN2(AIMAG(P15),REAL(P15))
      WRITE(6,530) PHIP,AMP,PHASE
530   FORMAT(1H ,2X,F5.1,6X,E12.5,5X,F7.2)
      PHIP=PHIP-5.
200   PHI=PHI+5.
      GO TO 100
      END
```

```
      COMPLEX FUNCTION FAIFA(A)
      COMPLEX A,COSA
      DATA PI/3.1415927/,PI33/.0951998/,P11/.2855993/
      COSA=CCOS(A/(11.,0.))
      FALFA=(COSA+COS( 4.*PI33))/(COSA+COS(PI33))*
     &      (COSA+COS( 2.*PI33))/(COSA+COS( 5.*PI33))*
     &      (COSA+COS( 8.*PI33))/(COSA+COS(11.*PI33))*
     &      (COSA+COS(14.*PI33))/(COSA+COS(17.*PI33))*
     &      (COSA+COS(20.*PI33))/(COSA+COS(23.*PI33))*
     &      (COSA+COS(26.*PI33))/(CCOS(A/(22.,0.)))*
     &      (COSA+COS(PI/12.))*
     &      (COSA+COS(3.*P11))/(COSA+COS(2.*P11))*
     &      (COSA+COS(5.*P11))/(COSA+COS(4.*P11))
      RETURN
      END
```

EDGE SCATTERING COEFFICIENT (15 DEGREES)

X = (1.34707,-0.13234)

PHI	MOD	ARG
180.0	0.35281E-01	100.93
175.0	0.35763E-01	102.58
170.0	0.37411E-01	107.33
165.0	0.40797E-01	114.54
160.0	0.46763E-01	123.06
155.0	0.56298E-01	131.60
150.0	0.70495E-01	139.20
145.0	0.90746E-01	145.48
140.0	0.11914E+00	150.45
135.0	0.15921E+00	154.31
130.0	0.21739E+00	157.29
125.0	0.30669E+00	159.58
120.0	0.45759E+00	161.35
115.0	0.76166E+00	162.70
110.0	0.16768E+01	163.73
105.0	0.68786E+05	164.50
100.0	0.19867E+01	-14.95
95.0	0.10699E+01	-14.59
90.0	0.76313E+00	-14.40
85.0	0.60831E+00	-14.36
80.0	0.51376E+00	-14.47
75.0	0.44882E+00	-14.73
70.0	0.40024E+00	-15.16
65.0	0.36124E+00	-15.76
60.0	0.32790E+00	-16.57
55.0	0.29762E+00	-17.62
50.0	0.26850E+00	-18.99
45.0	0.23889E+00	-20.76
40.0	0.20722E+00	-23.07
35.0	0.17179E+00	-26.15
30.0	0.13087E+00	-30.37
25.0	0.83354E-01	-36.40
20.0	0.32150E-01	-45.51
15.0	0.23747E-11	-60.39

EDGE SCATTERING COEFFICIENT (15 DEGREES)

X = (1.44423,-0.22407)

PHI	MOD	ARG
180.0	0.71446E-01	112.27
175.0	0.72400E-01	113.03
170.0	0.75389E-01	115.22
165.0	0.80796E-01	118.61
160.0	0.89249E-01	122.83
155.0	0.10165E+00	127.47
150.0	0.11922E+00	132.13
145.0	0.14372E+00	136.51
140.0	0.17783E+00	140.43
135.0	0.22596E+00	143.81
130.0	0.29606E+00	146.66
125.0	0.40406E+00	148.99
120.0	0.58720E+00	150.88
115.0	0.95725E+00	152.37
110.0	0.20734E+01	153.51
105.0	0.83987E+05	154.34
100.0	0.24025E+01	-25.11
95.0	0.12847E+01	-24.82
90.0	0.91180E+00	-24.77
85.0	0.72461E+00	-24.96
80.0	0.61117E+00	-25.41
75.0	0.53408E+00	-26.12
70.0	0.47714E+00	-27.12
65.0	0.43208E+00	-28.46
60.0	0.39410E+00	-30.21
55.0	0.36000E+00	-32.46
50.0	0.32734E+00	-35.36
45.0	0.29392E+00	-39.11
40.0	0.25748E+00	-44.04
35.0	0.21539E+00	-50.65
30.0	0.16478E+00	-59.76
25.0	0.10384E+00	-72.70
20.0	0.38029E-01	-91.68
15.0	0.23997E-11	-119.71

EDGE SCATTERING COEFFICIENT (15 DEGREES)

X = (1.57080,-0.25601)

PHI	MOD	ARG
180.0	0.10898E+00	125.22
175.0	0.11045E+00	125.65
170.0	0.11495E+00	126.88
165.0	0.12286E+00	128.80
160.0	0.13482E+00	131.21
155.0	0.15178E+00	133.90
150.0	0.17517E+00	136.66
145.0	0.20716E+00	139.35
140.0	0.25112E+00	141.83
135.0	0.31271E+00	144.04
130.0	0.40211E+00	145.95
125.0	0.53975E+00	147.54
120.0	0.77333E+00	148.83
115.0	0.12460E+01	149.82
110.0	0.26739E+01	150.54
105.0	0.10757E+06	150.98
100.0	0.30626E+01	-28.83
95.0	0.16334E+01	-28.91
90.0	0.11587E+01	-29.25
85.0	0.92223E+00	-29.87
80.0	0.78068E+00	-30.81
75.0	0.68616E+00	-32.09
70.0	0.61800E+00	-33.77
65.0	0.56564E+00	-35.96
60.0	0.52293E+00	-38.76
55.0	0.48566E+00	-42.35
50.0	0.45048E+00	-47.02
45.0	0.41398E+00	-53.14
40.0	0.37197E+00	-61.34
35.0	0.31872E+00	-72.58
30.0	0.24684E+00	-88.33
25.0	0.15164E+00	-110.60
20.0	0.49443E-01	-141.09
15.0	0.23954E-11	-178.31

APPENDIX B. ANALYTICAL APPROXIMATION

For a 15° half angle ogival cylinder subject to an impedance boundary condition and illuminated by an H polarized plane wave incident in a plane perpendicular to the generators, an analytical approximation to the backscattering cross section can be developed by adding expressions for the edge waves to the physical optics result. The method is equivalent to that of Ufimtsev (1962) or, alternatively, to the equivalent current method of Knott and Senior (1973).

B.1 Physical Optics

If the incident field is the plane wave having $\underline{H} = \hat{z}H_z$

with

$$H_z = e^{ik\,\hat{i}\,\cdot\,\underline{\rho}}\,,$$

the impedance analogue of the physical optics approximation is to assume

$$H_z = \frac{2\hat{n}\cdot\hat{i}}{\hat{n}\cdot\hat{i}-\eta}\; e^{ik\,\hat{i}\,\cdot\,\underline{\rho}}$$

over the lit portion of the surface and zero in the shadow. On substituting this into (6), the physical optics expression for the far field amplitude P becomes

$$P^{p\,\cdot\,o} = \frac{k}{2}\int_{lit}\left(\frac{\hat{n}'\cdot\hat{\rho}-\eta}{\hat{n}'\cdot\hat{i}-\eta}\right)\hat{n}'\cdot\hat{i}\;e^{ik(\hat{i}-\hat{\rho})\cdot\underline{\rho}'}\,ds\,,$$

and in the particular case of backscattering such that $\hat{i} = -\hat{\rho}$

$$P^{p\,\cdot\,o} = \frac{k}{2}\int_{lit}\left(\frac{\hat{n}'\cdot\hat{\rho}-\eta}{\hat{n}'\cdot\hat{\rho}+\eta}\right)\hat{n}'\cdot\hat{\rho}\;e^{-2ik\hat{\rho}\,\cdot\,\hat{\underline{\rho}}'}\,ds'. \qquad (B.1)$$

At the specular point $\hat{n}'\cdot\hat{\rho} = 1$.

Let us now apply this to a length ℓ of a wedge of uniform impedance η and interior half angle Ω. If the incidence is such that only the upper surface is illuminated, i.e., $\Omega < \phi < \pi - \Omega$, then

$$\hat{n}' \cdot \hat{\rho} = \sin(\phi - \Omega)$$

and

$$\hat{\rho} \cdot \underline{\rho}' = x' \cos(\phi - \Omega)$$

giving

$$p^{p \cdot o}(\phi) = \frac{k}{2} \frac{\sin(\phi - \Omega) - \eta}{\sin(\phi - \Omega) + \eta} \sin(\phi - \Omega) \int_0^{\ell} e^{-2ikx'\cos(\phi - \Omega)} dx'.$$

Hence

$$p^{p \cdot o}(\phi) = -\frac{i}{4} \frac{\sin(\phi - \Omega) - \eta}{\sin(\phi - \Omega) + \eta} \tan(\phi - \Omega) \left\{1 - e^{-2ik\ell\cos(\phi - \Omega)}\right\}$$

for $\phi \neq \pi/2 + \Omega$, reducing to

$$p^{p \cdot o}(\phi) = \frac{k\ell}{2} \frac{1 - \eta}{1 + \eta}$$

if $\phi = \pi/2 + \Omega$, and the contribution of the front edge is therefore

$$p^{p \cdot o}(\phi) = -\frac{i}{4} \frac{\sin(\phi - \Omega) - \eta}{\sin(\phi - \Omega) + \eta} \tan(\phi - \Omega). \qquad (b.2)$$

When $\phi \simeq \pi/2 + \Omega$ the expression reduces to that in (17), implying a singularity identical to that displayed by the exact edge diffraction coefficient (16).

If $\phi > \pi - \Omega$ the lower face of the wedge is also illuminated and its contribution to the edge diffraction is

$$p^{p \cdot o}(\phi) = \frac{i}{4} \frac{\sin(\phi + \Omega) - \eta}{\sin(\phi + \Omega) + \eta} \tan(\phi + \Omega) \qquad (B.3)$$

which is infinite when $\phi = 3\pi/2 - \Omega$, as expected.

In the case of an ogival cylinder of half angle Ω, it is convenient to specify the point of integration using the angle α subtended at the center of curvature. On the upper surface

$$\hat{n}' = \hat{x} \sin\alpha + \hat{y} \cos\alpha$$

$$\underline{\rho}' = R\{\hat{x} \sin\alpha + \hat{y}(\cos\alpha - \cos\Omega)\} \quad ,$$

giving

$$\hat{n}' \cdot \hat{\rho} = \sin(\emptyset + \alpha)$$

$$\hat{\rho} \cdot \underline{\rho}' = R \sin(\emptyset + \alpha) - R \sin\emptyset \cos\Omega.$$

From (B.1) the contribution of the upper surface is

$$P_u^p \cdot o(\emptyset) = \frac{kR}{2} e^{2ikR\sin\emptyset\cos\Omega} \int_{-\Omega}^{\gamma} \frac{\sin(\alpha + \emptyset) - \eta(\alpha)}{\sin(\alpha + \emptyset) + \eta(\alpha)} \sin(\alpha + \emptyset) e^{-2ikR\sin(\alpha + \emptyset)} d\alpha \tag{B.4}$$

for $\Omega < \emptyset \leq \pi$ where $\gamma = \min.(\pi - \emptyset, \Omega)$. If $\emptyset > \pi - \Omega$, however, a portion of the lower surface is also illuminated, and its contribution is

$$P_\ell^p \cdot o(\emptyset) = \frac{kR}{2} e^{-2ikR\sin\emptyset\cos\Omega} \int_{-\Omega}^{-(\pi-\emptyset)} \frac{\sin(\alpha - \emptyset) - \eta(\alpha)}{\sin(\alpha - \emptyset) + \eta(\alpha)} \sin(\alpha - \emptyset) e^{-2ikR\sin(\alpha - \emptyset)} d\alpha \tag{B.5}$$

The physical optics expression for P is therefore the sum of (B.4) and (B.5), i.e.,

$$P^p \cdot o(\emptyset) = \frac{kR}{2} e^{2ikR\sin\emptyset\cos\Omega} \int_{-\Omega}^{\gamma} \frac{\sin(\alpha + \emptyset) - \eta(\alpha)}{\sin(\alpha + \emptyset) + \eta(\alpha)} \sin(\alpha + \emptyset) e^{-2ikR\sin(\alpha + \emptyset)} d\alpha$$

$$+ \frac{kR}{2} e^{-2ikR\sin\emptyset\cos\Omega} \int_{-\Omega}^{-\gamma} \frac{\sin(\alpha - \emptyset) - \eta(\alpha)}{\sin(\alpha - \emptyset) + \eta(\alpha)} \sin(\alpha - \emptyset) e^{-2ikR\sin(\alpha - \emptyset)} d\alpha \tag{B.6}$$

valid for $\Omega < \emptyset \leq \pi$.

B.2 Inclusion of Edge Diffraction

The contributions of the front and rear edges to the backscattered field can be obtained from the edge diffraction coefficient for a wedge of half angle Ω, the exact expression for which is given in (16), reducing to (38) in the particular case $\Omega = 15°$. Were we to merely add them to (B.6), however, we would be guilty of tallying the edges twice, since the physical optics approximation already contains some edge contributions, albeit erroneous ones. The latter can be deduced from (B.2) and (B.3), and on subtracting them from (B.6) with account taken of the change in phase center, the scattering from the (unterminated) surfaces of the ogival cylinder is found to be

$$P^{surf}(\phi) = P^{p \cdot o}(\phi) + \frac{i}{4}\frac{\sin(\phi - \Omega) - \eta_1}{\sin(\phi - \Omega) + \eta_1}\tan(\phi - \Omega)e^{2ikR\cos\phi\sin\Omega}$$

$$- \frac{i}{4}\frac{\sin(\phi + \Omega) - \eta_1}{\sin(\phi + \Omega) + \eta_1}\tan(\phi + \Omega)e^{2ikR\cos\phi\sin\Omega}\, U(\phi + \Omega - \pi)$$

$$- \frac{i}{4}\frac{\sin(\phi + \Omega) - \eta_2}{\sin(\phi + \Omega) + \eta_2}\tan(\phi + \Omega)e^{-2ikR\cos\phi\sin\Omega}U(\pi - \phi - \Omega) \qquad (B.7)$$

where U is the unit step function and η_1, η_2 are the surface impedances at the front and rear edges respectively.

On the assumption that the surface impedance and all its derivatives are continuous (in practice it is sufficient if just η and $\partial\eta/\partial s$ are continuous), an approximation to the far field amplitude is then obtained by adding the wedge diffraction coefficients to P^{surf}. The result is

$$P(\phi) = P^{w}(\phi, \phi, \eta_1)e^{2ikR\cos\phi\sin\Omega}$$

$$+ P^{w}(\pi - \phi, \pi - \phi, \eta_2)e^{-2ikR\cos\phi\sin\Omega}\, U(\pi - \phi - \Omega) + P^{surf}(\phi) \qquad (B.8)$$

where $P^{W}(\emptyset, \emptyset, \eta)$ is given in (16) and $P^{surf}(\emptyset)$ in (B.7).

Some immediate deductions can be made. If $\Omega < \emptyset < \pi - \Omega$ and η is everywhere such that

$$\eta(\alpha) = \sin(\alpha + \emptyset) \tag{B.9}$$

implying

$$\eta_1 \equiv \eta(-\Omega) = \sin(\emptyset - \Omega)$$

$$\eta_2 \equiv \eta(\Omega) = \sin(\emptyset + \Omega) ,$$

then

$$P^{p \cdot o}(\emptyset) = P^{surf}(\emptyset) = 0 \tag{B.10}$$

and the scattering in the direction $\emptyset$ is entirely attributable to edge diffraction. In particular, for broadside incidence (B.9) requires $\eta(\alpha) = \cos \alpha$, in which case

$$P(\pi/2) = 2P^{W}(\pi/2, \pi/2, \cos \Omega). \tag{B.11}$$

On the other hand, if η_1 and η_2 are chosen to suppress the edge diffraction in accordance with (19), we are left with only the surface contribution and

$$P(\emptyset) = P^{surf}(\emptyset). \tag{B.12}$$

It would appear that the condition for this conflicts with (B.9) for all ogival cylinders and for all angles of incidence except for a strip ($\Omega = 0$) at broadside incidence ($\emptyset = \pi/2$) where the requirement is $\eta = 1$. To minimize the backscattering cross section in any given direction is now an optimization process.

When $\phi = \pi/2 + \Omega$ the wedge diffraction coefficient for the front edge is infinite unless $\eta = 1$. The physical optics estimate is likewise infinite, and since the two infinities are identical (and cancel), it is convenient for numerical purposes to regroup the terms in (B.8). On doing so we have

$$P(\phi) = P^f(\phi, \phi, \eta_1)e^{2ikR\cos\phi\sin\Omega} + P^r(\phi, \phi, \eta_2)e^{-2ikR\cos\phi\sin\Omega}\, U(\pi - \phi - \Omega)$$

$$+ P^{p \cdot o}(\phi) \qquad \text{(B.13)}$$

where the front edge contribution is

$$P^f(\phi, \phi, \eta_1) = P^w(\phi, \phi, \eta_1) + \frac{i}{4}\frac{\sin(\phi - \Omega) - \eta_1}{\sin(\phi - \Omega) + \eta_1}\tan(\phi - \Omega)$$

$$- \frac{i}{4}\frac{\sin(\phi + \Omega) - \eta_1}{\sin(\phi + \Omega) + \eta_1}\tan(\phi + \Omega)U(\phi + \Omega - \pi)\,, \qquad \text{(B.14)}$$

the rear contribution is

$$P^r(\phi, \phi, \eta_2) = P^w(\pi - \phi, \pi - \phi, \eta_2) - \frac{i}{4}\frac{\sin(\phi + \Omega) - \eta_2}{\sin(\phi + \Omega) + \eta_2}\tan(\phi + \Omega), \qquad \text{(B.15)}$$

and $P^{p \cdot o}(\phi)$ is given in (B.6). All three terms in (B.13) are finite for all finite η, but the regrouping has changed somewhat the conditions for suppressing the individual terms. Although $P^{p \cdot o}(\phi)$ still vanishes if (B.9) is satisfied, (19) is no longer relevant to the suppression of the remaining terms in (B.13). Thus if $\phi = \pi/2$ with $\Omega = 15°$,

$$P^{f,r}(\pi/2, \pi/2, \eta) = -i\left\{0.10134\left[1 + 7.02667\sin^2\frac{6\chi}{11}\right]\sec^2\frac{6}{11}\right.$$

$$\left. - 0.93301\tan\left[\chi - \frac{\pi}{12}\right]\tan\left[\chi + \frac{\pi}{12}\right]\right\}$$

(see 18) and vanishes if $\eta = \cos\chi = 1.390$, compared with the value $\eta = 1.237$ for which $P^w(\pi/2, \pi/2, \eta) = 0$.

Programs have been written to compute $P(\emptyset)$ for $\Omega = 15°$ and any desired impedance using both of the representations (B.8) and (B.13). The results are, of course, identical, and though (B.13) is more convenient numerically, the computation of the individual terms in (B.8) is helpful in seeking to minimize the scattering. Because we have not included any traveling wave effects per se, the accuracy of our formulae diminishes as end-on incidence ($\emptyset = \pi$) is approached, particular for surface impedances where these effects are significant.